Inelastic Random Earthquake Response and Reliability of Base-Isolated Nuclear Containment Vessels

（基礎免震を含む原子炉格納容器の非線形ランダム地震応答と信頼性）

1994年9月

Hiroshi ASADA

Inelastic Random Earthquake Response and Reliability of Ductile Frames Mixed with Brittle Elements

(脆性的要素を含む骨組の非線形ランダム地震応答と信頼性)

March, 1999

1999 年 3 月

Hafez AL-SADEQ
ハフェズ アルサデク

CONTENTS

CONTENTS i
SYMBOLS iii
FIGURES v
ACKNOWLEDGEMENTS vii
ABSTRACT viii
ABSTRACT (in Japanese) x

1. INTRODUCTION
   1.1 Statement of the problem 1
   1.2 Brief review of previous research 4
   1.3 Study objectives 8
   1.4 Study layout 8

2. EARTHQUAKE EXCITATION
   2.1 Introduction 10
   2.2 Simulation of real earthquake ground motions 10
   2.3 Artificial input motions 14
   2.4 Correspondence between real and artificial input motions 18

3. ADOPTED HYSTERETIC MODELS (Structural Models)
   3.1 Introduction 24
   3.2 Frame and brittle element hysteretic models 25
   3.3 Input motion and system input data 28
   3.4 Equilibrium equation of motion 28
   3.5 Response under individual white noise samples 30

4. INELASTIC DYNAMIC RESPONSE PREDICTION
4.1 Introduction 33
4.2 Energy balance equation 34
4.3 Simulation and prediction of average plastic energy 37
4.4 Simulation and prediction of average ductility factor 45
4.5 Simulation and prediction of plastic energy standard deviation 49
4.6 Simulation and prediction of ductility factor standard deviation 53
4.7 Verification for other post-yielding stiffness ratio 57
4.8 Expressions summary and general formula setup 60
4.9 Fitting agreement 61
4.10 Relationship between response quantities 63
4.11 General curves capturing the effect of brittle element on seismic response of ductile frame 68
4.12 Response under real earthquakes 71

5. RELIABILITY ANALYSIS
5.1 Introduction 80
5.2 Reliability analysis 80

6. CONCLUSIONS AND RECOMMENDATIONS
6.1 Conclusions 88
6.2 Recommendations for future research 89

REFERENCES 91
PUBLICATIONS 93

SYMBOLS

E_p = accumulated plastic energy dissipated by frame

$\bar{E}_p$ = average accumulated plastic energy dissipated by frame

$\bar{\lambda}_i$ = average normalized total input energy

$\bar{\lambda}$ = average normalized accumulated plastic energy dissipated by frame

ξ = normalized input motion intensity

α = frame yield acceleration

S_0 = power spectrum density of white noise

τ = time divided by frame natural period of vibration

τ_c = normalized time at which the frame response starts to be stationary

τ_0 = normalized time at which nonlinear response starts (previous work)

t = time

t_d = time duration of earthquake

ζ = average number of impulses during t_d

ω_0 = frame natural circular frequency of vibration

f_0 = frame natural frequency of vibration

T_0 = frame natural period of vibration

K_{w0} = brittle element initial stiffness

K_{f0} = frame initial stiffness

K_{fw0} = frame and brittle element total stiffness

Q_{fy} = frame yield shear strength

Q_{wy} = brittle element yield shear strength

Q_{fwy} = total frame and brittle element yield shear strength

δ_{fy} = frame yield displacement

ε = normalized potential energy of brittle element

μ = ductility factor

$\bar{\mu}$ = average ductility factor

σ_λ = standard deviation of λ

σ_μ = standard deviation of μ

β = brittle element post yield stiffness ratio

R_k = system stiffness ratio

R_q = system strength ratio

f_λ = probability density function for λ

f_μ = probability density function for μ

R_λ = energy-based reliability

R_μ = ductility based reliability

λ_F = assumed failure limit for λ

μ_F = assumed failure limit for μ

m = system mass

T = kinetic energy of mass m

A_i = magnitude of impulse i

FIGURES

Fig. 1.1.1: Infilled and empty frames
Fig. 1.1.2: Frame mixed with shear wall
Fig. 1.1.3: Parallel mixed system

Fig. 2.2.1: Concept of earthquake waves travel paths
Fig. 2.2.1: Proposed typical models for earthquake power spectrum
Fig. 2.2.2: probability density of power spectrum based on real earthquakes
Fig. 2.2.3: probability density of power spectrum based on white noise
Fig. 2.3.1: Assumed power spectrum
Fig. 2.3.2: Samples of white noises and corresponding power spectra
Fig. 2.4.1: Data processing for El Centro earthquake
Fig. 2.4.2: Data processing for Taft earthquake
Fig. 2.4.3: Data processing for Hachinohe earthquake
Fig. 2.4.4: Data processing for Miyagiken-oki earthquake
Fig. 2.4.5: Data processing for Kobe earthquake

Fig. 3.1.1: General load deformation relationships
Fig. 3.2.1: Adopted hysteretic models for brittle element and frame
Fig. 3.2.2: Failure scenario of the brittle element restoring force
Fig. 3.4.1: Idealized SDOF system subjected to horizontal ground motion
Fig. 3.5.1: Plastic energy and displacement response time histories (sample1)
Fig. 3.5.2: Shear force-displacement relationships (sample1)
Fig. 3.5.3: Plastic energy and displacement response time histories (sample2)
Fig. 3.5.4: Shear force-displacement relationships (sample2)

Fig. 4.2.1: Accumulated plastic deformations
Fig. 4.3.1: Sampling curves of $\bar{\lambda} - \tau$
Fig. 4.3.2: $\bar{\lambda} - \tau$ formula setup

Fig. 4.3.3: Parameter of τ_c with respect to ξ, ε/ξ and β
Fig. 4.3.4: Evaluation of coefficient l
Fig. 4.3.5: Evaluation of coefficients d
Fig. 4.3.6: Simulated and predicted $\bar{\lambda}-\tau$ curves (R_k = 6 and 8, β = –0.1)
Fig. 4.3.7: Simulated and predicted $\bar{\lambda}-\tau$ curves (R_k = 10 and 12, β = –0.1)
Fig. 4.4.1: Coefficients of $a2$ and $b2$
Fig. 4.4.2: Simulated and predicted $\bar{\mu}-\tau$ curves (R_k = 6 and 8, β = –0.1
Fig. 4.4.3: Simulated and predicted $\bar{\mu}-\tau$ curves (R_k = 10 and 12, β = –0.1)
Fig. 4.5.1 : Evaluation of coefficient a_3
Fig. 4.5.2: Evaluating the coefficient b_3 of σ_λ formula
Fig. 4.5.3: Simulated and predicted $\sigma_\lambda-\tau$ curves (R_k = 6 and 8 , β = –0.1)
Fig. 4.5.4: Simulated and predicted $\sigma_\lambda-\tau$ curves (R_k = 10 and 12 β = –0.1)
Fig. 4.6.1: Evaluating the coefficient a_4 of $\sigma_\mu-\tau$ formula
Fig. 4.6.2: Evaluating the coefficient b_4 of $\sigma_\mu-\tau$ formula
Fig. 4.6.3: Simulated and predicted $\sigma_\mu-\tau$ curves (R_k = 6 and 8 , β = –0.1)
Fig. 4.6.4: Simulated and predicted $\sigma_\mu-\tau$ curves (R_k = 10 and 12 , β = –0.1)
Fig. 4.7.1: Simulation and prediction curves (R_q= 1.4, R_k =8 and β = –0.2 , – 0.05)
Fig. 4.7.2: Simulation and prediction curves (R_q= 1.6, R_k =12 and β = –0.2 , – 0.05)
Fig. 4.10.1: Relationships of (a) $\bar{\mu}$ - $\bar{\lambda}$ and (b): σ_μ - σ_λ (ε/ξ = 0,10)
Fig. 4.10.2: Relationships of (a) $\bar{\mu}$ - $\bar{\lambda}$ and (b): σ_μ - σ_λ (R_q = 1.7, R_k = 14)
Fig. 4.11.1: Absolute response quantities based on prediction
Fig. 4.11.2: Relative response quantities based on prediction
Fig. 4.12.1: Response under El Centro earthquake (ξ =0.05)
Fig. 4.12.2: Response under Taft earthquake (ξ =0.05)
Fig. 4.12.3: Response under Hachinohe earthquake (ξ =0.05)
Fig. 4.12.4: Response under Miyagiken-oki earthquake (ξ =0.05)
Fig. 4.12.5: Response under Kobe earthquake (ξ =0.05)
Fig. 4.12.6: Response of bare frame for real earthquakes
Fig. 4.12.7: Relationships of μ - λ under real earthquakes

Fig. 5.2.1: Probability density functions of 3 distributions
Fig. 5.2.2: Reliability curves based on 3 probability distributions
Fig. 5.2.3: Reliability curves based on plastic energy dissipation
Fig. 5.2.4: Reliability curves based on ductility factor

ACKNOWLEDGMENTS

I have no adequate way of expressing my sincere gratitude, heartfelt thanks and appreciation to the academic advisor of this study; Prof. Dr. Yutaka Matsushima of the Institute of Engineering Mechanics, University of Tsukuba, who was of great help and gave me persistent encouragement throughout the Doctoral program.

Special thanks and appreciation are due to Prof. Dr. Takashi Nishioka, Prof. Dr. Yasuhiko Yamamoto, Prof. Dr. Hiroyuki Suzuki and Prof. Dr. Hiroshi Imai of the Institute of Engineering Mechanics, University of Tsukuba for their very fruitful comments and constructive suggestions and for reviewing the manuscript.

Since I entered Matsushima Earthquake Engineering Research Laboratory, I had the chance to know many students who were very kind and cooperative. A lot of useful discussions and ideas were exchanged from which I learned a lot. I wish to sincerely thank all of them. In particular, I express my thanks to Dr. Bujar Myslimaj for his valuable comments.

I would like to take this opportunity to extend my thanks and appreciation to the Japanese language teaching group of University of Tsukuba for getting sincere help when undertaking Japanese language course. Also, I sincerely acknowledge indispensable consultations made with the Science Information Processing Center, University of Tsukuba. Also, discussions with Dr. Toshiyuki Kanakubo of Institute of Engineering Mechanics and Dr. Jose Caringal Adajar of A. J. International Integrated Structures & Services were helpful.

I also appreciate and thank staff members of the Syrian National Seismological Center for encouragement and support. Thanks are also due to Dr. Satteh Badawi and Dr. Wael Mualla of the Faculty of Civil Engineering, University of Damascus.

The financial support provided by Ministry of Education, Science, Sports and Culture (Monbusho) of Japan is greatly acknowledged. It was a great opportunity not only from academic perspective, but also to learn and get to know about the specific culture and people of this nice country.

Finally, I feel in debt to my children Nesrin, Mustafa and Maher for not giving them enough time when they were in need and thank my wife for her quite understanding. Also, during my long absence from home, my parents, brother and sisters were very patient encouraging and supporting me all the time. I thank them from my deep heart.

ABSTRACT

A mixed structural system of frames and brittle failure-type elements like infill walls are widely used in many parts of the world, especially in developing countries as a cheap and simple method for enclosing and partitioning spaces in office and residential frame building structures. The frame whose elements surround infill wall is called infilled frame which is considered as a typical example of mixed system in this study. Brittle elements are made from variety of local materials and in case of masonry infill walls, they are usually made from hollow/solid bricks or concrete blocks with mortar bond. In most cases, brittle elements are considered as non-structural elements and their influence on the response of the structural frame is ignored in design practice. Seismic behavior of the mixed system is rarely mentioned in seismic design codes and lack of guidance on this subject has motivated this study.

Recent experimental and analytical studies have shown that introducing secondary elements like infill walls to moment-resisting frames generally enhance lateral stiffness, strength and energy absorption and dissipation capacity of the ductile frames. Nevertheless, the research already made in this subject have failed to quantify the effect of the brittle elements on the overall seismic response of the frames in convenient forms usable for design purpose. It is the aim of this study to bridge this gap and provide approximate-closed form expressions for that objective. Based on experimental data of infilled frame behavior under lateral loads, a simplified multi-linear hysteretic model is proposed for modeling restoring force in the brittle element with minimum controlling parameters. The restoring force model accounts for the brittle character of the secondary element by considering negative post-yielding stiffness parameter where stiffness degradation is assumed proportional to strength reduction, leading to its gradual failure and the force which was holding is gradually transferred to the frame. The model is incorporated into a

general nonlinear dynamic response analysis program in which frame element has a simple bilinear hysteretic model with zero stiffness beyond yielding. Restoring force for the whole system is assumed as a combination of the frame and brittle element hysteretic loops. A flat power spectral density function is considered for generating one-hundred statistically independent stationary white noise acceleration time histories used as input motions. Parametric study is performed on wide ranges of mixed system stiffness, strength and input motion intensity.

The attention is focused on two main response quantities: Accumulated plastic energy dissipated by frame element and frame ductility factor which are calculated for wide range of selected system data and input motion intensity. Statistical manipulations are made on the results and approximate expressions for the averages and standard deviations of the defined responses are developed. Making use of that expressions, reliability analysis for mixed system and pure frame system are performed and the drawn reliability curves are verified using direct probabilistic methods. Fitting agreements between simulation results and prediction estimates are analyzed and discussed as well. The mixed system response under real earthquake ground motions are performed for reference. To do that, real earthquake ground motions are processed in such a way that an approximate correspondence between real and artificial motions is made possible through selecting stationary-like part of each real input motion, then, relevant parameters are computed considering the selected motion as series of shot noise impulses.

The mixed system response expressed in terms of accumulated plastic energy and ductility demands on the frame can be predicted using the developed formulations which are functions of the influential parameters. In general, seismic response of the frame in a mixed system is found to be lower relative to pure frame system, the degree of which depends on level and duration of input motion, and the system geometrical and mechanical characteristics. Finally, conclusions are drawn and recommendations for future research are given for the purpose of improving and extending the analysis and its application.

論文概要

延性的な骨組の中に組みこまれた壁（infill wall）のような脆性的要素を含む混合構造系が広く世界で用いられている。多くの発展途上国では建築物の空間を仕切る安価で簡単な方法としてこのような混合構造がよく使われる。骨組要素が壁要素を含む場合、その骨組を壁付骨組（infilled frame）と呼ぶ。本研究で対象としている混合系の典型的な例がこの壁付骨組である。脆性的要素にはいろいろな材料が使われる。組積造の壁の場合には煉瓦やコンクリートブロックなどが用いられる。通常脆性的要素は非構造部材とみなされ、骨組の応答に与えるその影響は設計では無視される。混合系の地震時挙動が耐震設計基準に記述されることはほとんどなく、この種の問題に対する指針がないことが本研究を行う動機となっている。

最近の実験と解析によれば、骨組に壁のような二次要素を加えると一般に剛性、強度、エネルギー吸収能が増加することが分かる。しかし、脆性的要素が骨組の地震応答に与える影響を実際の設計に使えるような便利な形で評価する研究成果はまだ得られていない。この溝をうめ、閉じた形の近似表現を用意することが本研究の目標である。水平力を受ける壁付骨組の挙動に関する実験資料に基づき、単純化された多折線の履歴モデルを脆性的要素の復元力特性として設定する。このモデルは二次要素の脆性的特性を降伏後の負剛性で表している。剛性の低下は強度の低下に比例するとし、脆性的要素の損傷に応じて荷重がその要素から延性的な骨組に移っていくものとする。このモデルが汎用の非線形応答解析プラグラムに組みこまれる。延性骨組は塑性剛性がゼロの単純なバイリニア型履歴特性をもつとする。混合系の復元力は脆性的要素と延性的骨組の復元力を足したものとする。入力加速度は一定のパワースペクトル密度関数をもつ平均値ゼロの定常ホワイトノイズとし、互いに独立な１００個の時刻歴を発生させて入力地震動とする。混合系の剛性と強度、入力強度などの広い範囲の値に対するパラメータ解析を行う。

二つの応答量に注目する。骨組によって消費される累積塑性エネルギーと骨組の塑性率である。得られた結果を統計的に処理し、これらの応答量の平均値

と標準偏差の近似的表現式を作成する。この表現式を用いて混合系の信頼性解析を行い、シミュレーション解析によって求められた信頼性関数と比較する。近似解と数値解は実用的に許容できる範囲で互いによく一致することが分かる。 参考のために実際の地震動による混合系の応答も解析する。このとき実際の地震動の定常部分を近似的に等価な定常ショットノイズとみなして、ホワイトノイズによる応答と対応させている。

累積塑性エネルギーと塑性率で表される混合系の応答は、影響するパラメータの関数である作成された表現式によって精度よく予測することができる。一般に、混合系における骨組の地震応答は骨組だけの応答に比べて小さく、その程度は入力の強度と継続時間および系の特性を表すパラメータに依存する。最後に本論文の結論と将来の研究の方向に言及している。

Chapter One

INTRODUCTION

1.1 *Statement of the problem*

1.2 *Brief review of previous research*

1.3 *Study objectives*

1.4 *Study layout*

Chapter 1

INTRODUCTION

1.1 Statement of the problem

Structures composed of ductile frames mixed with brittle elements are often found in existing and newly designed buildings. Probably, moment-resisting frames behavior under lateral loading enjoys quite good understanding from the structural engineering community mainly due to the extensive experimental and analytical research devoted to that purpose during the past few years. However, a little progress is achieved concerning the behavior of structural system having ductile frames mixed with brittle-failure type elements under the same loading condition. One reason behind that may be attributed to the complicated behavior of the brittle-failure type element itself (otherwise denoted herein as brittle element for short) and especially when mixed with frame system. Therefore, design codes reflecting this fact of our limited knowledge and shortcomings, lacks reliable guidance concerning the mixed system design and leaving that to the designer judgment who save time and treats the real mixed system of frame and brittle element as a pure frame system, thus the brittle element presence is largely ignored.

Infilled frame structure in which interior and/or exterior frames are infilled with wall elements known as infill walls are considered as typical example of mixed system in this study (Fig. 1.1.1). The current design practice is having the walls in contact with frame elements using mortar bond only and in most cases, no special connection with the bounding frame is introduced. Infill walls are frequently made from variety of local materials like hollow or solid bricks with/without grout or concrete blocks. Mixed system of infilled frame is widely used in South Europe, Latin America, and most of the developing countries as a

cheap and simple way for enclosing and partitioning spaces in frame building structures. Since infill walls elements are considered as non-structural elements, their influence on the behavior of the bounding frame is ignored in seismic design practice.

Moreover, in a bid to reduce lateral displacement, shear wall element which also has brittle failure mode, in most cases, is used in multi-bay frames, but its presence is often ignored in the design process and the mixed system is designed just like pure frame one (Fig.1.1.2). In Japan, parallel-mixed system is noticed in low-rise school buildings (Fig. 1.1.3), in which lateral load resisting mechanism in the east-west direction have an open frame in the south-side behaving in a ductile manner whereas the exterior north-side has a rigid frame or walled frame of wide columns and deep beams, thus creating short columns of brittle failure character. Again, the practice is often designing for frames and no account is paid for the existence of the brittle elements.

Available experimental and analytical investigations have shown that introducing brittle elements like infill walls to bare frames enhance the lateral stiffness, strength and energy dissipation capacity of the mixed frame system. However, giving that infill walls are made of brittle materials, it is recognized that as soon as infill wall reaches yield strength limit, its stiffness and strength are rapidly dropped. This drop is externally caused by bond separation between the infill wall and the bounding frame elements, and internally by excessive cracks and crushes reflecting the brittle behavior of infill walls under increased lateral deformation demands.

Generally, there are many experimental researches regarding the behavior of infilled frames under lateral loads and the effect of infill walls on the lateral response of the frame. However, there are limited analytical studies dealing with modeling techniques and nonlinear dynamic response of mixed systems under strong earthquake ground motions and contribution of brittle elements to the overall seismic response of the frames. This short of guidance on the behavior of mixed frame system has led to a poor and misjudgment of the system behavior when rarely debated and introduced in seismic design codes. This study is contribution in the ongoing research trend toward better understanding of the seismic behavior of the mixed frame systems by taking

advantage of available experimental data and setting analytical model to come up with useful analytical expressions capable of predicting roughly the seismic demand of the frames when mixed with brittle elements like infill walls.

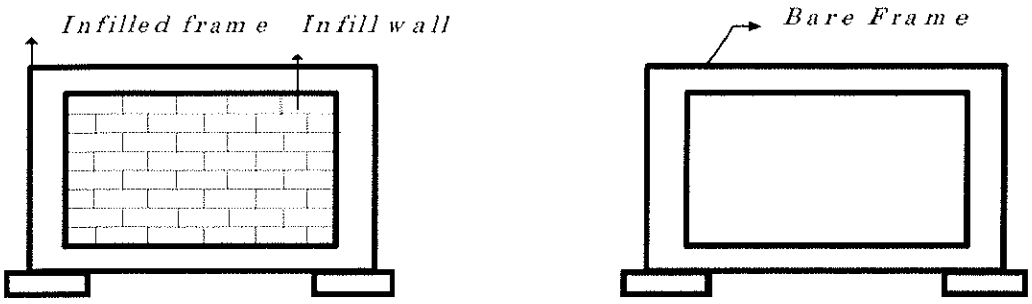

(a) : Infilled frame (b): Empty or bare frame

Fig.1.1.1 Infilled and empty frames

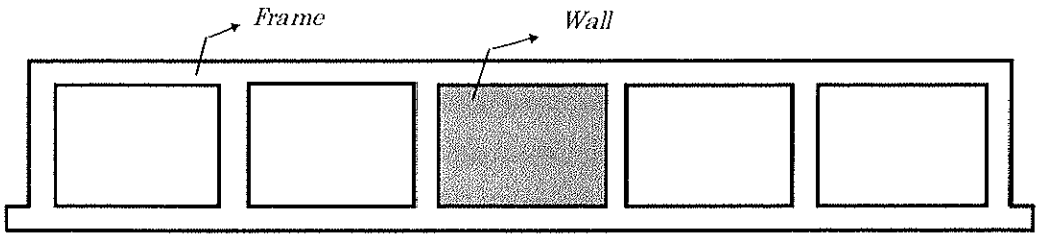

Fig.1.1.2 Frame mixed with shear wall

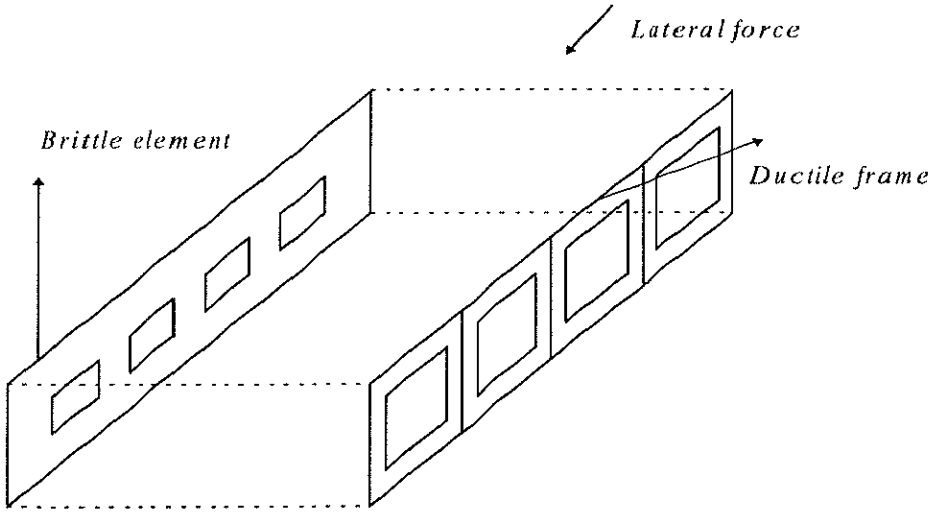

Fig. 1.1.3 Parallel mixed system

1.2 Brief review of previous research

The review made herein is about mixed frame-brittle element system in which the brittle element is made of infill wall, due to the limited data available on other types of mixed systems, thus, the mixed system will be called here as infilled frame (frame mixed with infill wall). The behavior of structures composed of frames mixed with infill walls under lateral loads have been experimentally investigated by many researchers. Early work is reported by Polyakov (1956) who observed the typical separation of the infill wall and surrounding frame under moderate loading and suggested that infill wall could be modeled as "equivalent strut" element. This simple idealization was a breakthrough step toward analytical modeling of infilled frames by which rough estimation of infilled frame stiffness and strength is made possible. Subsequent research works were concentrated on formulating the relation between the equivalent strut size and the frame-infill wall mechanical and geometrical characteristics. As a result of experimental test on steel frame filled with concrete infill wall, Holmes (1961) proposed that width of the equivalent strut be taken as 1/3 of the diagonal infill wall length. Smith and Carter (1969) developed analytical expressions for evaluating the equivalent strut width based on a beam-on-elastic foundation analogy modified by experimental results. They concluded that effective width of the equivalent strut depends on the relative stiffness of frame and infill wall, material stress strain curves, and the load level. The results indicate also that equivalent strut width falls in the range between 1/4 and 1/11 of the infill wall diagonal length. Those experimental results were based on monotonic loading and carried on one-storey one-bay infilled frames. However, early findings of Polyakov, Holmes and Smith assured that infill wall elements contribute to the infilled frame stiffness and strength and this contribution is not negligible.

Later experimental works were performed under quasi-static cyclic loading in a clear attempt to simulate the earthquake loads. In fact, there are limited experimental research concerning the infilled frame behavior under cyclic loading and most of the experiments were also conducted on simple one-storey one-bay infilled frame sub-assemblages. Many experimental results also show

that introducing a brittle element like infill wall into bare frame has beneficial effect on the seismic performance of frame as it contributes to increasing the ultimate strength and initial stiffness of the whole mixed system. Attempt is made here to find out and trace the initial and post-yielding dynamic characteristics of the infill wall element as well as its energy dissipation capacity when confined by structural frame elements as there are more uncertainty involved for this element compared with the main structural frame element. Main concern is the hysteretic shear force-interstorey drift relationship of the infill wall element from which the ultimate strength, lateral initial and post-yielding stiffness can approximately be captured for parametric study.

Brokken and Bertero (1981), as a result of their experimental investigation on three-storey infilled frame models with infill walls made from masonry concrete blocks and other materials, found that lateral initial stiffness of infilled frames could be in the range between 5-20 times that of the surrounding frame and the corresponding yield strength ratio falling in the range 1.5-2.5 times. Also, it has been observed that infill walls suffered considerable stiffness degradation with increasing inter-storey drift. The study has provided load-displacement diagrams for infilled frame with different frame and infill wall characteristics from which one can approximately extract the infilled frame post-yielding stiffness ratio defined here as the post-yielding stiffness divided by initial stiffness. On average, it is found that this ratio falls in the range (-20,-8)%. But, it is expected that this ratio will be a little lower for infill wall elements alone under the same deformation level.

Mehrabi et al. (1996) have conducted experimental tests on 1/2 scale one-storey one-bay infilled RC frame specimens into which infill walls made of concrete blocks were introduced. It was shown that infill walls can significantly improve the performance of RC frames to a degree that depends on their relative structural characteristics. The stiffness of infilled frame units was about 15 times as large as that of bare frame, and the maximum load resistance of the infilled frames was about 1.5-2.3 times that of bare frame. Also, from the envelopes of the force-deformation hysteresis curves of the infilled frames, the post-yielding stiffness ratios are estimated around the range (-27,-3)%.

Gavrilovic and Sendova (1992) performed experimental tests on 1/2 scale

three-storey one-bay models using many types of infills (masonry, syporex, gypsum and eltozol). They pointed out that infill wall, depending on its characteristics, can considerably increase the initial stiffness and strength of the structure and plays important role in elastic, and particularly, post elastic range by limiting the lateral displacement. They also found that infill wall modifies the dynamic characteristics of the structure, its energy absorption capacity and failure mechanism. Besides, the study have shown wide range of infilled frame stiffness and strength ratios when different materials for infill wall element are used. The average stiffness and strength ratios fell in the range 5.0 and 2.2, respectively, and infill wall post-yielding stiffness ratio is roughly estimated around (-12,-6) % which is extracted from the idealized storey shear force-interstorey drift relationships.

Abrams (1992) noted that the behavior for loading in one direction of masonry walls did not appear to be influenced by previous damage in the other loading direction, concluding that the cyclic behavior of the walls can be fairly characterized by its behavior when subjected to monotonically increasing loads. However, Teran-Gilmore et al. (1995) reported experimental results performed by Klingner (1980) who found that after reaching a given resistance level in one direction, an infilled frame model was not able to develop more than this resistance in the other direction upon load reversal. The aforementioned results, which seems to contradict each other, reflects the state of current limited knowledge regarding the infill wall (as representative type of brittle element which is often mixed with frames) cyclic behavior , and thus, the need for more investigation for deeper clarification of the problem.

Recently, Negro and Verzeletti (1996) have performed a series of pseudo-dynamic tests on full-scale four story reinforced concrete building designed according to European codes 2 and 8. The tests were conducted on bare frame, uniformly infilled frame, and soft storey infilled frame. Infill walls are made of hollow brick masonry which is a typical one used in Europe. The results confirmed previous findings and assured that presence of a regular pattern of infill walls prevents energy dissipation from taking place in the frame to a large extent and the effect of the non-structural infill panels cannot be neglected in design. Their study found that Single Degree of Freedom (SDOF) input energy

was sufficient to highlight the differing global structural behavior for the different infill configuration. To account for infill wall distributions in the moment-resisting frames, the study stressed the need for exploring a method based on simple modification of the design forces according to the difference in the SDOF energy demand with respect to the bare frame.

Performance of infilled framed buildings under real earthquake ground motion is observed during 1985 Mexico earthquake. Several cases of adequate seismic performance, as well as failure and poor behavior were reported in a large number of modern-medium-rise framed buildings with unreinforced masonry infills. In general, it has been considered that the presence of unreinforced masonry infills was beneficial for majority of infilled framed buildings, and prevented the collapse of several buildings in the zone of highest seismic sensitivity. This usually was the case when unreinforced infills were placed symmetrically in plan and within all the stories of the building. Although some of these infills showed extensive shear cracking after earthquake, they resisted the majority of the lateral loads acting on the building, protecting the column from possible failure and helping dissipate earthquake input energy. However, infill walls contributed to poor seismic performance of framed building in some cases. Large percentage of these cases are attributed to irregular distribution of infill walls in plan and elevation of the building created in the original design or caused by failure of infills during earthquake, thus leading to torsional response and/or soft story condition normally not accounted for in the original seismic design (Wakabayashi and Martines 1988).

It can be viewed that experimental works on the behavior of infilled frame is more or less available to some extent. In general, the results indicated that infill walls affect behavior of the surrounding frame and should not be ignored in its design process. However, not much work has been reported on the analytical modeling of the hysteretic dynamic response of infilled frames, and as results, so little, if any, is materialized and put into the form of guidelines in seismic design codes. The problem which still remained unsolved is how you can account for the presence of brittle elements like infill walls in the seismic design of frames. The present study falls in this direction where presence of brittle element is accounted for by means of different energy and ductility

demands of the pure and mixed frames and steps are followed to evaluate the effect produced on reliability assessment of these two systems.

1.3 Study objectives

The main objectives of this study are:

- To investigate the nonlinear dynamic response of ductile frames when mixed with brittle elements and the effect of these secondary elements on the overall seismic performance of the frame elements.
- To provide useful closed form expressions capable of predicting the important response quantities of accumulated plastic energy and ductility factor of the frame with or without brittle failure-type elements and the fluctuations of these expressions about the average estimates.
- To assess the reliability of frames with or without brittle elements based on accumulated plastic dissipated energy and ductility factor demands using the developed expressions and direct probabilistic approach.

1.4 Study layout

The study is organized in six chapters. The first chapter provides an introduction to the subject under investigation. It starts with stating the problem to be addressed and the motivation behind that, then it gives brief review of the previous researches which are most relevant to this study. The objectives of this study are also highlighted in this chapter.

The second chapter deals with earthquake excitation. At first, it briefly describes the characteristics of the real input motions starting from the source, then it explains the simulated input motions which is generated to be used for nonlinear dynamic response analysis and how correspondence is made between the real and artificial input motions.

The third chapter describes the behavior of the brittle element under cyclic loading taking infill wall as a typical example and using available experimental data, then the main controlling parameters are selected for setting up an approximate analytical hysteretic model for the brittle element. It also gives the

range within which the input data parameters are selected including the level of the input motion intensity.

The fourth chapter constitutes the main chapter of this dissertation where the dynamic analysis is conducted on wide range of input data for the structural characteristics of the system and level input motion intensity. The results are discussed and statistically analyzed leading to the derivation of the closed form expressions for the main response quantities. Fitting agreement between the simulation data and prediction estimates are investigated. Also, confidence intervals for the response quantities are computed and discussed. The relations between response quantities are addressed and compared with other research results when available. Besides, response of mixed frame systems under typical real earthquake ground motions are performed having the real input motions processed earlier in the second chapter.

The fifth chapter extends the analysis to deal with reliability assessments of frames with or without brittle elements in terms of accumulated plastic energy and ductility factor demands. Discussion is made on how reliability curves can be utilized for reliability-based design.

The final chapter summarizes the studies that have been conducted and the main conclusions that have been drawn. Also, recommendations for future research are presented to help further understanding of the seismic behavior of the mixed frame systems and promotes introduction of guidelines into seismic design codes.

Chapter Two

EARTHQUAKE EXCITATION

2.1 *Introduction*
2.2 *Simulation of real earthquake ground motions*
2.3 *Artificial input motions*
2.4 *Correspondence between real and artificial input motions*

Chapter 2

EARTHQUAKE EXCITATION

2.1 Introduction

It is well known that the information that can be obtained from structural seismic response studies based on a single earthquake record only has limited application and do not serve the design purpose because of the statistical nature of the earthquakes. An earthquake that occurred in the past which has its own specific parameters of magnitude, focal depth, attenuation characteristics, frequency content and duration may never occurs again in the future. It would be desirable for design purpose to have large number of recorded-strong motion earthquake accelerograms for each class of earthquake parameters. However, there are limited records available for destructive strong ground motions to serve for statistical purpose. Therefore, the need has emerged for constructing an artificial motions that can be put in place of earthquake accelerograms to study the structural response.

As one aim of this thesis is to study the random seismic response of the considered mixed frame system or pure frame system, the earthquake as input motion can be represented as a limited duration segment of stationary random function having a prescribed acceleration power spectral density function $S(\omega)$. This useful and simple representation will allow the application of some important results of stationary probabilistic dynamic analysis. The following discussion will be concentrated on selection of $S(\omega)$ function upon which the generation of artificial input motions are based.

2.2 Simulation of real earthquake ground motions

The analysis of power spectral density functions of real earthquake strong motion accelerograms recorded at free fields shows that the spectral amplitude is never held constant with frequency even over a short-band. The reason for such oscillatory characteristic is generally attributed to three main effects: The source where the earthquake is initially erupted, propagation path through which the seismic waves travel long distance in a firm ground layers and the local site conditions where soft soil deposits turn to amplify the amplitude of the seismic waves in most cases (note Fig. 2.2.1).

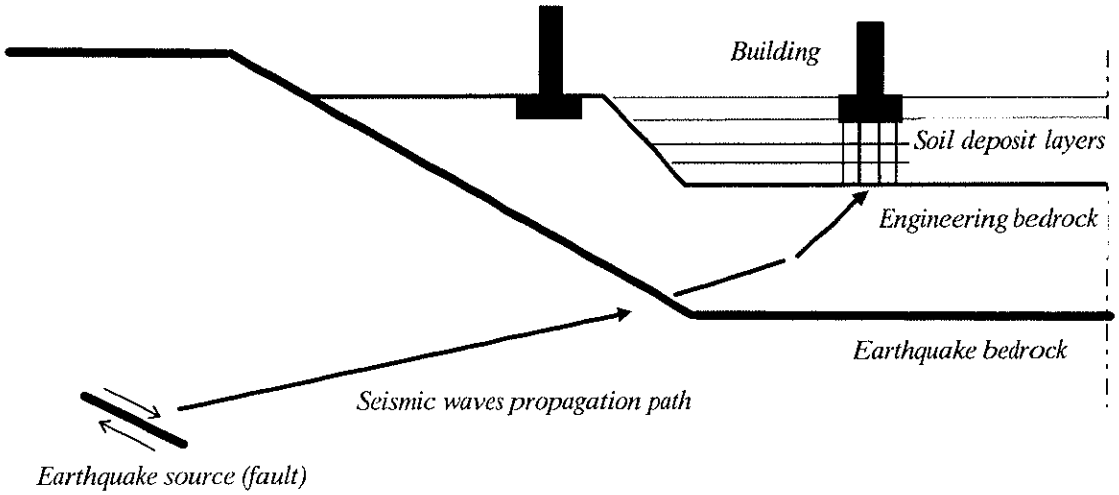

Fig.2.2.1 Concept of earthquake waves travel paths

Source effect is widely modeled by well-known ω^2 model which has its acceleration power spectrum close to white noise over long range of frequencies and has the characteristic of high pass-filter, meaning that the high frequencies pass through and low frequencies are stopped or eliminated. One of the models suggested for considering the source-site travel path (or propagation path) effect, is the Markov spectrum which has the characteristic of low-pass filter, where the low frequencies are passed and high stopped. Markov spectrum is often used for its simplicity (Myslimaj and Matsushima, 1998). The forms of ω^2 model and Markov model are given in Eqs. (2.2.1) and (2.2.2) respectively,

$$S(\omega) = S_0[\frac{(\omega/\omega_c)^2}{1+(\omega/\omega_c)^2}]^2 \qquad (2.2.1)$$

and

$$S(\omega) = S_0 \frac{1}{1 + (\omega / \omega_m)^2} \tag{2.2.2}$$

where ω_m and ω_c are two corner frequencies and S_0 represents the level of power spectral density. Besides, representative curves of those equations are drawn in Fig. 2.2.2 (dotted and broken lines, respectively) using logarithmic scale. The third effect; i.e., local site condition is widely modeled by Kanai-Tajimi ground acceleration model (Kanai, 1957; Tajimi, 1960) which attenuates the higher-frequency components and amplifies those frequency components close to predominant natural frequency of soil deposits at specific site. If the acceleration power spectrum for many sites having different soil conditions are computed, the average power spectrum is expected to be again close to constant value over wide range of frequencies. Kanai-Tajimi model is given by

$$S(\omega) = S_0 \{ \frac{1 + 4h_g^2(\omega / \omega_g)}{[1 - (\omega / \omega_g)^2]^2 + 4h_g^2(\omega / \omega_g)^2} \} \tag{2.2.3}$$

where h_g and ω_g stand for the soil damping ratio and natural frequency, respectively. Tajimi has suggested 15.6 rad/sec for ω_g and 0.6 for h_g as being representative of firm soil condition. Typical curve of Eq. (2.2.3) is shown in Fig. 2.2.2 (solid line).

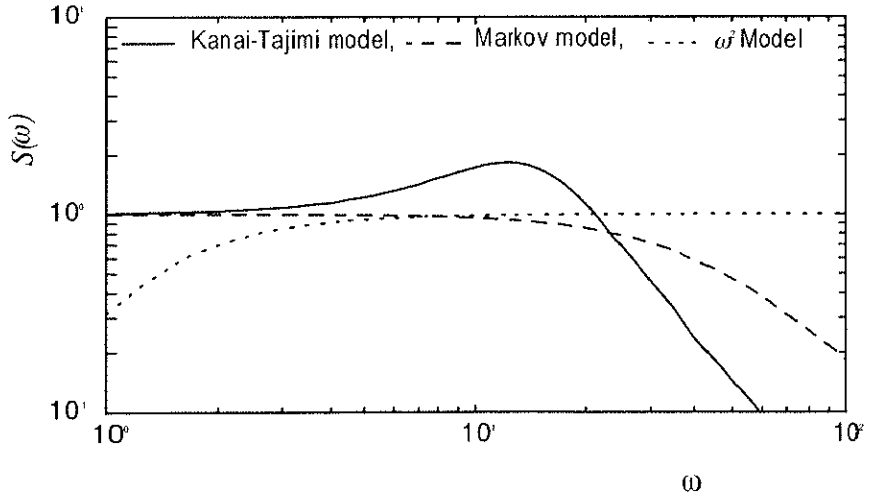

Fig. 2.2.2 Proposed typical models for earthquake power spectrum

Bycroft (1960) studied extreme values of response for a SDOF system using 20 separate accelerograms of stationary white noise with 25 seconds time duration each and having band limited constant power spectral density function. After proper scaling, Bycroft compared his results with Housner's design velocity spectra which is based on real input motions. Bycroft's results indicated that white noise could be a reasonable representation of real earthquake ground accelerations at a given intensity level.

Recently, Goto and Matsushima (1999) have found that the probability distribution of average power spectrum (PDAPS) of white noise accelerograms are close to the PDAPS taken for real earthquakes. Fig. 2.2.3 shows the PDAPS based on the real earthquakes drawn in bar lines where the records of the horizontal north-south components of El-Centro (Imperial Valley, California, 1940), Taft-Lincoln (Kern County, California, 1952), Hachinohe (Tokachi-oki, 1968), THO30-1FL (Miyagiken-oki, 1978) and Kushiro (Kushiro-oki, 1993) are used. Normalization of power spectra of real earthquakes are made according to Eqs (2.2.4) and (2.2.5), taking into account the different intensities of real earthquakes and making the process comparable with white noise power spectra,

$$S''(\omega) = S(\omega) / \int S(\omega) d\omega \tag{2.2.4}$$

and

$$S'(\omega) = S''(\omega) / E[S''(\omega)] \tag{2.2.5}$$

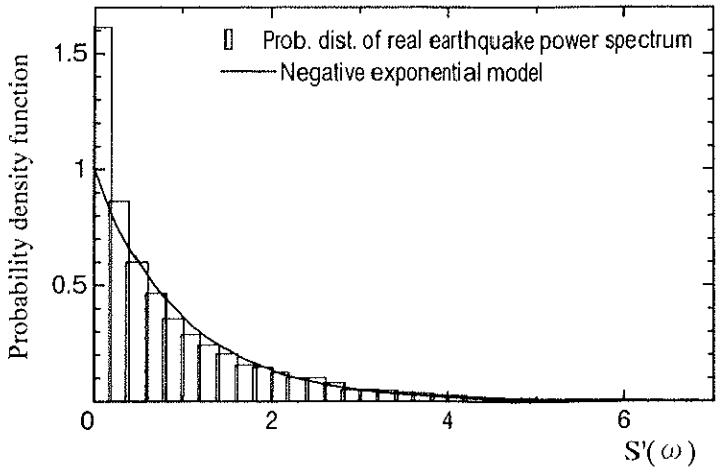

Fig.2.2.3 Probability density function from real earthquakes

The simulated data in Fig. 2.2.3 has negative exponential distribution model which is, in principle, a member of chi-square probability density curves given by Eq. (2.2.6).

$$f_c(y) = \frac{1}{2^{\nu/2}\Gamma(\nu/2)} y^{\nu/2-1} e^{-y/2} \qquad (2.2.6)$$

in which ν is a positive integer standing for degrees of freedom and with ν=2, PSAPS of real earthquake is chi-square distributed. On the other hand, PSAPS of white noises is shown in Fig.2.2.4 (bar lines), where one hundred white noise samples are used to compute the simulated distribution. Chi-square distribution with ν=2 is plotted in Fig 2.2.4 where good agreement with simulation data is observed. The above findings support the view that earthquake ground motions, on average, could be modeled as white noise accelerograms.

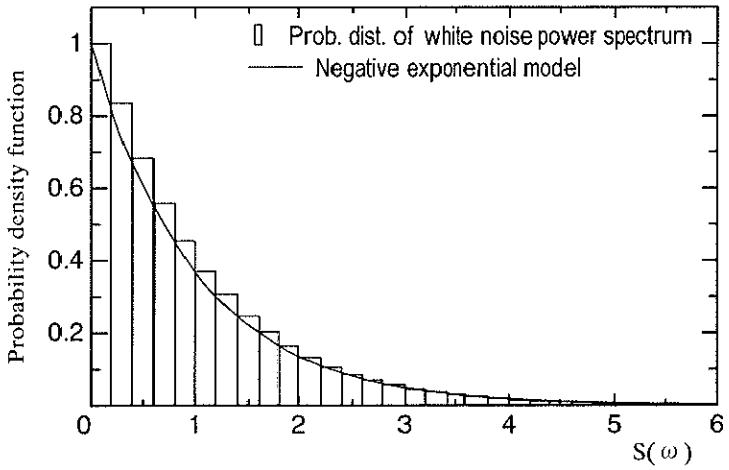

Fig. 2.2.4 Probability density function from white noises

Judging from the purpose of this study and from the above conclusions, the earthquake ground motions are roughly modeled here as stationary band-limited and statistically independent white noise accelerograms with limited period of time.

2.3 Artificial input motions

Based on the above discussions, that real earthquake ground motions could

roughly be approximated in its steady state as white noise motions for which $S(\omega)$ is theoretically constant for all frequency range. However, in practice, the simplest real form of $S(\omega)$ is that corresponding to band-limited white noise, for which the power spectral density function is constant in the circular frequency range $|\omega| < \omega_1$ and zero elsewhere as expressed in Eq. (2.3.1) and shown in Fig. 2.3.1 where $S(\omega)$ is always two-sided symmetric function about the vertical axis.

$$S(\omega) = \begin{cases} S_0 & |\omega| \le \omega_1 \\ 0 & |\omega| > \omega_1 \end{cases} \tag{2.3.1}$$

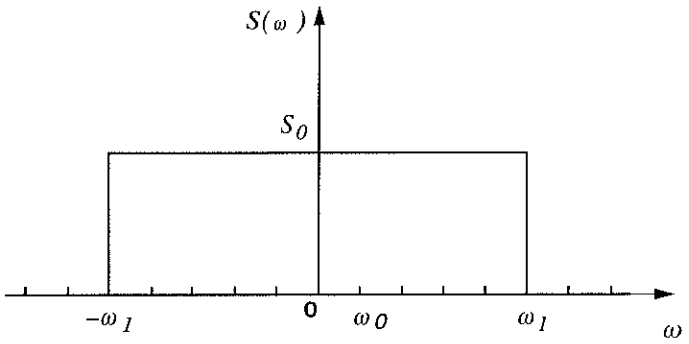

Fig. 2.3.1 Assumed power spectrum

The method used by the computer program for artificial motion generation is based on the fact that any periodic function can be expanded into series of sinusoidal waves as:

$$\ddot{x}(t) = \sum_n A_n \sin(\omega_n t + \phi_n) \tag{2.3.2}$$

where A_n is the amplitude and ϕ_n is the random phase angle of the n contributing sinusoid. The amplitude A_n is related to the two-sided spectral density function $S(\omega)$ by the relation $A_n^2/2 = 2S(\omega_n)\Delta\omega$ where the total power can be written as,

$$\sum_n \frac{A_n^2}{2} = 2\sum S(\omega_n)\Delta\omega \cong 2\int_0^\infty S(\omega)d\omega \tag{2.3.3}$$

and according to the previous assumption of constant power spectrum, all amplitudes have the same value given by $A_n = \sqrt{2S_0\Delta\omega}$. The series of different phase angles ϕ_n are given by random number generation subroutine which produces series of phase angles with uniform probability distribution in the range between 0 and 2π. The mean square value of the generated motions is computed as:

$$E(\ddot{x}^2) = 2S_0\omega_1 \tag{2.3.4}$$

and as the motions have zero mean, this gives

$$\sigma_{\ddot{x}} = \sqrt{E(\ddot{x}^2)} \tag{2.3.5}$$

where $\sigma_{\ddot{x}}$ is the standard deviation of the resulted motions. In this study, a set of one-hundred statistically independent stationary band-limited white noise samples used as acceleration time histories are generated and used for response analysis. The samples will have similar general appearance but different details. It is assumed that frequency band limit falls in the range $[-5, 5]\omega_0$, where ω_0 is the natural vibration circular frequency of the bare frame system. The selected frequency band width is believed to be reasonable from practical view point. Samples of the generated white noise and their corresponding power spectra are shown in Figs. 2.3.2(a) and 2.3.2(b), respectively, where τ and f_0 are equal respectively to t/T_0 and $\omega_0/2\pi$. T_0 is the natural vibration period of pure frame system, which equals $1/f_0$.

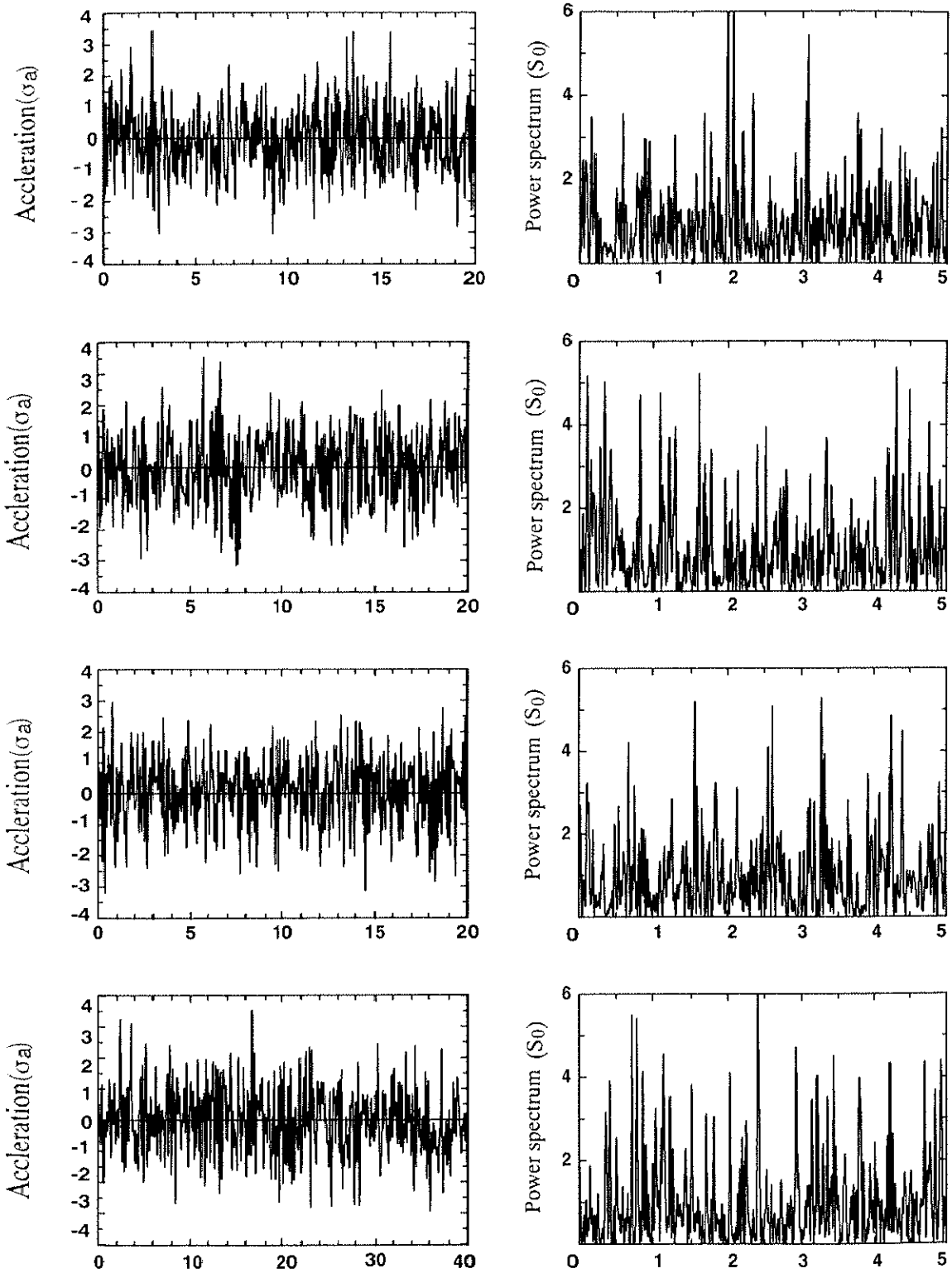

Fig. 2.3.2 (a) Samples of white noise; (b) corresponding power spectra

2.4 Correspondence between real and artificial input motions

In order that inelastic response analysis under real strong motions be performed, the selected real earthquake accelerograms are processed in a way that simulates stationary white noise motions. The horizontal north-south components of El-Centro (1940), Taft-Lincoln (1952), Hachinohe (1968), Miyagiken-oki (1978) and Kobe (Kobe Marine Observatory, 1995) are utilized as typical real input motions. Real earthquake input motion consists of transient or buildup part, relatively stationary part which contains most of the input motion intensity and decaying part. Approximate correspondence between stationary white noise accelerograms and real earthquake input motion is made possible through selecting the likely stationary part of each real input motion which is considered as sequence of shot noises. The constant power spectral density function S_0 for the shot noises train is calculated by

$$S_0 = \frac{\zeta E(A^2)}{2\pi} \qquad (2.4.1); \qquad \zeta = \frac{N_s}{t_d} \qquad (2.4.2)$$

where ζ denotes the average number of impulses per unit time, $E(A^2)$ stands for the average square areas of impulses assuming that $E(A) \approx 0$, and N_s is the total number of impulses during the selected period t_d. Table 2.4.1 gives the above coefficients which led to the calculation of S_0. Figs. 2.4.1 through 2.4.5 show the steps done for each real earthquake input motion, starting from the full acceleration time history where the stationary-like part of the accelerogram is picked up, then, the impulse train is setup for computing the power spectral density using Eqs. (2.4.1) and (2.4.2) after confirming that $E(A) \approx 0$.

Table 2.4.1 Earthquakes data

Parameters / Earthquake	time range(sec)	t_d (sec)	N_s	$E(A^2)$ (cm^2/sec^2)	$E(A) \approx 0$ (cm/sec)	S_0 (cm^2/sec^3)
El Centro-Ns	1.30-12.3	11.0	90	174	-0.17	226
Taft-Ns	2.76-14.6	11.8	93	45.4	-0.09	56.9
Hachinohe-Ns	1.41-22.4	21.0	105	126	0.25	101
Miyagiken-oki(Ns)	1.00-11.0	10.0	77	139.4	0.01	171
Kobe-Ns	4.20-12.58	8.38	41	2685	-0.04	2092

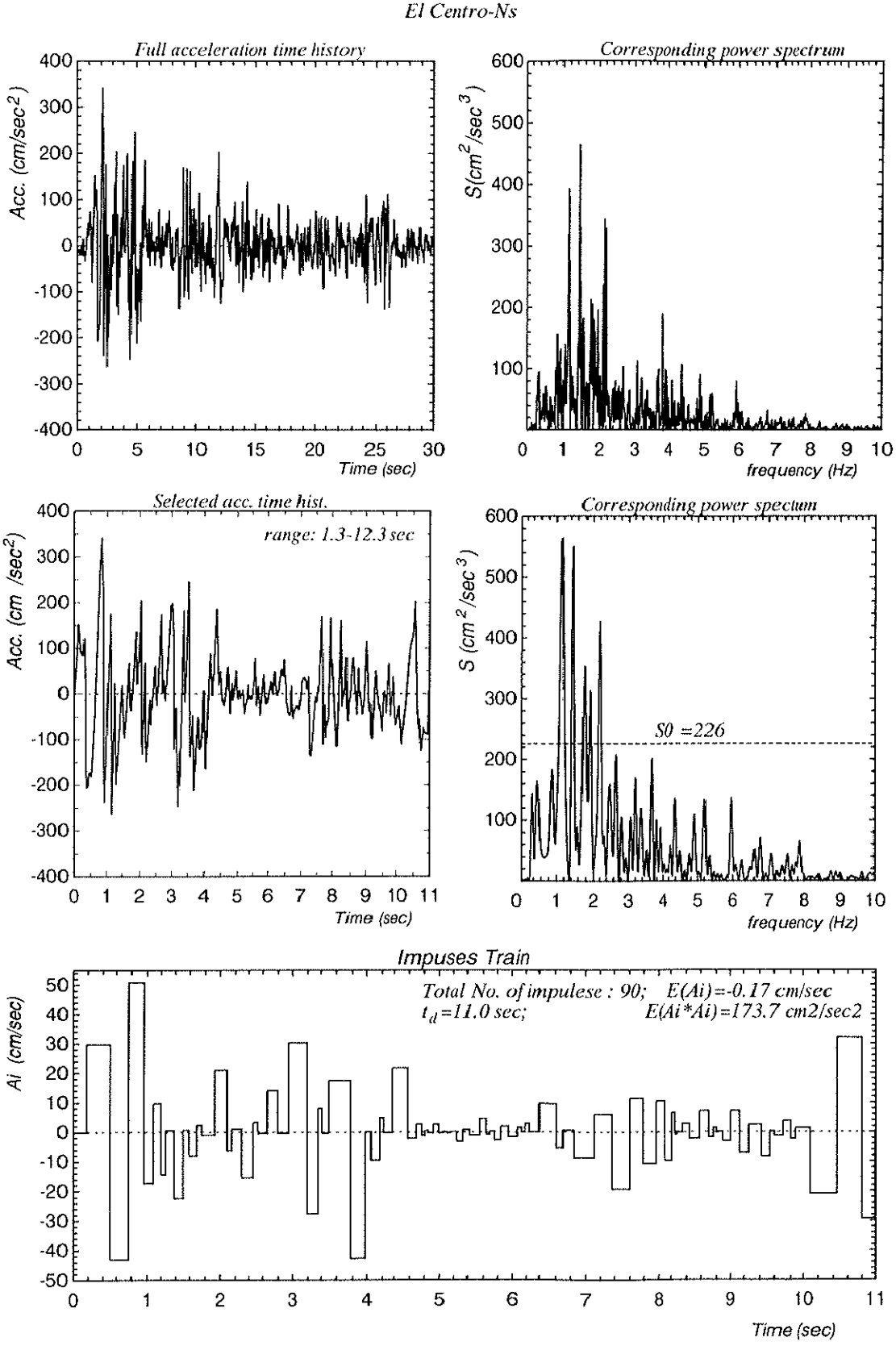

Fig. 2.4.1 El Centro data processing

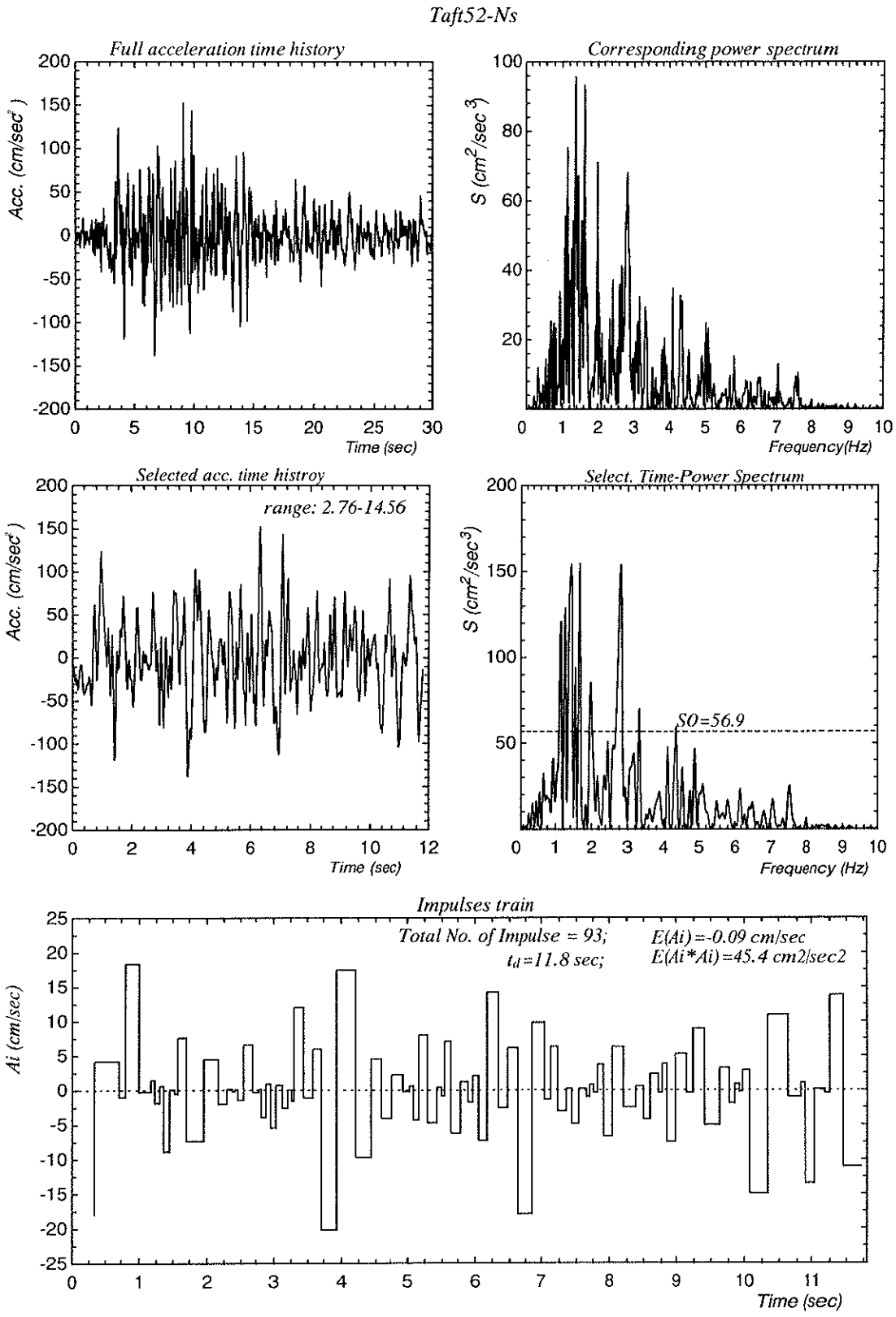

Fig. 2.4.2 Taft data processing

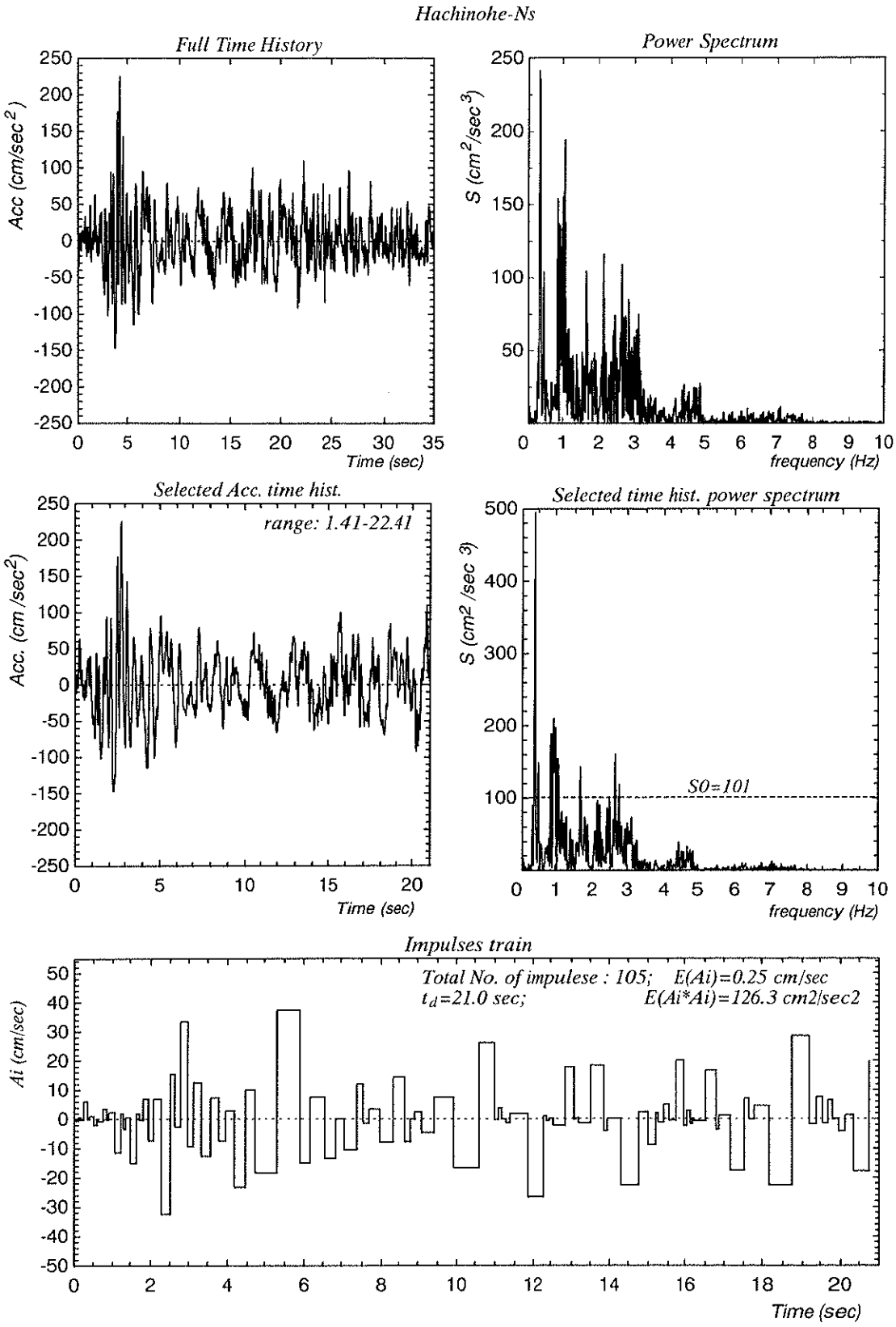

Fig. 2.4.3 Hachinohe data processing

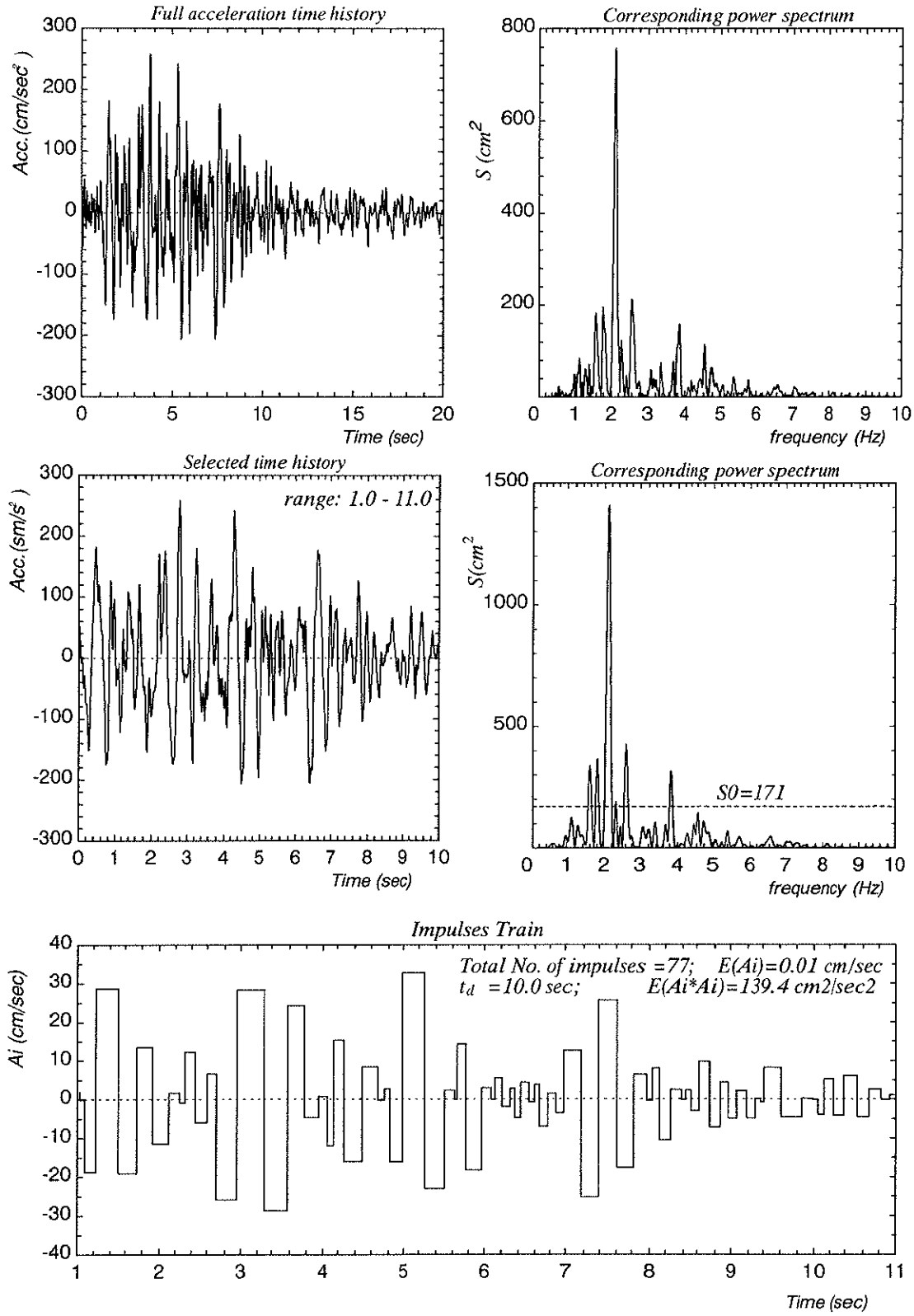

Fig. 2.4.4 Miyagiken-oki data processing

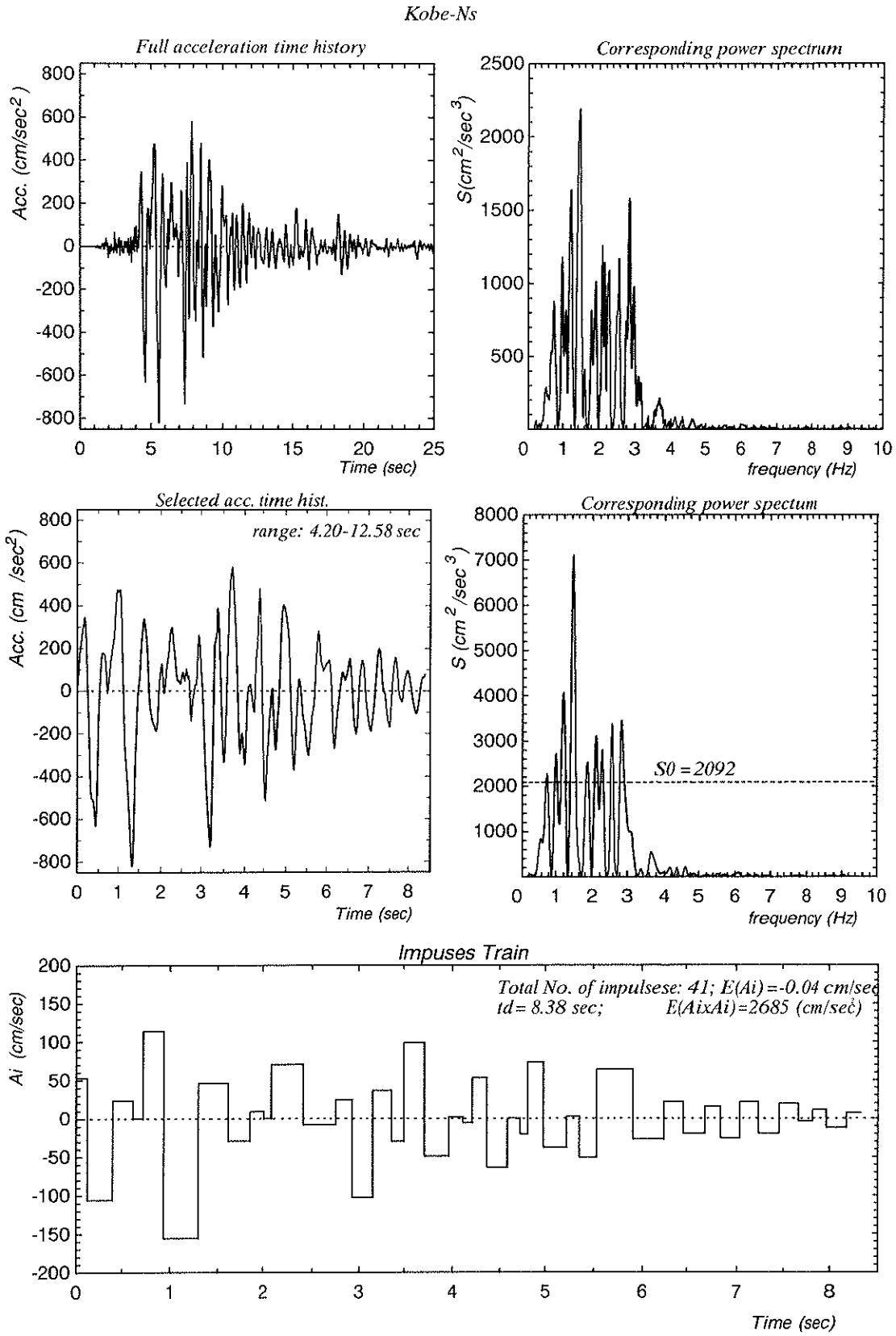

Fig. 2.4.5 Kobe data processing

Chapter Three

ADOPTED HYSTERETIC MODELS (Structural Models)

3.1 Introduction

3.2 Ductile frame and brittle element hysteretic models

3.3 Input motion and system input data

3.4 *Equilibrium equation of motion*

3.5 *Response under individual white noise samples*

Chapter 3

ADOPTED HYSTERETIC MODELS

3.1 Introduction

Many available experimental data reported on the behavior of ductile frames mixed with brittle elements, in particular, frames with infill walls show that the brittle elements reduce the plastic energy and ductility demands on the main lateral load carrying frame system. Experimental data also show a wide range of scatter as how much these secondary elements are contributing to the stiffness, strength and energy dissipation capacity of the whole mixed system in different loading stages and conditions. This range of scatter could be attributed to many factors, of which are the different geometrical and mechanical characteristics of these elements and their constitutive materials (masonry units and mortar with/without grout in case of infill wall brittle element), besides, structural properties of the frame itself. Generally, available experimental data show that lateral stiffness of mixed system fall in the range between 5-20 times that of the bare frames and the corresponding yield shear strength ratio is in the range between 1.4-2.5 times. Also, mixed system post-yielding stiffness falls in the range -27 up to -3 % of its initial stiffness.

In general, idealized load-deformation relationships of brittle element, bare frame, and the whole mixed system could be roughly summarized in Fig. 3.1.1. The figure indicates that as soon as the secondary element reach its yield strength, its stiffness and strength are rapidly dropped. This drop is externally caused by excessive cracks and crushes reflecting the brittle behavior of the secondary element under increased deformation demand. A simplified hysteretic model for the cyclic nonlinear behavior of the secondary element is

introduced in this chapter with its parameters definition based on the total structural characteristic of the mixed system, while bilinear model is adopted for capturing the hysteretic behavior of the frame. The cyclic behavior of the mixed system is defined as a combination of both primary and secondary elements.

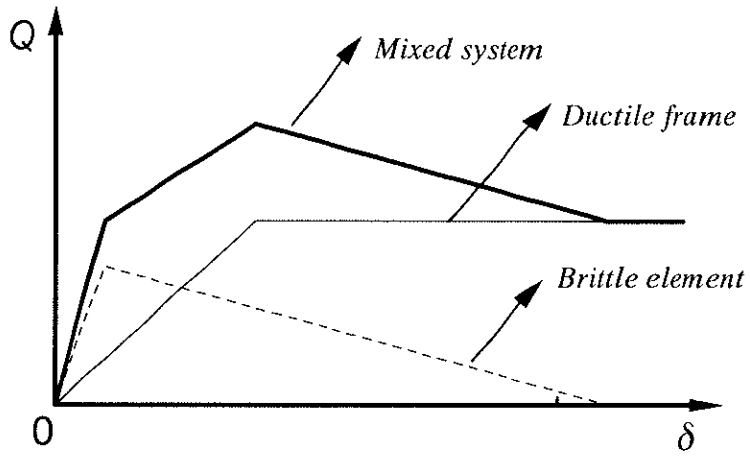

Fig. 3.1.1 Idealized load-deformation relationship of the mixed system

3.2 Ductile frame and brittle element hysteretic models

Based on previous investigation, a simplified multi-linear hysteretic model shown in Fig. 3.2.1(a) is proposed for modeling restoring force in the brittle element (Al-Sadeq and Matsushima, 1998). The model conservatively assumes sudden drop at ultimate strength and accounts for the brittle character of the element through considering negative post-yielding stiffness characteristic. The stiffness degradation is assumed proportional to strength reduction leading to a gradual failure of the brittle element after which the mixed system of frame and brittle element behaves like bare frame.

The controlling parameters are, initial stiffness (K_{w0}), yield strength (Q_{wy}) and post-yielding negative slope of the envelope curve (βK_{w0}), where β is the ratio between the brittle element post-yielding stiffness to its initial stiffness. A bilinear elasto-plastic model with zero plastic stiffness shown in Fig. 3.2.1(b) is used for modeling restoring shear force in ductile frame element which has

initial stiffness (K_{f0}) and yield strength (Q_{fy}) as controlling parameters. Frame parameters are assumed not to be affected by brittle element existence. Mixed system initial stiffness (K_{fw0}) and yielding strength (Q_{fwy}) are taken as multiples R_k and R_q of the bare frame initial stiffness (K_{f0}) and yield strength (Q_{fy}), respectively as given in relations (3.2.1) and (3.2.2),

$$R_k = K_{fw0} / K_{f0} \qquad (3.2.1); \qquad R_q = Q_{fwy} / Q_{fy} \qquad (3.2.2)$$

where it is assumed that K_{fw0} and Q_{fwy} can be given in relations (3.2.3) and (3.2.4), respectively.

$$K_{fw0} = K_{f0} + K_{w0} \qquad (3.2.3); \qquad Q_{fwy} = Q_{fy} + Q_{wy} \qquad (3.2.4)$$

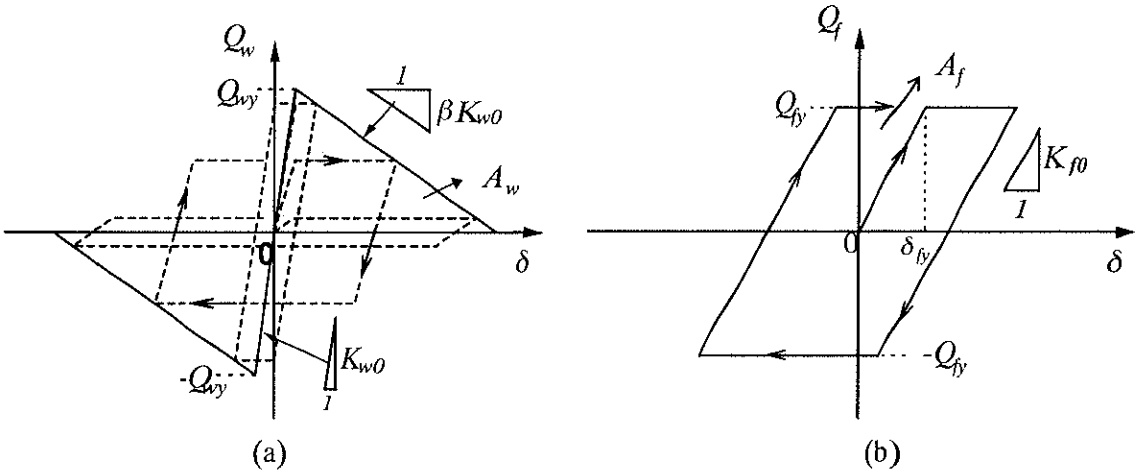

Fig. 3.2.1 Adopted hysteretic models for; (a) brittle element; (b) ductile frame

The proposed brittle element model is incorporated into a more general nonlinear dynamic analysis program DRAIN2D+ (Tsai and Li, 1994) for which, the brittle element is decomposed into series of parallel sub-elements, each of which is assumed to have shear type load-deformation relationship. As shown in Fig. 3.2.2, stiffness and strength of the brittle element are equally divided among the sub-elements and given gradually increased ductility in comply with the slope of the post-yielding envelope curve of the hysteretic model. A single sub-element will be failed once the given ductility is reached and the resisting force which was holding will be transmitted to the existing frame element.

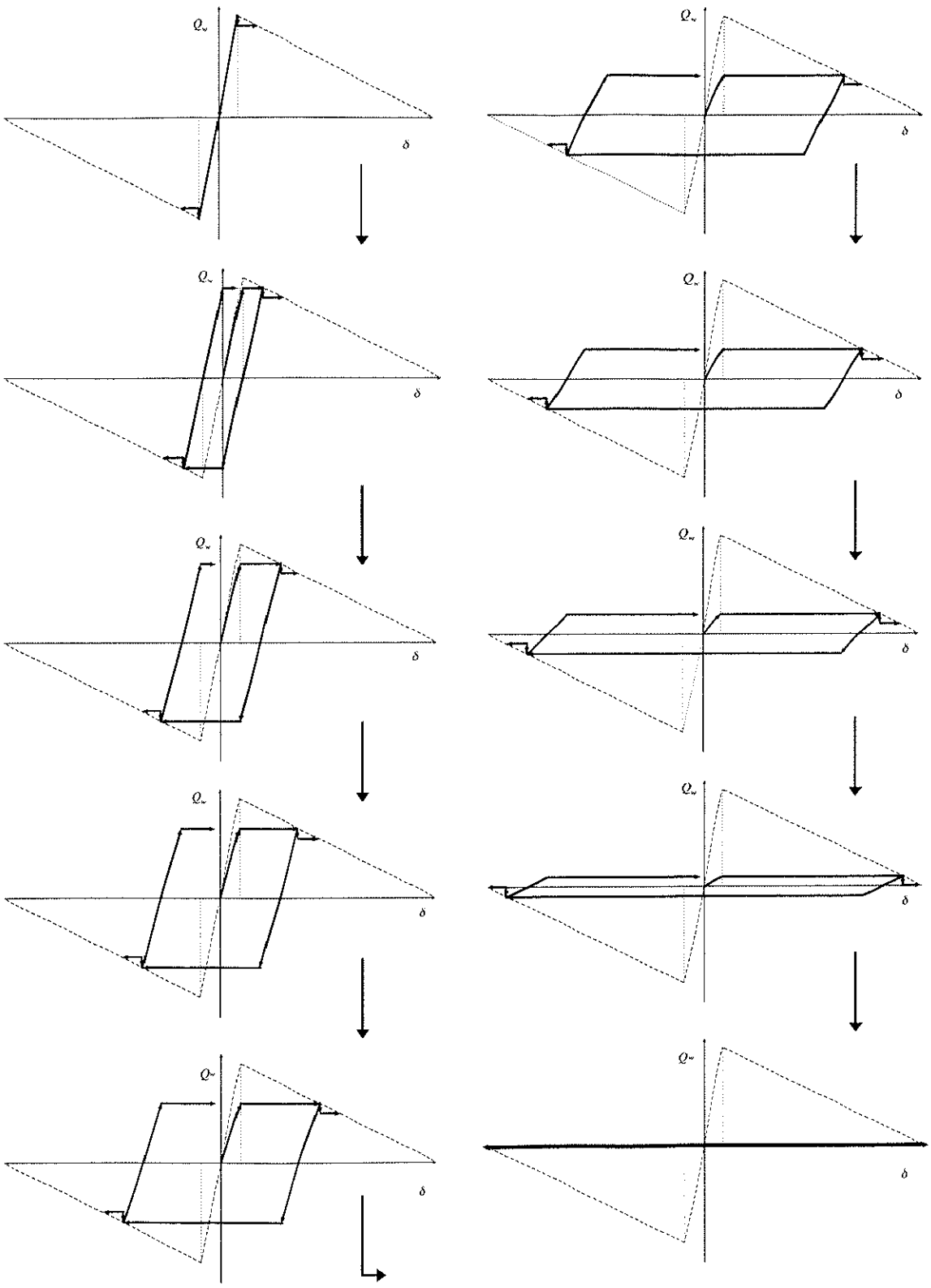

Fig 3.2.2 Failure scenario of the brittle element restoring force

3.3 Input motion and system input data

A flat power spectral density function is assumed for generating one hundred statistically independent white noise acceleration time histories used as input motions. Response analysis is performed for four levels of ξ which denotes the ratio of the input motion intensity to bare frame strength. ξ is defined as:

$$\xi = \frac{\omega_0 S_0}{\alpha^2} \qquad (3.3.1)$$

in which, α denotes the frame yield acceleration given by $\alpha = Q_{fy}/m$, ω_0 is the bare frame initial circular frequency given by $\omega_0 = 2\pi/T_0$ where T_0 is its initial natural period of vibration, and S_0 is the constant power spectral density of the excitation. The typical chosen gradually increased values for ξ are 0.0125, 0.025, 0.0375 and 0.05. Mixed system stiffness ratio R_k is taken as 1, 6, 8, 10, 12 and 14 and for the corresponding yield shear strength ratio R_q, the values of 1.0, 1.4, 1.5, 1.6, 1.7, 1.8, 1.9 and 2.0 are considered. The value of unity in R_q or R_k corresponds to pure frame condition which is viewed here as a special case of mixed frame system. The post-yielding stiffness ratios of the brittle element model β are taken as -0.2, -0.1 and -0.05 . In this study, the considered values for R_q, R_k and β parameters are concluded from investigating the available experimental data and considered to cover wide range of the mixed frame-brittle element structural characteristics. Any combination of R_k, R_q, β, and ξ values corresponds to one case of analysis. The adopted ranges of R_q, R_k, ξ and β totally form 424 analytical cases.

3. 4 Equilibrium equation of motion

The mixed frame-brittle element system is idealized by undamped mass-spring system having single-degree-of-freedom. The system has restoring force equal to the sum of two hysteretic loops which are the brittle element hysteresis proposed in this study and shown in Fig. 3.2.1(a) and the frame hysteresis shown in Fig. 3.2.1(b). The equation of motion is given by

$$\ddot{x}(t) + \frac{Q_{fw}(t)}{m} = -\ddot{x}_g(t) \tag{3.4.1}$$

where $x(t)$ is the system relative displacement with respect to its base and dots denote the second derivative with respect to time. $Q_{fw}(t)$ represents the restoring force of the mixed system which has oscillating reactive mass m, and $\ddot{x}_g(t)$ is the stationary white noise taken as horizontal ground acceleration for exciting a system initially rested on the ground as shown in Fig. 3.4.1. The equation of motion is solved using step-by step integration procedure based on constant acceleration Newmark method adopted in program DRAIN2D+.

The attention is focused on two important response quantities, i.e., average accumulated plastic energy dissipated by the frame $\overline{E}_p$ which has its normalized form $\overline{\lambda}$ given by $\overline{\lambda} = \overline{E}_p / Q_{fy}\delta_{fy}$ and average ductility factor $\overline{\mu}$ defined here as the average maximum absolute displacement divided by yield displacement of the frame. Standard deviations for λ denoted by σ_λ and for μ denoted by σ_μ are computed as well.

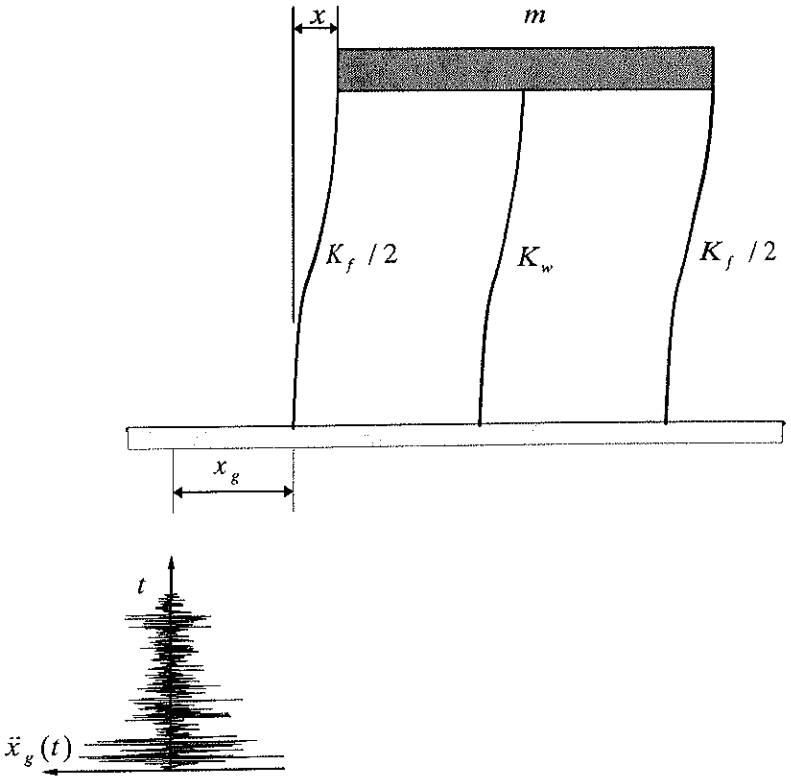

Fig. 3.4.1 Idealized SDOF system subjected to horizontal ground motion

3.5 Response under individual white noise samples

Response analysis under some white noise samples is performed having the hysteretic models for frame and brittle element already defined and acceleration input motions explained and prepared before. The purpose of this section is to show how the mixed system components, i.e., ductile frame and brittle element are working and the contribution made by each of them to the overall system response. Accumulated plastic energy time history, displacement time history and shear force-displacement relationship for the assumed ductile frame, brittle element and whole mixed system are presented for illustration. System and input motion data are taken as $R_q = 1.8$, $R_k = 8$, $\tau = 0 - 40$, and $\xi = 0.025$. Fig. 3.5.1(a) shows the time history of the accumulated plastic energy dissipated by frame element in case of brittle element existence (dashed line) and nonexistence (solid line). The figure also shows that the frame element in mixed system stays in elastic state longer time compared with pure frame system, but as soon as the brittle element energy dissipation capacity is exploited, the main structural frame takes the whole seismic response. Fig. 3.5.1(b) shows the displacement time history for the frame with/without brittle element, where it indicates that brittle element contributes to controlling displacement of the frame and may prevent excessive deformation demand that frame may not be designed for.

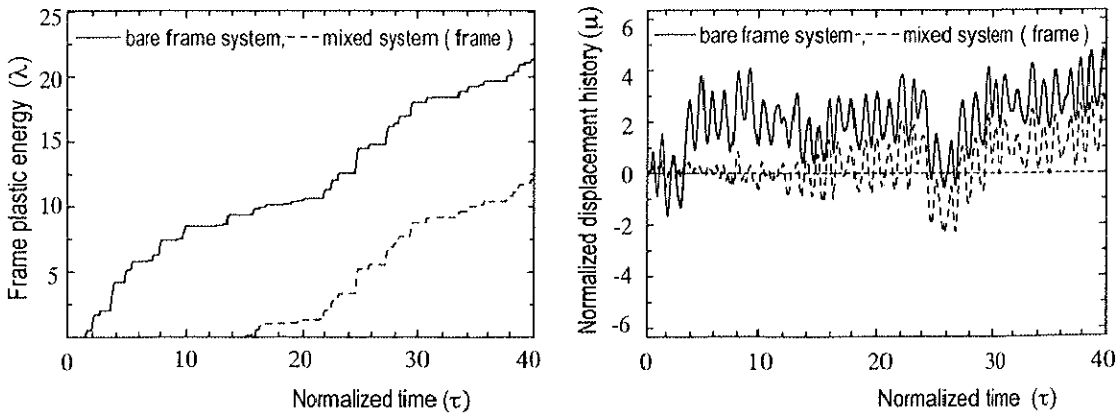

Fig. 3.5.1 (a) Plastic energy time history; (b) displacement time history

Shown in Fig. 3.5.2(a) is shear force-displacement relationship for frame without secondary element whereas Fig. 3.5.2(b) shows the same relationship in case of mixed system. Fig. 3.5.2(c) shows the force-displacement relationship for the assumed brittle element where its gradual failure mechanism can be observed. Fig. 3.5.2(d) shows the storey shear force-displacement relationship where it can be seen the contribution made by the brittle element and the mixed ductile frame-brittle element system attenuates rapidly to stable frame system.

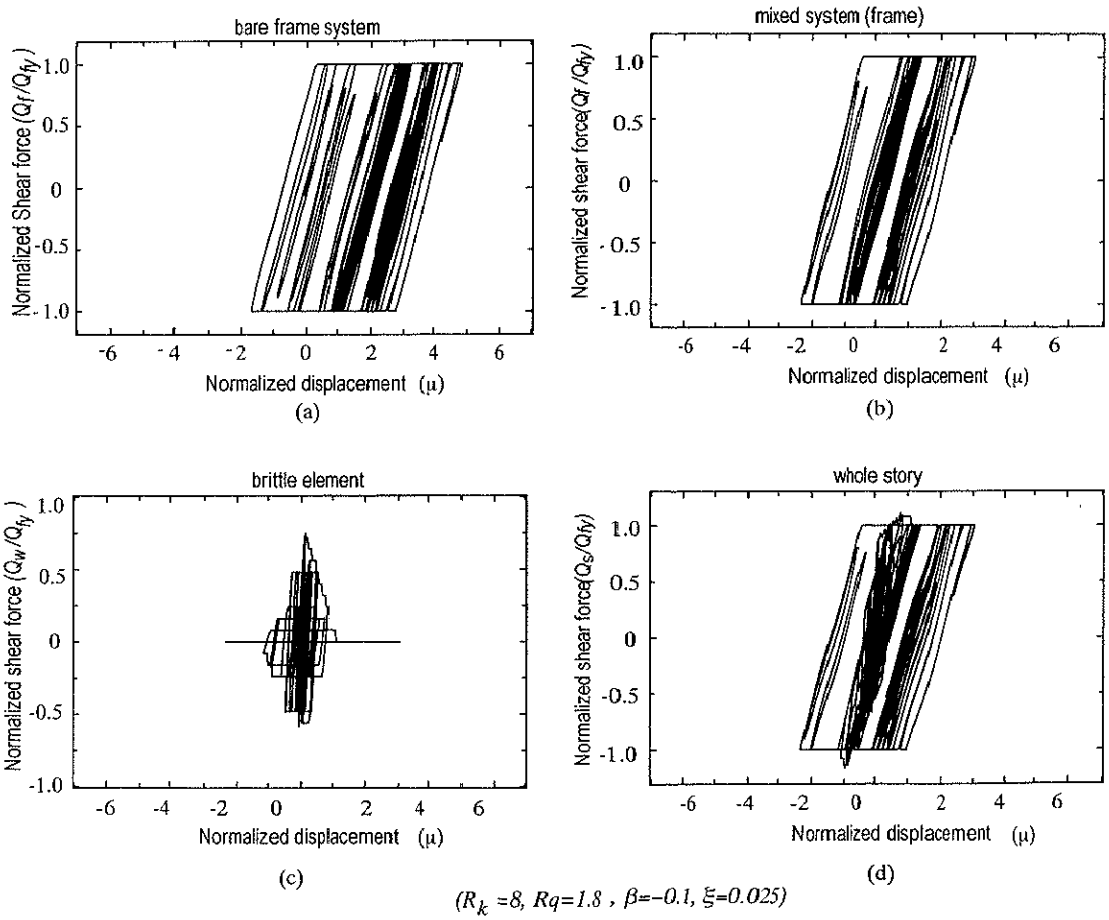

Fig. 3.5.2 Shear force-displacement relationship for: (a) empty frame system; (b) frame in mixed system; (c) brittle element; (d) whole storey

Another curves showing the response in terms of accumulated plastic energy and displacement time histories under another sample white noise input motion is shown in Figs. 3.5.3(a) and 3.5.3(b), respectively. The system parameters have $R_q = 1.8$, $R_K = 6$, $\tau = 0 - 40$, and input motion intensity is taken

as $\xi = 0.05$. Displacement time history indicates that not only the maximum displacement of the mixed system is less than its counterpart in case of frame system, but also a complete change of the system hysteretic behavior about the balanced position is made and its ability to return to the balanced state turns out better.

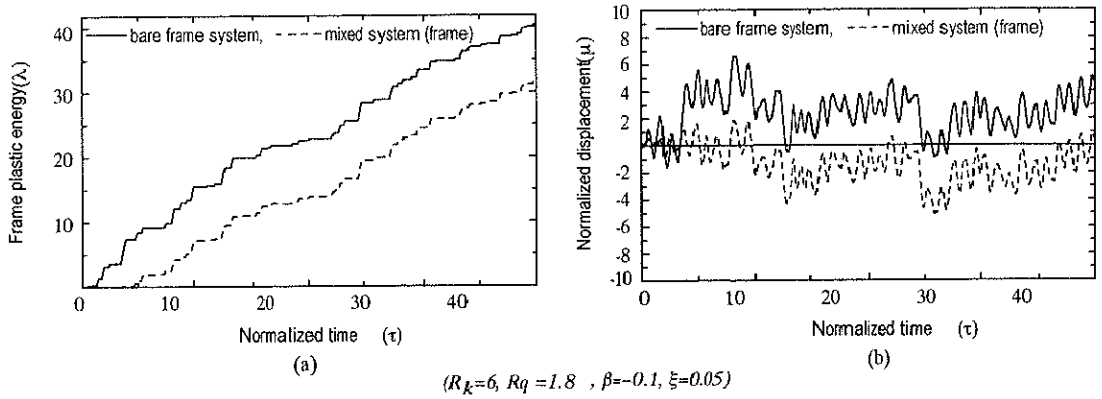

Fig. 3.5.3 (a) Plastic energy time history; (b) displacement time history

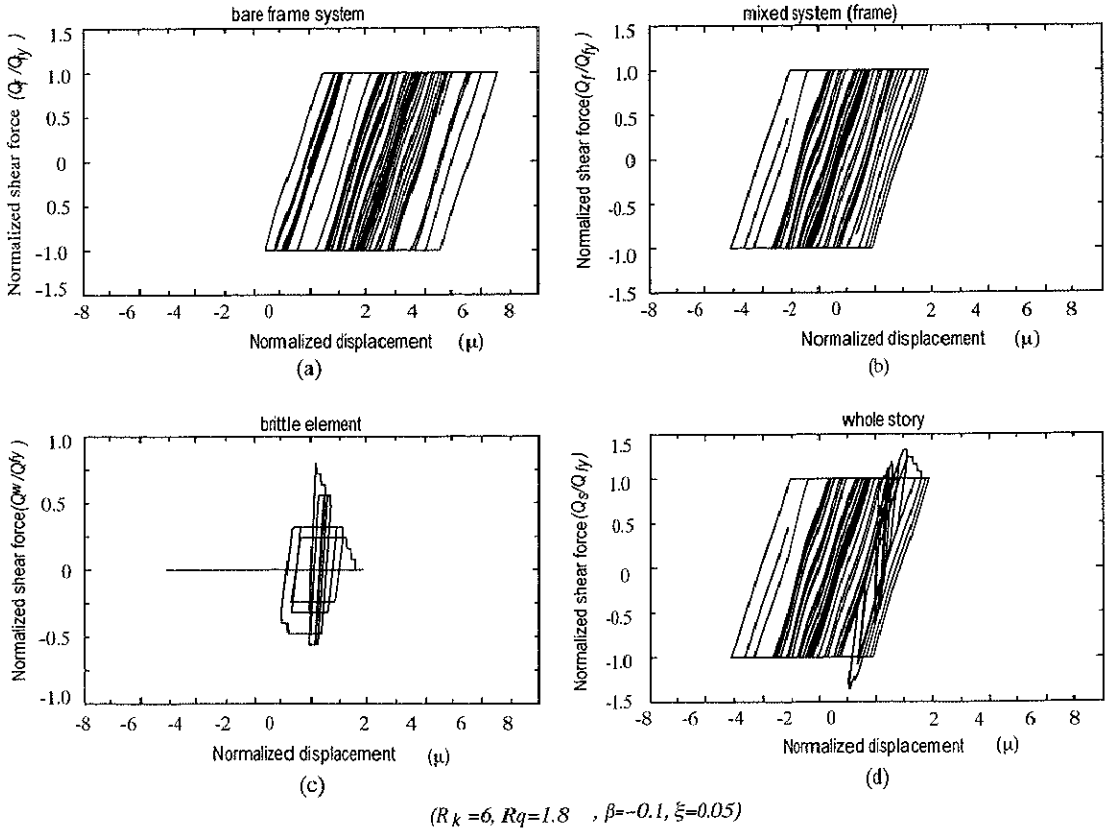

Fig. 3.5.4 Shear force-displacement relationship for: (a) bare frame system; (b) frame in mixed system; (c) brittle element; (d) whole storey

Chapter Four

INELASTIC DYNAMIC RESPONSE PREDICTION

4.1 Introduction
4.2 Energy balance equation
4.3 Simulation and prediction of average plastic energy
4.4 Simulation and prediction of average ductility factor
4.5 Simulation and prediction of plastic energy standard deviation
4.6 Simulation and prediction of ductility factor standard deviation
4.7 Verification for other post-yielding stiffness ratio
4.8 Expressions summary and general formula setup
4.9 Fitting agreement
4.10 Relationship between response quantities
4.11 General curves capturing the effect of brittle element on seismic response of mixed systems
4.12 Response under real earthquakes

Chapter 4

INELASTIC DYNAMIC RESPONSE PREDICTION

4.1 Introduction

Traditionally, earthquake-resistant design of buildings is based on strength and ductility concepts, but energy-based design approach has been gaining high reputation since its early introduction by Housner (1956). However, combining both accumulated plastic energy and ductility factor required by earthquake shaking may give reliable indices for design purpose, in addition to the conventional strength demand. As far as a system of ductile frame mixed with brittle element dealt with in this study is concerned, the brittle element due to its higher stiffness and lower strength starts to dissipate energy in early stage while frame elements are still in elastic response state. But, as the input motions are progressing forward and the fact that the brittle element has limited energy dissipation capacity, its complete failure is expected and the original frame alone is left to withstands the excitation by means of its own energy dissipation and deformability capacities. The accumulated plastic energy and ductility factor experienced by frame element are focused on.

Having input motions, system data, and hysteretic models for the frame and brittle element set in previous chapters, response analysis is performed in this chapter. The resulted simulation data for the average and standard deviation of accumulated plastic energy and ductility factor of the frame are analyzed. The relevant parameters deemed to influence the response are traced out utilizing statistical methods. Accordingly, closed form expressions are developed for predicting average and standard deviation of the response quantities. Besides, fitting agreements are investigated and the confidence intervals related to the

sufficiency of sample size are discussed. Having established the formulations, relationships between the response quantities are established and compared with corresponding previous research when available. For reference, corresponding response under real earthquakes is conducted having the real earthquake data being processed earlier in the second chapter.

4.2 Energy balance equation

The equilibrium equation of motion of a mass-spring oscillatory system having single-degree-of-freedom (SDOF) and subjected to horizontal excitation force $F(t)$, is generally given by

$$m\ddot{x}(t) + c\dot{x}(t) + Q(t) = F(t) \tag{4.2.1}$$

where $x(t)$ is the system relative displacement with respect to its base, $\dot{x}(t)$ and $\ddot{x}(t)$ denote the first and second derivatives with respect to time, respectively (otherwise denoted herein as x, $\dot{x}$, $\ddot{x}$). c is the damping coefficient, m is the reactive mass and $Q(t)$ is the system restoring force. If Eq. (4.2.1) is integrated with respect to $x(t)$ from the time that $F(t)$ starts, gives

$$\int m\ddot{x}dx + \int c\dot{x}dx + \int Q dx = \int F(t)dx \tag{4.2.2}$$

The first term on the left-hand-side of Eq. (4.2.2) is the recoverable kinetic energy which can be written as

$$\int m\ddot{x}dx = m\int \frac{d\dot{x}}{dt}dx = m\int \dot{x}d\dot{x} = \frac{m\dot{x}^2}{2} \tag{4.2.3}$$

The second term on the left-hand-side of Eq. (4.2.2.) is the irrecoverable viscous damping energy which is also non-negative as

$$\int c\dot{x}dx = \int c\dot{x}(\dot{x}dt) = \int c\dot{x}^2 dt \tag{4.2.4}$$

The third term on the left-hand-side in Eq. (4.2.2) is the absorbed energy which

is composed of recoverable elastic strain energy and irrecoverable plastic hysteretic energy,

$$\int Q dx = E_s + E_p \tag{4.2.5}$$

where the elastic strain energy for a linear elastic system can be defined as $E_s = Qx/2$ where x is the system displacement. The plastic dissipated energy E_p, in case of bilinear restoring force system, equals the sum of accumulated positive and negative plastic deformations multiplied by yield strength as shown in Fig. 4.2.1.

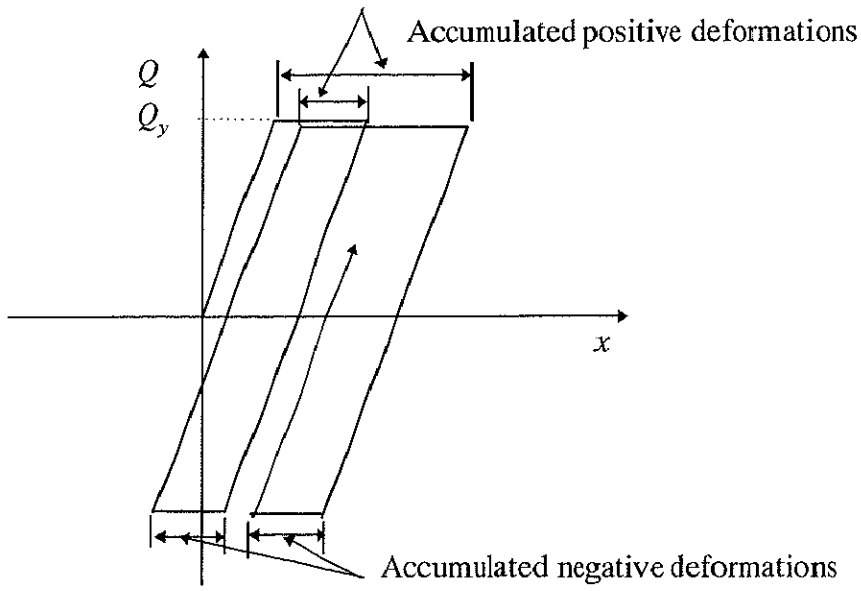

Fig. 4.2.1 Accumulated plastic deformations

The right-hand-side term in Eq. (4.2.2) is by definition the input energy E_i defined as

$$E_i = \int F(t) dx \tag{4.2.6}$$

Assume that F (t) is a white noise exciting force composed of a string of equally positive and negative impulses of magnitude A_i, their arrival time have Poisson distribution, average number of impulses per unit time is ζ, and a constant power spectral density S_0 defined by

$$S_0 = \frac{\zeta E(A_i^2)}{2\pi} \tag{4.2.7}$$

where the impulses have zero average $E(A_i) \cong 0$. If a change in the kinetic energy of the mass as defined in Eq. (4.2.3), $T = m\dot{x}^2/2$, is computed for one impulse in $F(t)$ as

$$\Delta T = \frac{m}{2}[(\dot{x} + \Delta\dot{x})^2 - \dot{x}^2] = m[\dot{x}\Delta\dot{x} + \Delta\dot{x}^2/2] \tag{4.2.8}$$

where $\Delta\dot{x} = A_i/m$, and $x(t)$ is also assumed to be a stationary random process with zero average, then $E(\dot{x}\Delta\dot{x}) = 0$ and

$$E(\Delta T) = m(\Delta\dot{x})^2/2 = E(A_i^2)/2m \tag{4.2.9}$$

The average rate of power (input energy) E_{av} delivered to the system is then the average increment in energy per impulse times the average number of impulses per unit time derived from Eqs (4.2.9) and (4.2.7) respectively,

$$E_{av} = \frac{E(A_i^2)}{2m}\frac{2\pi S_0}{E(A_i^2)} = \frac{\pi S_0}{m} \tag{4.2.10}$$

where in case of linear damped system, input energy is dissipated through damper. Average rate of input energy E_{av} which is equal to the corresponding average rate of energy dissipation is proved to be independent of damping coefficient c as indicated by Eq. (4.2.10). On the other hand, for undamped SDOF system with inelastic behavior, the case which is dealt with in this study, the input energy will be dissipated in the form of hysteretic plastic energy. If the system has its base excited by white noise acceleration input motion $\ddot{x}_g(t)$, then the equilibrium equation of motion (4.2.1) can be rewritten as

$$m\ddot{x}(t) + Q(t) = -m\ddot{x}_g(t) \tag{4.2.11}$$

in which $\ddot{x}_g(t)$ has its constant power spectrum density S_0. The power spectrum density of the excitation force $(-m\ddot{x}_g)$ is obtained knowing that; increasing the

acceleration by factor of m leads to increasing the power spectrum density by factor of m^2. As the system is undamped, the average input energy $\overline{E_i}$ is equal to the plastic dissipated energy and by making use of Eq. (4.2.10), $\overline{E_i}$ can be written as

$$\overline{E_i} = \frac{\pi(m^2 S_0)}{m} t = m\pi S_0 t \tag{4.2.12}$$

then, normalizing the above relation by two times the maximum elastic strain energy of the frame, gives

$$\overline{\lambda_i} = \frac{\overline{E_i}}{Q_{fy}\delta_{fy}} \tag{4.2.13}$$

where

$$\delta_{fy} = \frac{Q_{fy}}{K_{f0}} = \frac{Q_{fy}}{m\omega_0^2} \tag{4.2.14}$$

then, substituting Eqs. (4.2.12) and (4.2.14) into Eq. (4.2.13) yields

$$\overline{\lambda_i} = \pi \frac{\omega_0 S_0}{(Q_y / m)^2} \frac{t}{2\pi / \omega_0} 2\pi \tag{4.2.15}$$

and recalling that $\xi = \omega_0 S_0 / \alpha^2$, $\tau = t / T_0$, and $\alpha = Q_{fy} / m$, leads to the final form of $\overline{\lambda_i}$ as summarized in Eq. (4.2.16),

$$\overline{\lambda_i} = 2\pi^2 \xi \tau \tag{4.2.16}$$

which is the total normalized input energy delivered to the system at τ.

4.3 Simulation and prediction of accumulated plastic energy

The accumulated plastic energy dissipated by the frame element E_p^f is computed for each case under the 100 simulated input motions and the average value $\overline{E_p^f}$ is taken. The non-dimensional form of $\overline{E_p^f}$ is denoted by $\overline{\lambda}$ and defined as

$$\overline{\lambda} = \overline{E_p^f} / Q_{fy}\delta_{fy} \tag{4.3.1}$$

where the denominator equals two times the elastic strain energy of the frame. Sampling simulation curves of $\bar{\lambda} - \tau$ are displayed in Fig 4.3.1, where the non-dimensional time τ defined earlier as $\tau = t / T_0$, lies between 0 - 40. In principle, normalization is aimed at minimizing parameters dealt with in this study and implies an important physical meaning in case of τ, where systems of different first natural periods will have the same value of $\bar{\lambda}$ as far as they have the same value of τ, the case which is only possible when white noise excitation is applied .

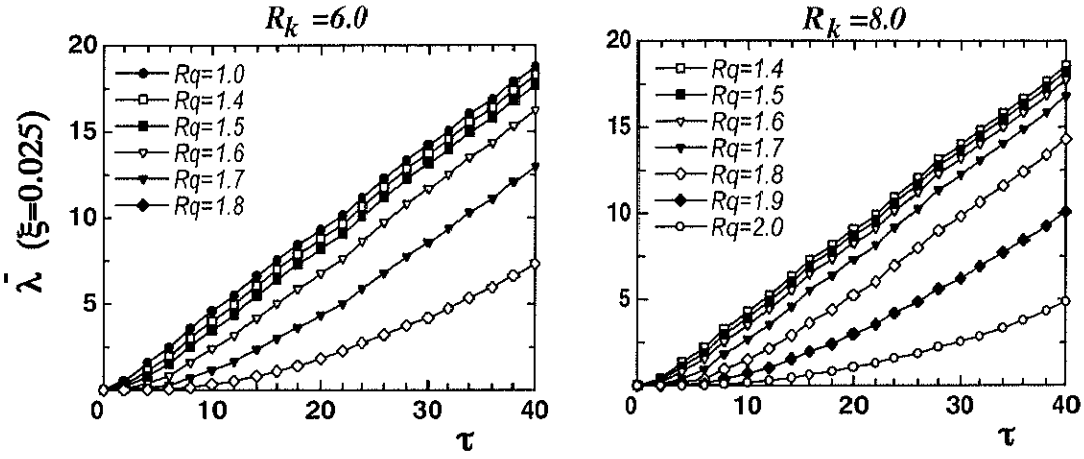

Fig. 4.3.1 Sampling curves of $\bar{\lambda} - \tau$ ($\beta = -0.1$)

Previous research to predict $\bar{\lambda} - \tau$ curves in case of bare frame condition and in stationary response state was made by Matsushima (1991) who found that $\bar{\lambda}$ could be given by

$$\bar{\lambda} = 2\pi^2 \xi (\tau - \tau_0) \qquad (4.3.2)$$

where τ_0 is the expected non-dimensional time for the response to arrive at elastic limit. In an attempt to draw up a general formula capable of predicting $\bar{\lambda} - \tau$ curves in both stationary and transient response states and when mixed systems as well as pure frame systems are concerned, statistical computations are made on the simulation data with all cases of input data for the system and excitation being included. Giving that the utilized input motion is stationary, the response is also expected to be stationary after transient period. As shown in Fig. 4.3.2 (general case), the difference between input energy $\bar{\lambda}_i$ and plastic

energy of the frame $\bar{\lambda}$ is function of τ as far as the response is in the transient state and then turns to become nearly constant value once the system entered stationary phase. The transient period seems to be much longer when mixed system is dealt with due to the energy absorbed by the secondary element which upon its complete failure, the mixed system turns to behave just like pure frame system where all the input energy will be undertaken by the frame only.

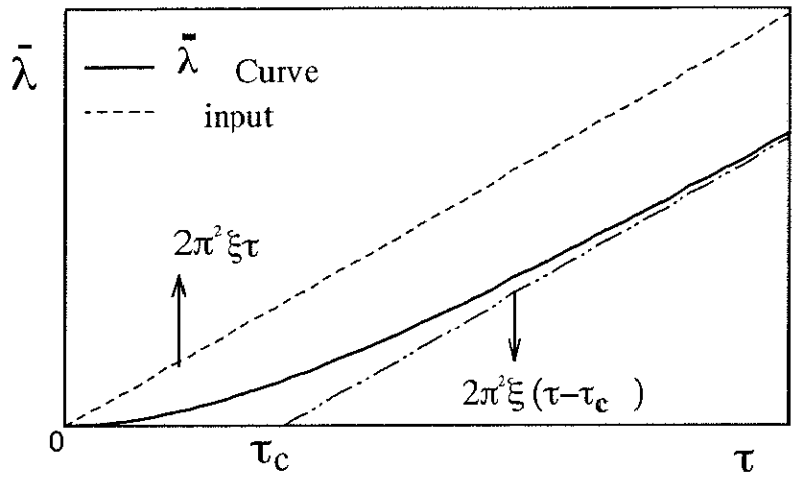

Fig. 4.3.2 $\bar{\lambda}-\tau$ Formula setup

It can be concluded that the second term in the right-hand-side of Eq. (4.3.2), i.e.; $2\pi^2\xi\,\tau_0$ which was constant term when accounting for stationary response, will become function of τ when transient state response is included as well. Besides, $\bar{\lambda}$ curve seem to have exponential form with respect to the line of input energy, then, it can be suggested that prediction estimates of $\bar{\lambda}-\tau$ may be described with a general formula given by

$$\bar{\lambda} = a_1(\tau - \tau_c(1 - e^{-\tau/\tau_c}))^{b_1} \qquad (4.3.3)$$

where a_1 and b_1 are taken as $a_1 = 2\pi^2\xi$ and $b_1 = 1$. In the limits of $\bar{\lambda}$ formula, $lim(\bar{\lambda}) = 0$ as $\tau \to 0$ and $lim(\bar{\lambda}) = 2\pi^2\xi(\tau - \tau_c)$ as $\tau \to \infty$. Also, the slope of $\bar{\lambda}$ is decreased to zero as τ approaches zero, i.e., $lim(d\bar{\lambda}/d\tau) = 0$ as $\tau \to 0$.

Parameter τ_c is selected such that formula (4.3.3) fits the simulation data of $\bar{\lambda}$ by means of least squares technique. The resulted τ_c values derived from

fitting the simulation data of $\bar{\lambda}-\tau$ curves to the model of Eq. (4.3.3), are found to be function of three relevant parameters ξ, ε/ξ and β against which τ_c values are plotted in Fig. 4.3.3.

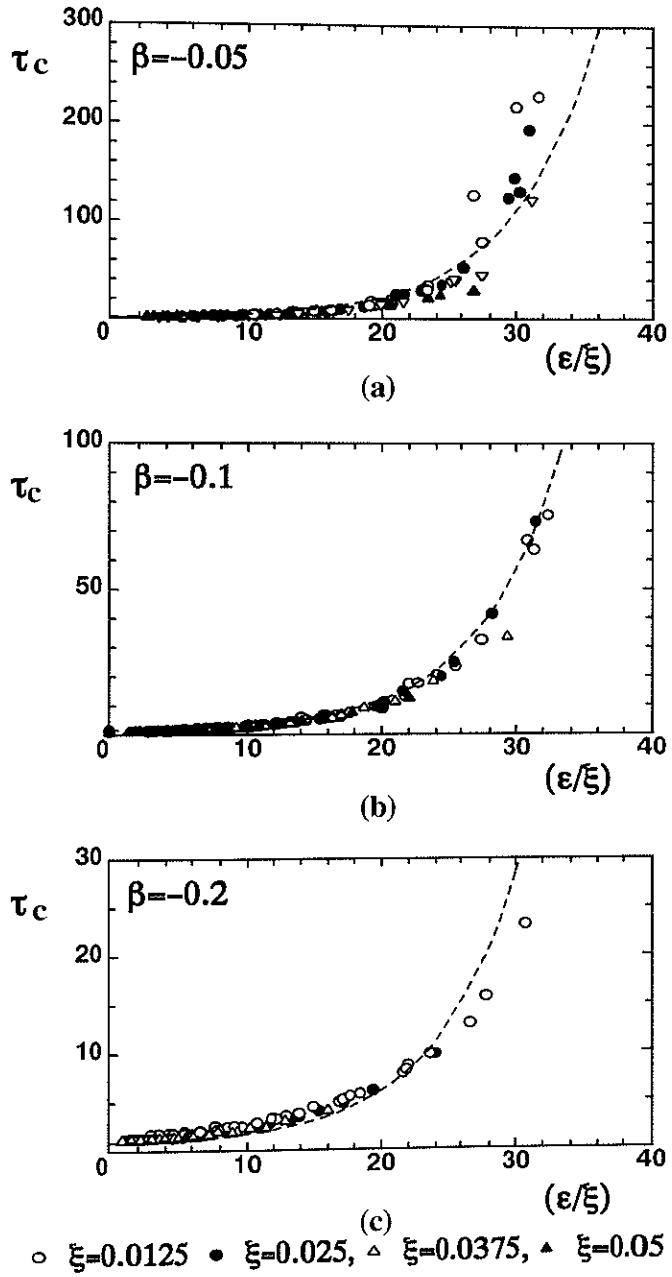

Fig.4.3.3 Parameter of τ_c with respect to ξ, ε/ξ and β

Parameter ε is defined as $\varepsilon = A_w / A_f$ where A_w and $A_f (= Q_{fy}\delta_{fy})$ are the shaded areas shown earlier in Figs. 3.2.1(a) and 3.2.1(b), respectively. A_w may physically expresses the brittle element potential energy capacity, whereas A_f

represents two times the elastic strain energy of the frame. ε can also be written in terms of R_k, R_q and β as given in the following relation,

$$\varepsilon = \frac{(R_q - 1)^2}{2(R_k - 1)}\left(1 - \frac{1}{\beta}\right) \qquad (4.3.4)$$

where the special case of $\varepsilon = 0$ or $\varepsilon/\xi = 0$ accounts for bare frame condition. It can be noted from Fig. 4.3.3 that τ_c value is composed of two main terms; first term is affected by frame element (ξ) and the second term is affected by brittle element presence (ε/ξ and β). Fitting model which accounts for those two effects is proposed in Eq. (4.3.5), where best fitting is obtained when ε/ξ falls in the range $0 \le \varepsilon/\xi \le 32$,

$$\tau_c = l + d\,(e^{f(\varepsilon/\xi)} - 1) \qquad (4.3.5)$$

Coefficient l is found to be function of ξ as shown in Fig. 4.3.4. It accounts for frame effect and takes the form: $l = r\xi^s$, where r and s have values of r=0.242 and s=-0.429 as fitting results.

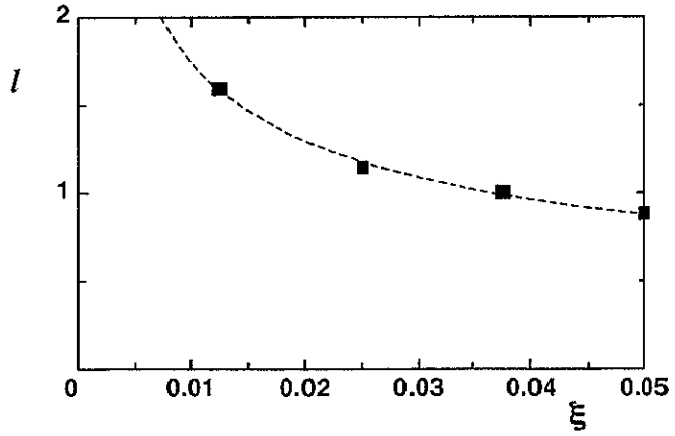

Fig. 4.3.4 Evaluation of coefficients l

Coefficient d is found to be function of β as shown in Fig. 4.3.3 and summarized in Fig. 4.3.5 where it takes the form $d = u/\beta$ in which u=-0.0407. Coefficient f has average constant value given by f = 0.164.

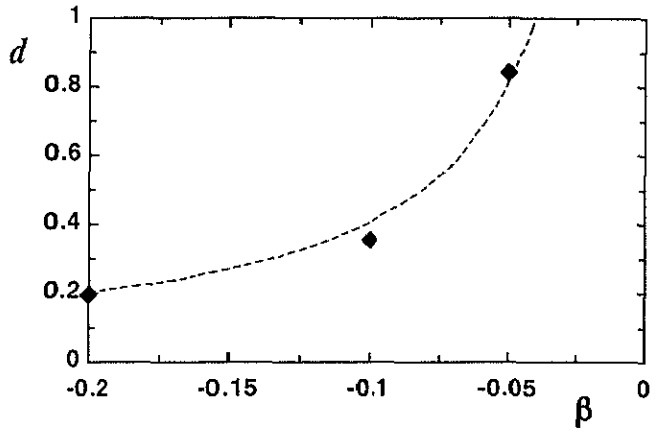

Fig. 4.3.5 Evaluation of coefficient d

As can be noted, the first term in the right-hand-side of formula (4.3.5) is a function of ξ which is frame and input motion related parameter whereas the second term is a function of ε/ξ and β, giving the brittle element contribution to τ_c value and eventually to $\bar{\lambda}$. It is found that ε parameter is an important index of the brittle element energy dissipation capacity relative to frame elastic strain energy. In the limits of τ_c, when $\xi \to \infty$ then $\tau_c \to 0$ and when $\varepsilon \to 0$ then $\tau_c \to 0.242\xi^{-0.429}$, the case of which corresponds to pure frame condition. Simulated and predicted curves of $\bar{\lambda} - \tau$ and for cases corresponding to R_k = 6-8 and 10-12 are plotted in Figs. 4.3.6 and 4.3.7, respectively for β=-0.1 where dashed lines stand for $\bar{\lambda}$ prediction based on formula (4.3.3). It is noticed that good agreement between the predicted and simulated estimates are found in most cases.

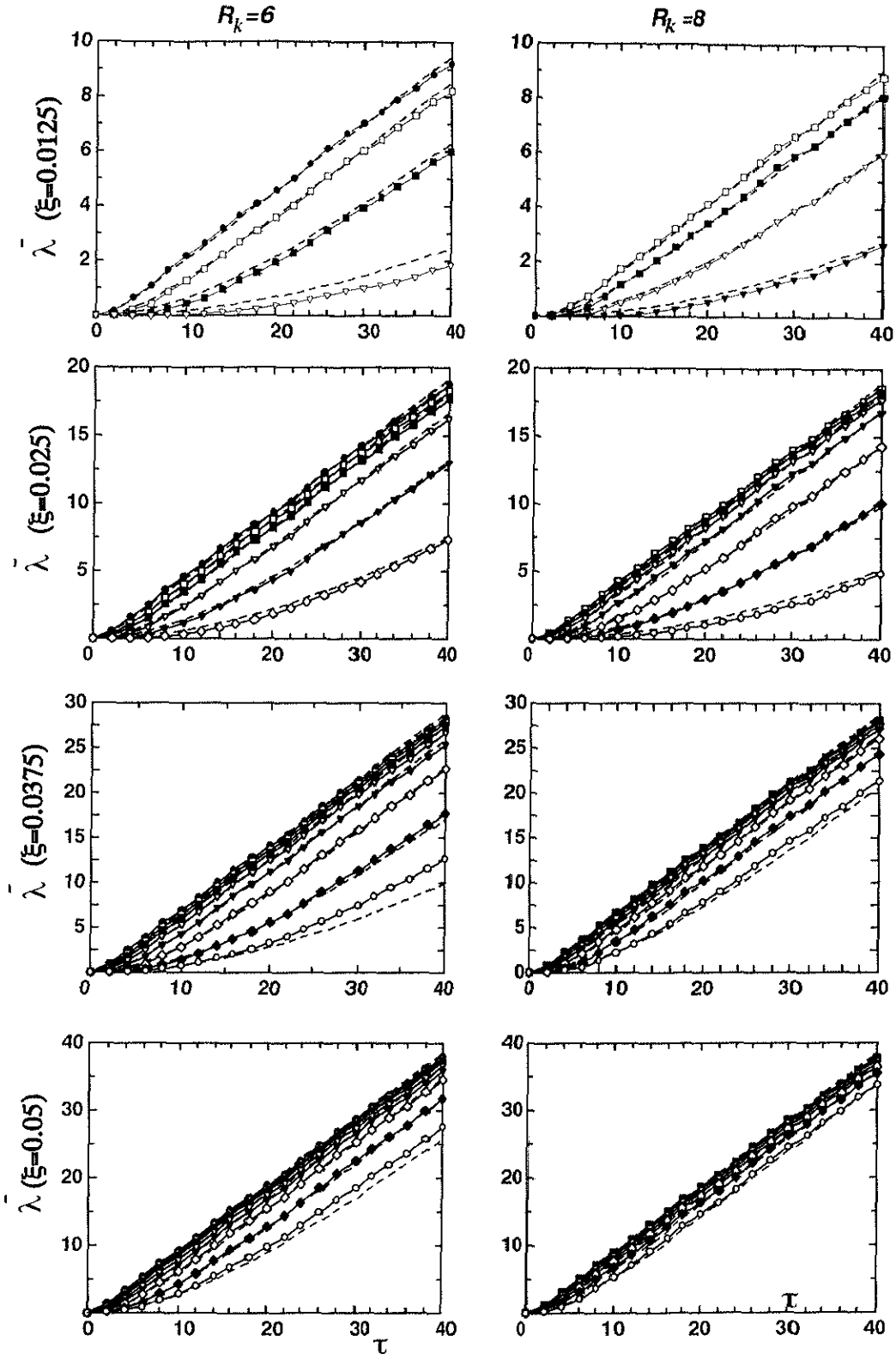

Fig.4.3.6 Simulated and predicted $\bar{\lambda} - \tau$ curves (R_k = 6 and 8, β = -0.1)

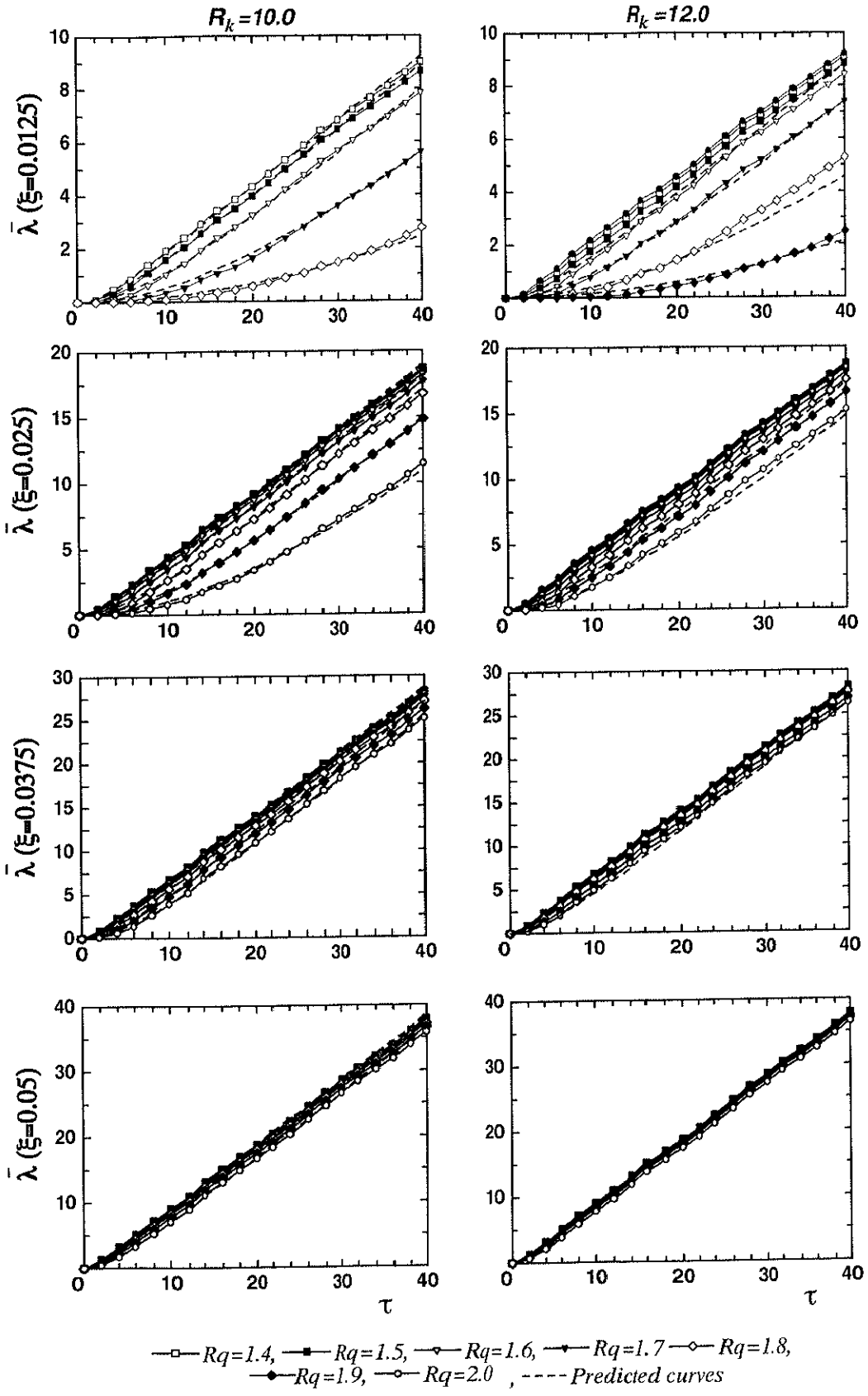

Fig.4.3.7 Simulated and predicted $\bar{\lambda} - \tau$ curves (R_k = 10 and 12, β = -0.1)

4.4 Simulation and Prediction of ductility factor

Ductility factor μ is defined as the absolute maximum displacement divided by displacement corresponding to frame yield point, where the average ductility factor $\bar{\mu}$ will be dealt with as far as the response under 100 white noise samples is concerned. Typical simulation results of $\bar{\mu}-\tau$ corresponding to R_k = 6-8 and 10-12 are plotted in Figs. 4.4.2 and 4.4.3 for $\beta = -0.1$, respectively. In an attempt to conclude a formula capable of predicting $\bar{\mu}$ in any case falling within the limit $(0 \le \varepsilon/\xi \le 32)$, the generalized form given in formula (4.3.3) is found to be applicable by keeping τ_c as defined earlier in Eq. (4.3.5), but leaving the other two coefficients, named here as a_2 and b_2, to be selected such that $\bar{\mu}$ model fits the simulation data of $\bar{\mu}-\tau$ by means of least squares method, i.e., $\bar{\mu}-\tau$ may be given by

$$\overline{\mu} = a_2 (\tau - \tau_c (1 - e^{-\tau/\tau_c}))^{b_2} \qquad (4.4.1)$$

as fitting results, coefficient a_2 with respect to ε/ξ and for the four values of ξ (0.0125, 0.025, 0.0375 and 0.05) are shown in Fig. 4.4.1(a) where it can be concluded that the average value of a_2 is function of ξ as shown in Fig. 4.4.1(b) from which a_2 can have the form expressed in Eq.(4.4.2) where c_2 and d_2 coefficients are obtained using the same previous statistical method giving the following values as results: $c_2 = 14.5$, $d_2 = 0.700$.

$$a_2 = c_2 \xi^{d_2} \qquad (4.4.2)$$

Also, in a similar manner, b_2 coefficient is shown in Fig. 4.4.1(c) with respect to ε/ξ for which Eq. (4.3.3) is proposed to fit the simulation data where g_2, h_2 and j_2 are obtained using fitting method which gives $g_2 = 0.417$, $h_2 = -0.00296$ and $j_2 = 0.177$.

$$b_2 = g_2 + h_2 (e^{j_2 (\varepsilon/\xi)} - 1) \qquad (4.4.3)$$

The first term of the right-hand-side of Eq. (4.4.3) which is a constant value takes frame effect on b_2, while the second term which is function of ε/ξ considers the influence of brittle element on that value.

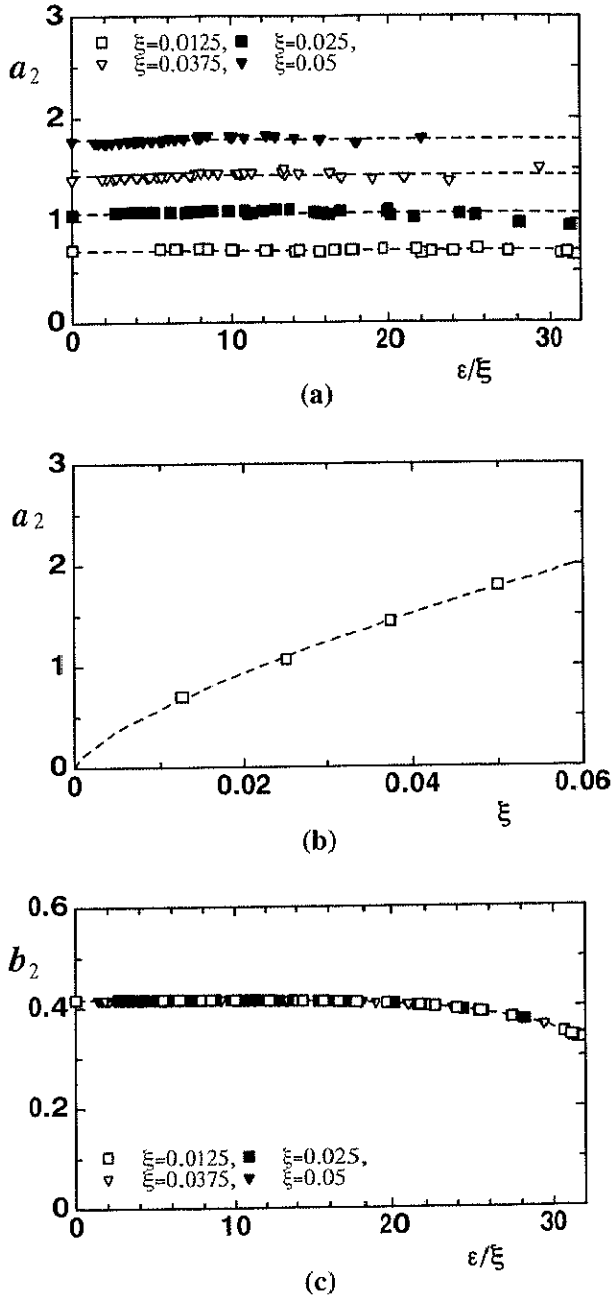

Fig. 4.4.1 Coefficients of $a2$ and $b2$

In the limits of Eq. (4.4.3), $b_2 \rightarrow g_2$ as $\varepsilon \rightarrow 0$ which covers the case of pure frame system. The dashed lines in Figs. 4.4.2 and 4.4.3 stand for $\bar{\mu}$ prediction estimates based on formula (4.4.1). The agreement between simulation and prediction estimates of $\bar{\mu}$ is seen to be satisfactory from practical viewpoint as rough estimation of $\bar{\mu}$ is needed for the purpose of this study, though fitting agreement will be discussed later in this chapter.

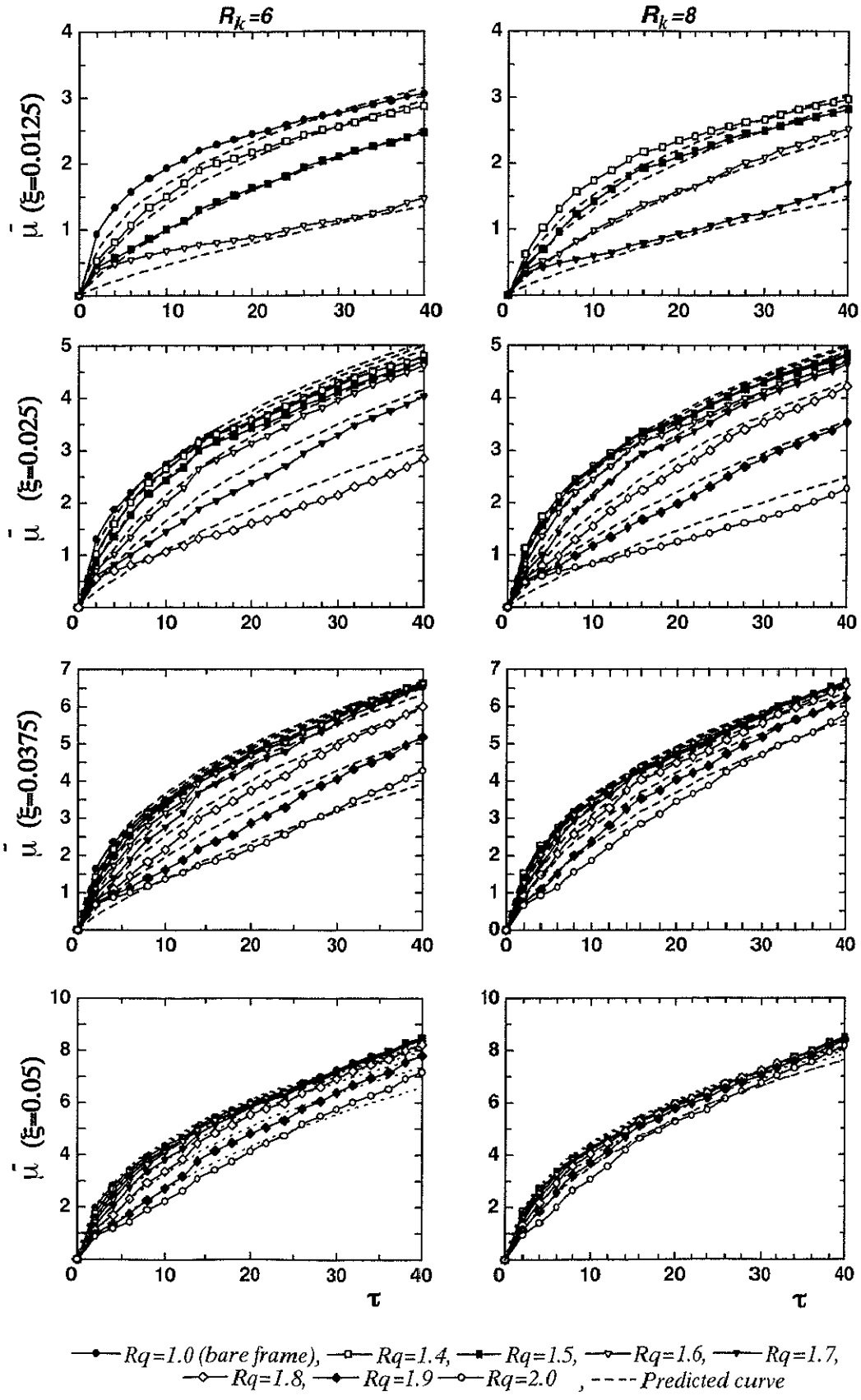

Fig. 4.4.2 Simulated and predicted $\bar{\mu} - \tau$ curves ($R_k = 6$ and 8, $\beta = -0.1$)

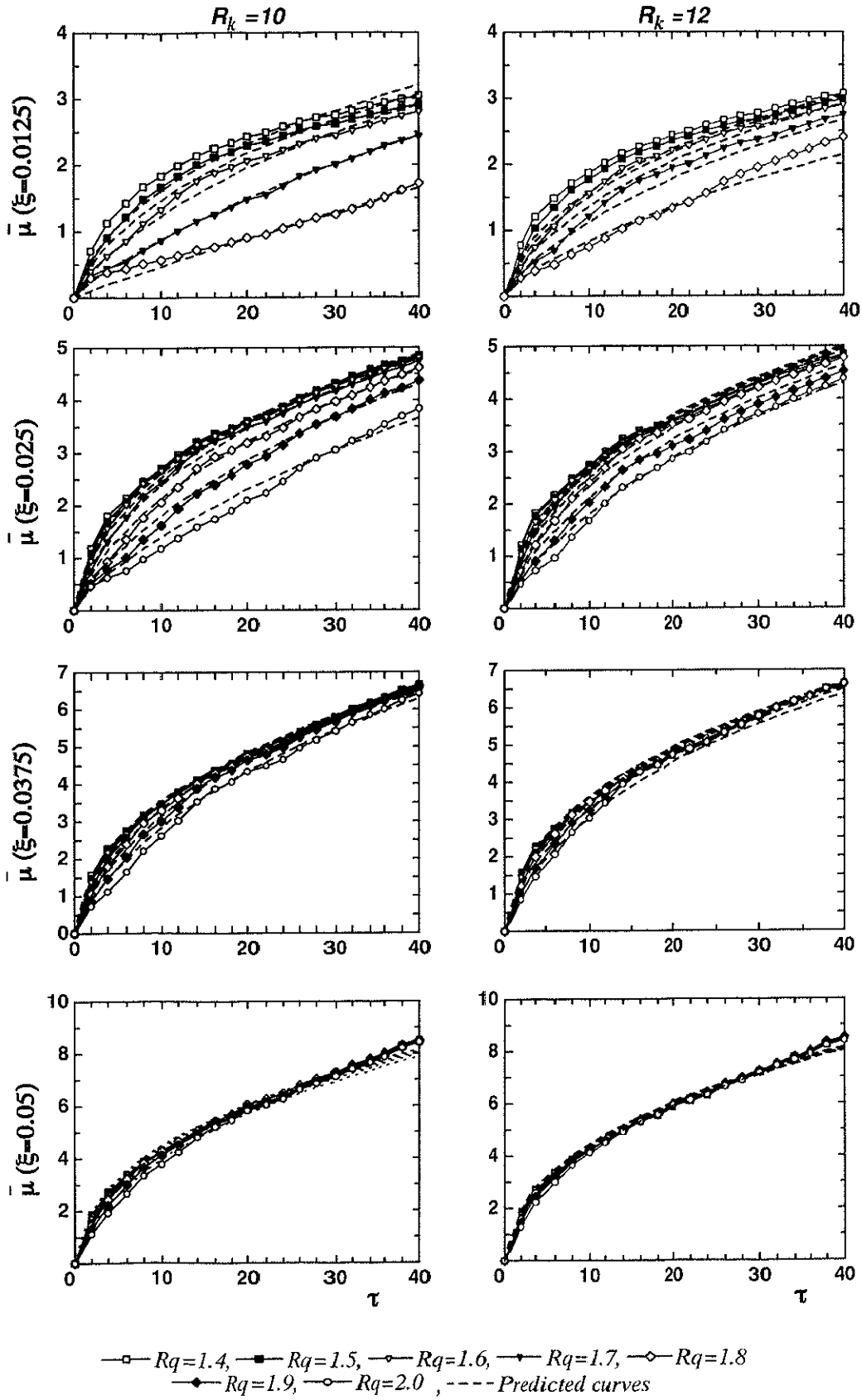

Fig. 4.4.3 Simulated and predicted $\bar{\mu} - \tau$ curves (R_k = 10 and 12, β = –0.1)

4.5 Simulation and prediction of plastic energy standard deviation

Standard deviation of frame accumulated plastic dissipated energy for all cases are computed and typical simulation data of $\sigma_\lambda - \tau$ curves covering cases of R_k = 6-8 and 10-12 for β = -0.1, are plotted in Figs. 4.5.3 and 4.5.4. Prediction estimates of $\sigma_\lambda - \tau$ curves is investigated, where it is found that $\sigma_\lambda - \tau$ prediction could be given in the general form expressed by Eq. (4.5.1),

$$\sigma_\lambda = a_3(\tau - \tau_c(1 - e^{-\tau/\tau_c}))^{b_3} \qquad (4.5.1)$$

where coefficient τ_c seems to go well with the previously defined model of Eq. (4.3.5). Coefficients a_3 and b_3 are to be simultaneously determined by fitting the simulation estimates of $\sigma_\lambda - \tau$ curves to the proposed model given in Eq.(4.5.1) using least squares method. a_3 values are plotted against ε/ξ in Fig. 4.5.1(a) for all values of ξ,

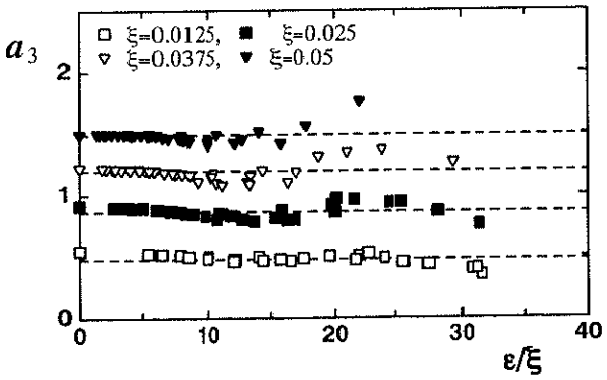

(a)

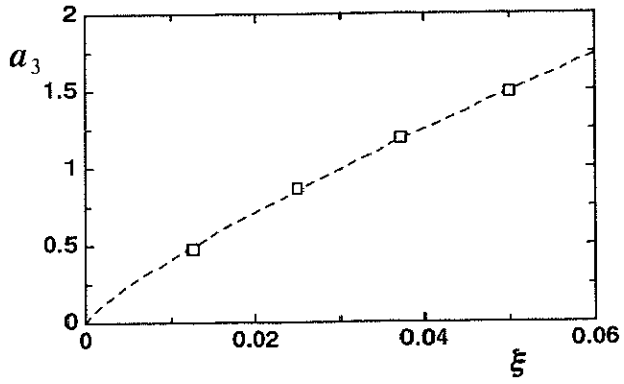

(b)

Fig. 4.5.1 Evaluation of coefficient a_3

where it is seen that coefficient a_3 is likely a function of ξ rather than ε/ξ as shown in the figure. Therefore, the mean value of a_3 for each level of ξ is taken and plotted in Fig. 4.5.1(b) as a function of ξ. The fitting model written in Eq.(4.5.2) is suggested for a_3 prediction,

$$a_3 = c_3 \xi^{d_3} \tag{4.5.2}$$

where c_3 and d_3 are given by $c_3 = 16.8$ and $d_3 = 0.807$. Also, fitting data of b_3 coefficient is presented in Fig. 4.5.2 as a function of ε/ξ and fitted to a model given by Eq. (4.5.3),

$$b_3 = g_3 + h_3(e^{j_3(\varepsilon/\xi)} - 1) \tag{4.5.3}$$

where g_3, h_3 and j_3 are determined again by fitting method and the following values are given as results $g_3 = 0.389$, $h_3 = 0.0226$ and $j_3 = 0.102$.

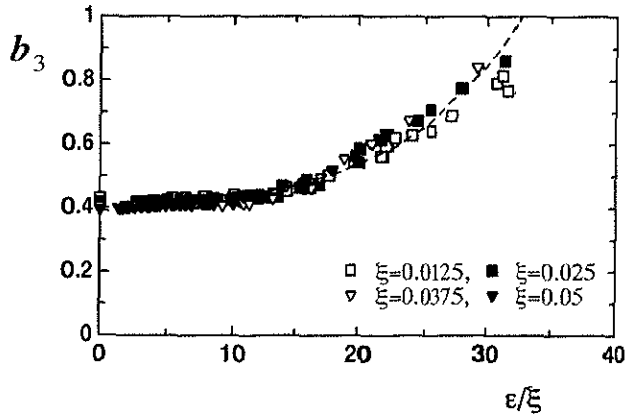

Fig. 4.5.2 Evaluating the coefficient b_3 of σ_λ formula

The corresponding curves of $\sigma_\lambda - \tau$ prediction based on formula (4.5.1) are shown in Figs. 4.5.3 and 4.5.4 with dashed lines for each corresponding simulation curve. The agreement between simulation and prediction estimates is seen to be satisfactory from practical viewpoint giving the fact that fluctuation of standard deviation estimates are expected to be higher compared with the average quantities which have more stable tendency. Fitting agreement of $\sigma_\lambda - \tau$ will also be addressed in this chapter.

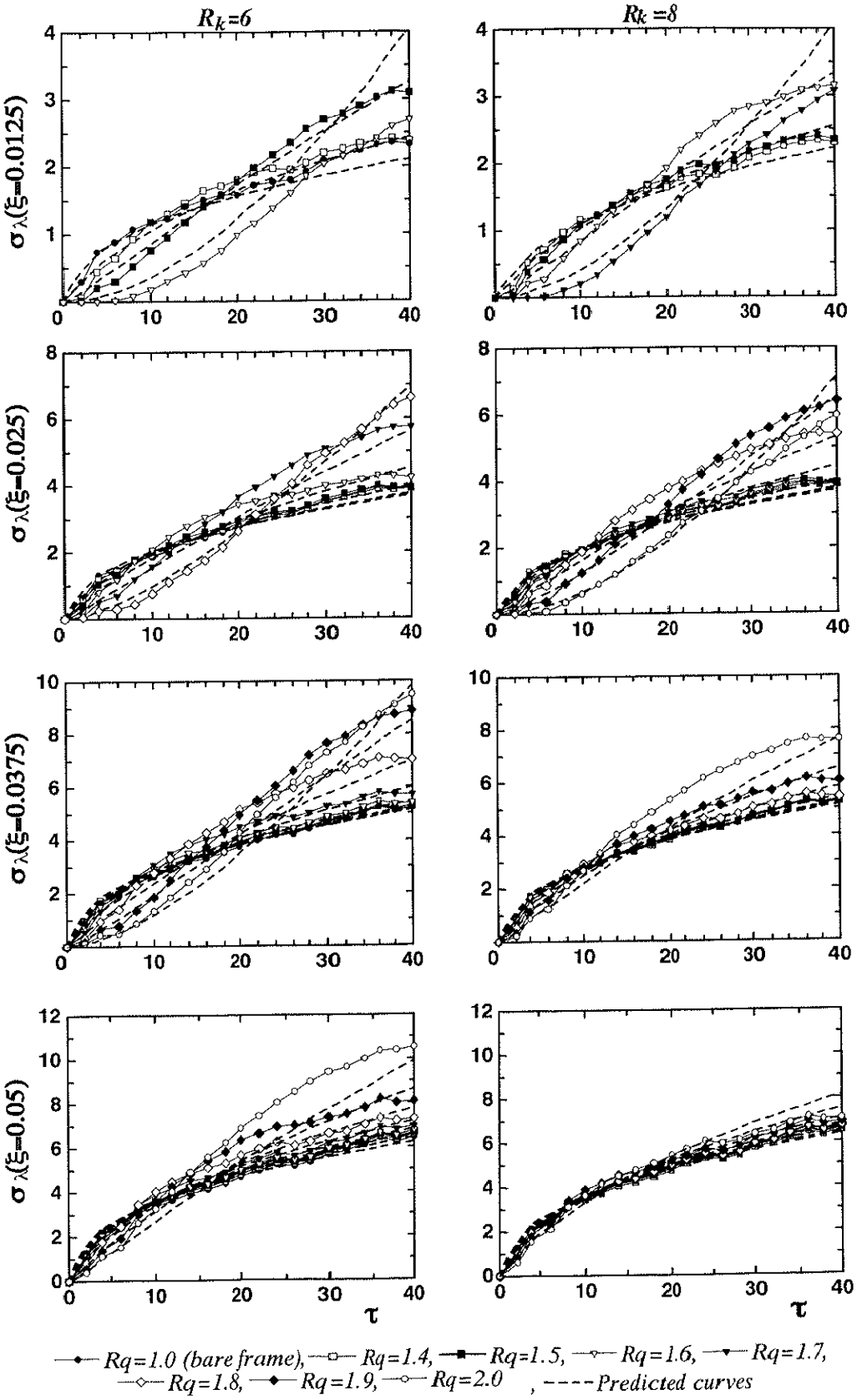

Fig. 4.5.3 Simulated and predicted $\sigma_\lambda - \tau$ curves (R_k = 6 and 8 , β = -0.1)

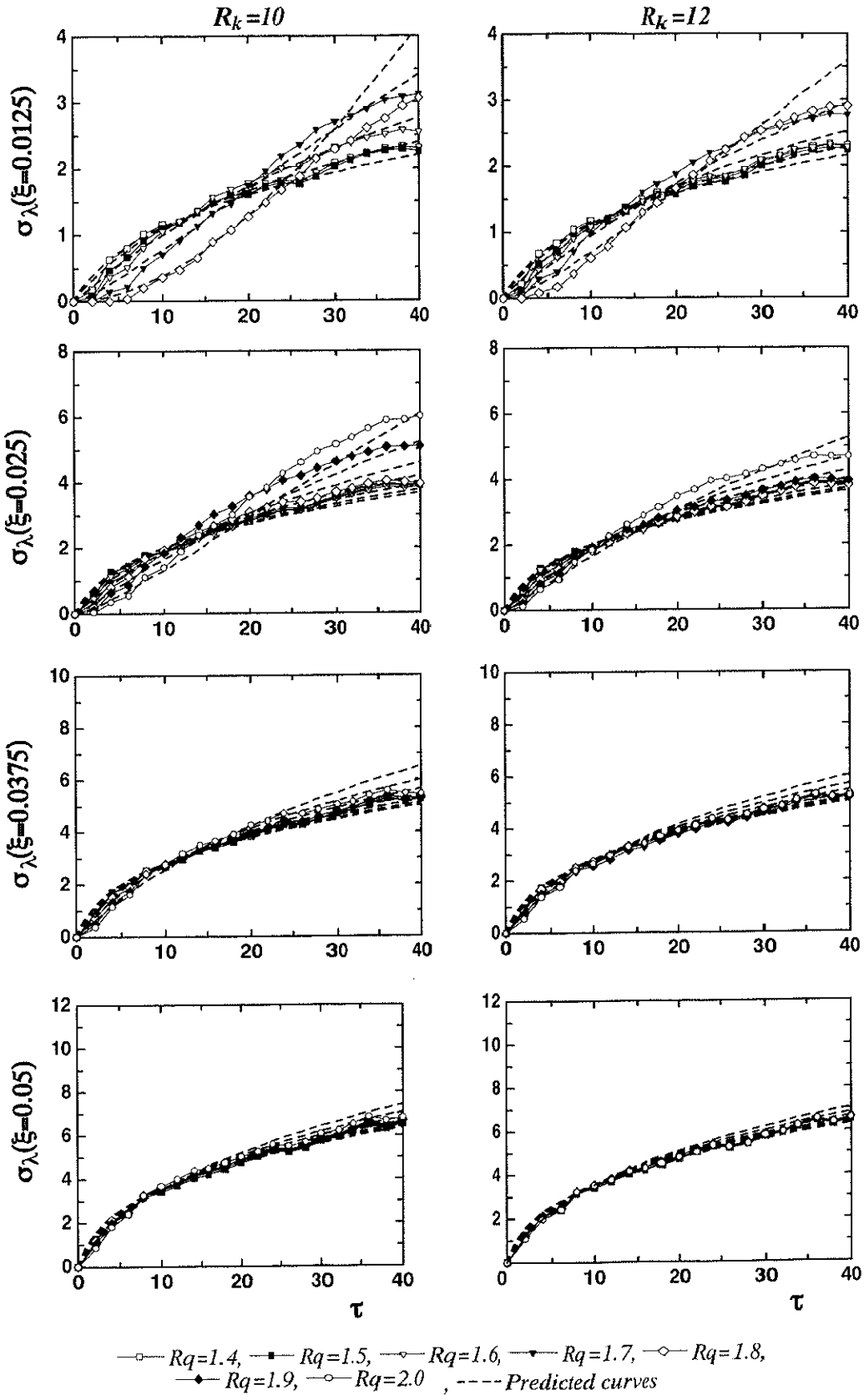

Fig. 4.5.4 Simulated and predicted $\sigma_\lambda - \tau$ curves (R_k = 10 and 12 β = -0.1)

4.6 Simulation and prediction of ductility factor standard deviation

Similarly, simulation analysis of the standard deviation of frame ductility factor σ_μ is performed with respect to τ. The curves of $\sigma_\mu - \tau$ representing typical simulation results are shown in Figs. 4.6.3 and 4.6.4 corresponding to cases of R_k = 6-8 and 10-12, respectively for β = -0.1. The same general form used for the previous response quantities is tested again here for the prediction estimates of $\sigma_\mu - \tau$ with new coefficients a_4 and b_4 as written in Eq. (4.6.1),

$$\sigma_\mu = a_4(\tau - \tau_c(1 - e^{-\tau/\tau_c}))^{b_4} \tag{4.6.1}$$

where τ_c can also be defined according to Eq. (4.3.5). Applying the same fitting method used before, the coefficients a_4 and b_4 are simultaneously computed by fitting $\sigma_\mu - \tau$ simulation curves to the model given in Eq. (4.6.1). Fitting results for a_4 values are drawn in Fig. 4.6.1(a),

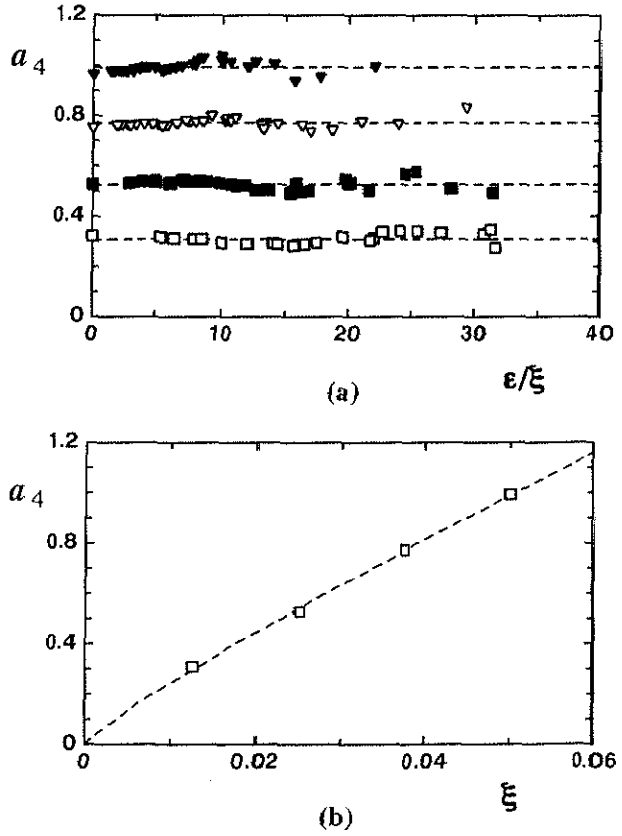

Fig. 4.6.1 Evaluating the coefficient a_4 of $\sigma_\mu - \tau$ formula

which suggests that value of a_4 can fairly be modeled as a function of ξ. The average values of a_4 are taken for each ξ and drawn in Fig. 4.6.1(b) where it is found that Eq. (4.6.2) could fit the simulation data of a_4,

$$a_4 = c_4 \xi^{d_4} \tag{4.6.2}$$

the coefficients c_4 and d_4 are concluded from fitting results and given as $c_4 = 13.5$, $d_4 = 0.871$. The coefficient b_4 is drawn in Fig. 4.6.2 with respect to ε / ξ from which the model given in Eq. (4.6.3) could give best fit to the its simulation data,

$$b_4 = g_4 + h_4 (e^{j_4(\varepsilon/\xi)} - 1) \tag{4.6.3}$$

where the coefficients g_4, h_4 and j_4 are also calculated by fitting method and found to have the following values: $g_4 = 0.309$, $h_4 = 0.00556$ and $j_4 = 0.115$.

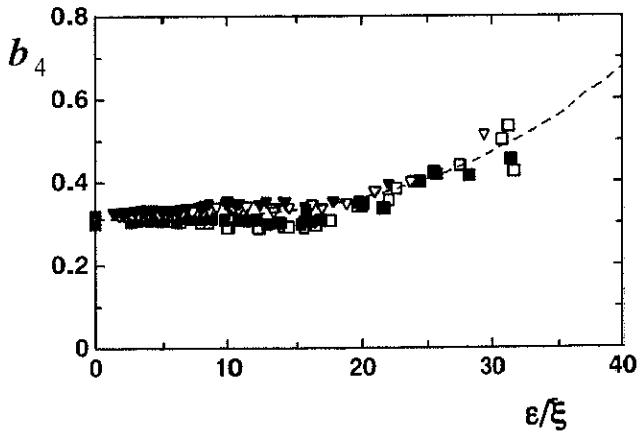

Fig. 4.6.2 Evaluating the coefficient b_4 of $\sigma_\mu - \tau$ formula

Dashed lines in Figs. 4.6.3 and 4.6.4 show the corresponding prediction curves of $\sigma_\mu - \tau$ based on formula (4.6.1). Satisfactory agreement could be noticed between the simulated and predicted results giving the fluctuated nature of standard deviation and the aim of this study which seeks rough estimation of these response quantities. Also, further discussion about fitting agreement is given later on in this chapter.

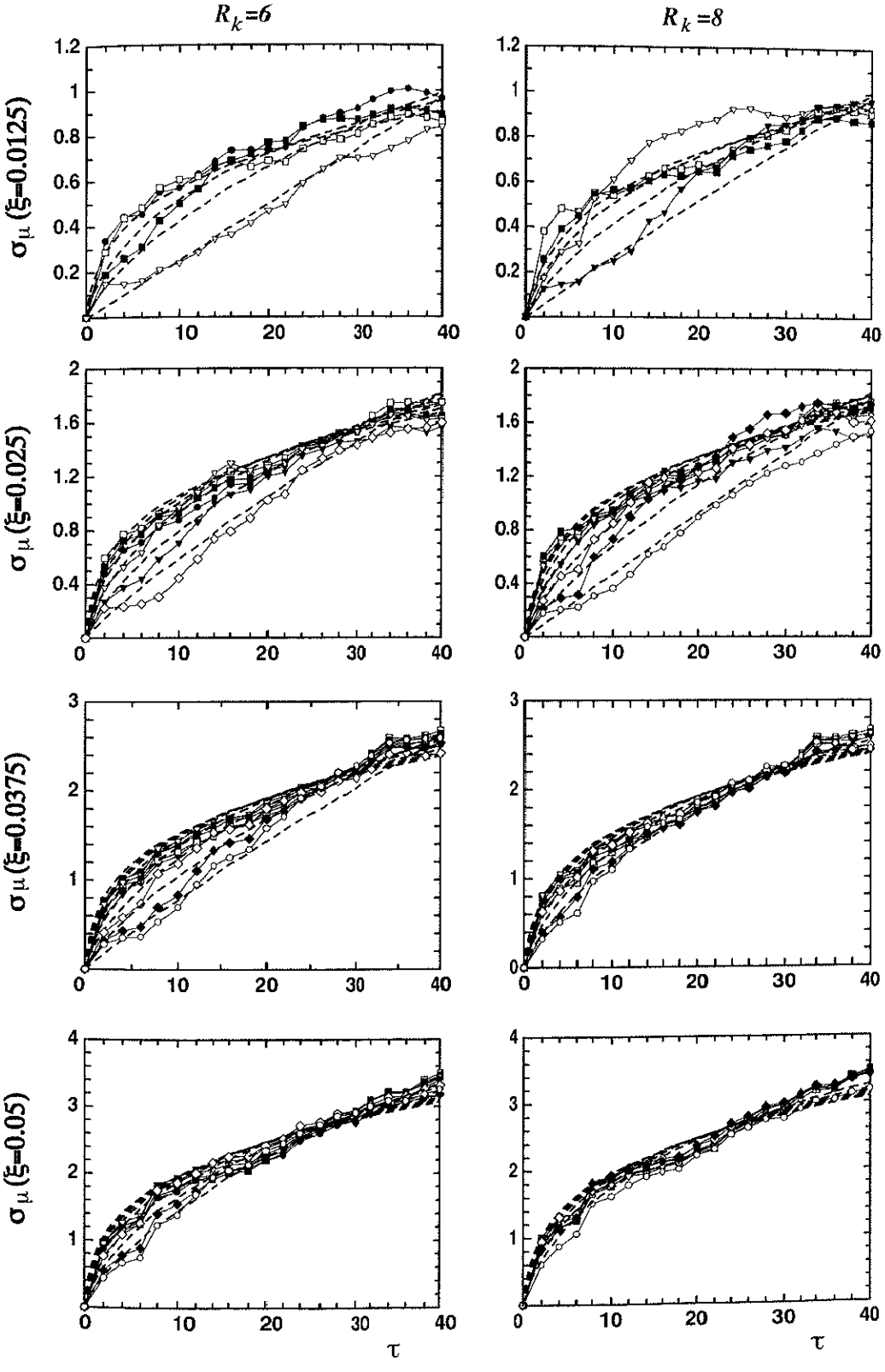

Fig. 4.6.3 Simulated and predicted $\sigma_\mu - \tau$ curves (R_k = 6 and 8 , β = −0.1)

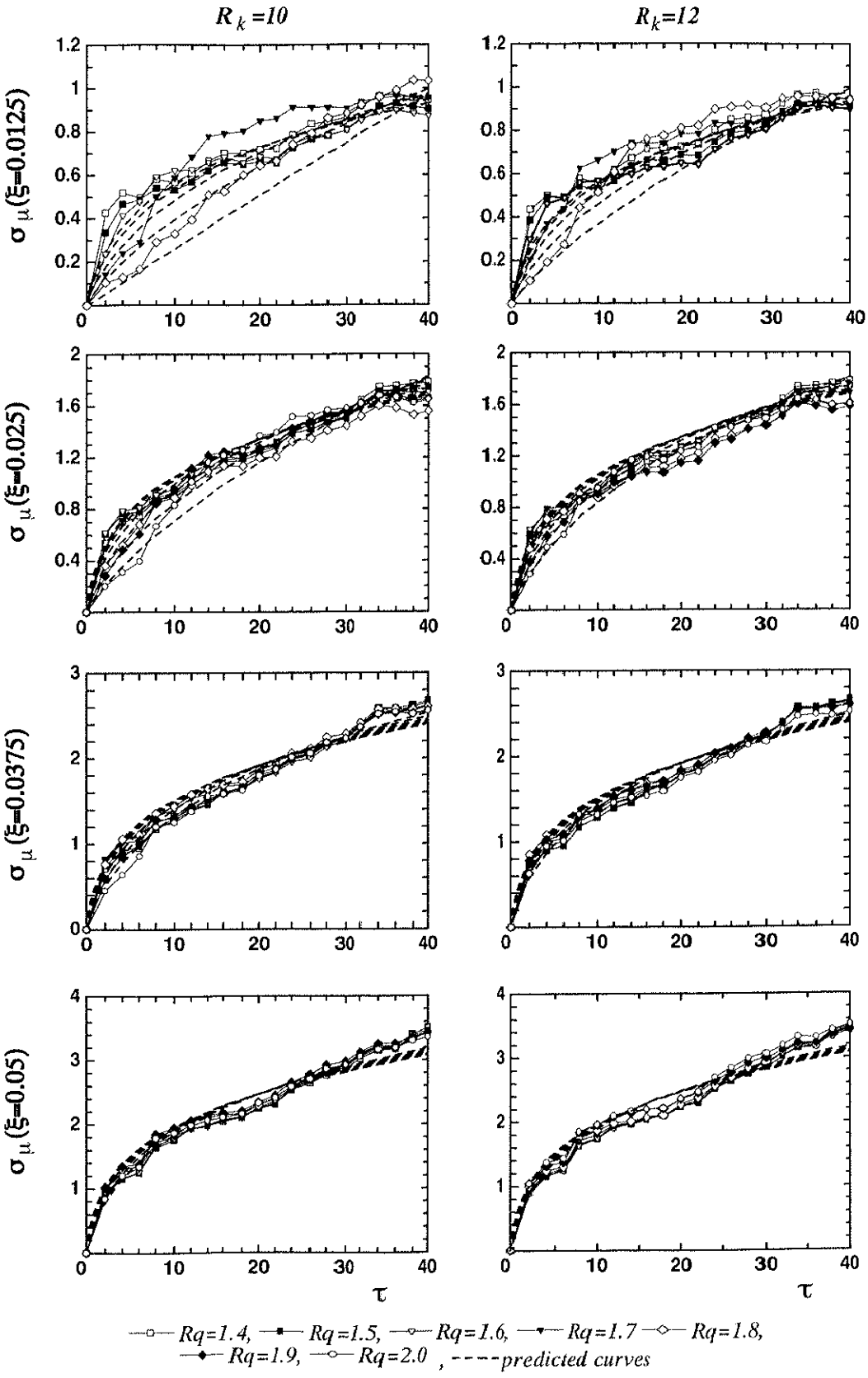

Fig. 4.6.4 Simulated and predicted $\sigma_\mu - \tau$ curves (R_k = 10 and 12 , β = -0.1)

4. 7 Verification for other value of β

The simulation and prediction curves of $\bar{\lambda}-\tau$, $\bar{\mu}-\tau$, $\sigma_{\lambda}-\tau$ and $\sigma_{\mu}-\tau$ shown in previous sections correspond to $\beta=-0.1$ which is viewed as more practical average value of the brittle element post-yielding stiffness ratio. However, the above formulations are derived and hold applicable when the value of β falls within the range of $-0.2 \leq \beta \leq -0.05$. Sampling cases are displayed in Figs. 4.7.1.and 4.7.2 where the cases of $(R_q=1.4, R_k=8)$ and $(R_q=1.6, R_k=12)$, respectively, are considered with the full range of ξ, i.e., $\xi=0.0125-0.050$.

In general, it can be observed that applicability of the formulations is also found to be satisfactory in the two end limits of β (-0.2, -0.05) which are viewed as two extremes ranging from very brittle to less brittle elements. Degree of agreement between simulation data and prediction estimates is to be discussed in more details in section 4.9. The effect of β parameter is seen quite important in the formulations as it reflects the post-yielding behavior of the secondary element. β is included in ε parameter which influences coefficients of a_i, b_i and τ_c for all formulas, except $\bar{\lambda}-\tau$ where it is only appeared in τ_c formula.

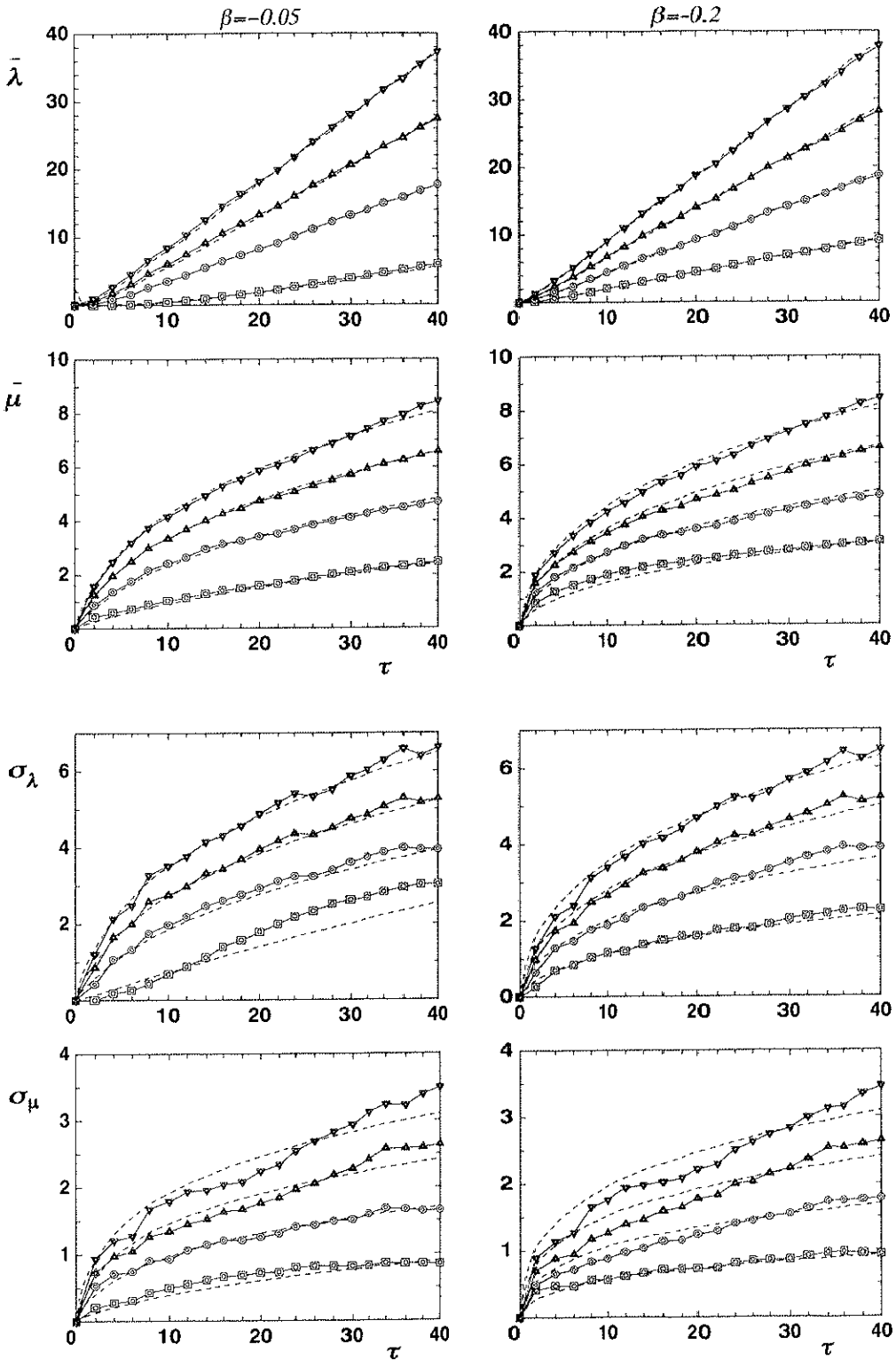

Fig. 4.7.1 Simulation and prediction curves ($R_q = 1.4, R_k = 8$ and $\beta = -0.2, -0.05$)

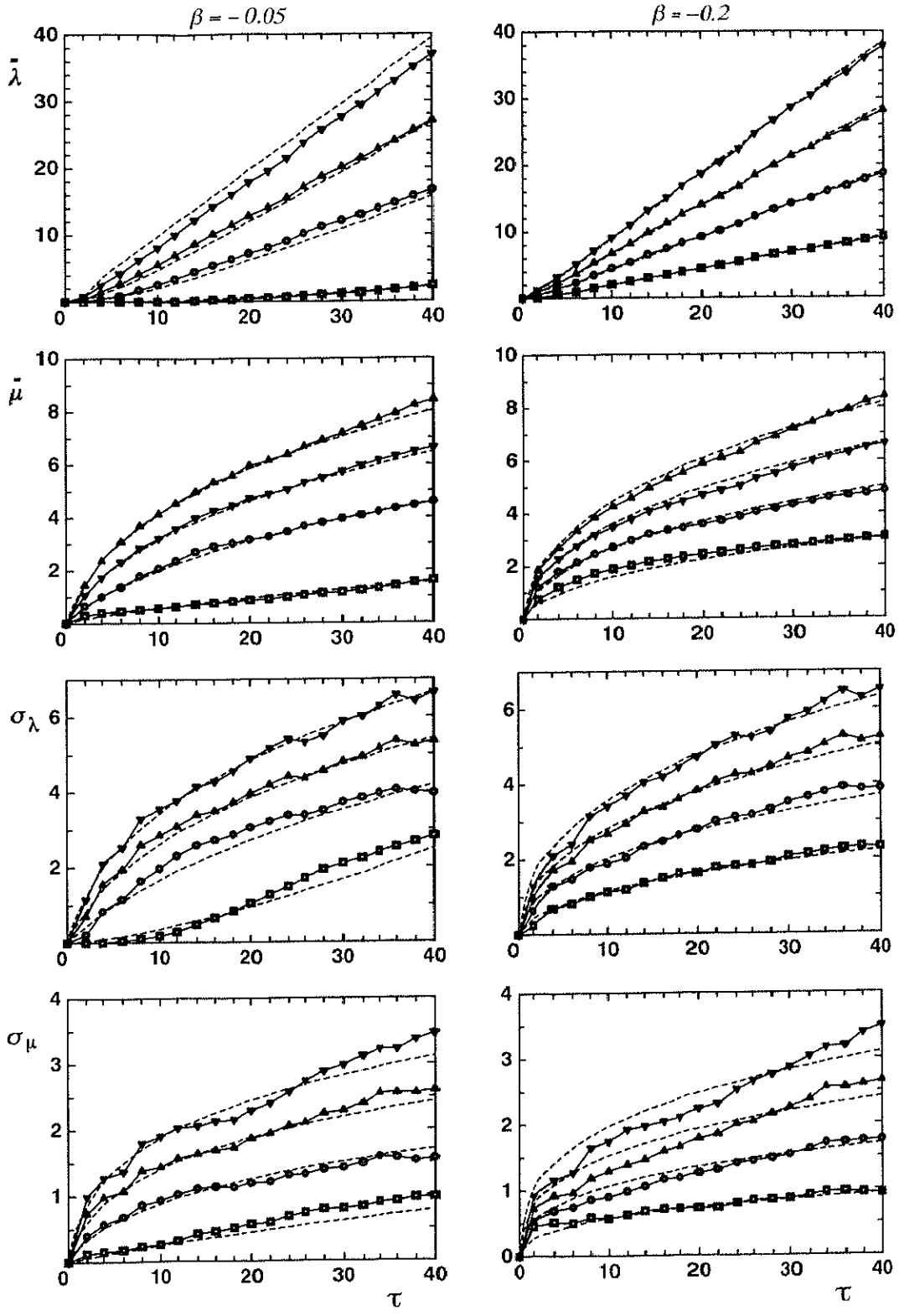

Fig. 4.7.2 Simulation and prediction curves ($R_q = 1.6, R_k = 12$ and $\beta = -0.2, -0.05$)

4. 8 Expressions summary and general formula setup

It can be noted that the already derived closed-form expressions for predicting the response quantities of $\bar{\lambda}-\tau$, $\bar{\mu}-\tau$, $\sigma_\lambda-\tau$ and $\sigma_\mu-\tau$ have general form which could be written as in Eq. (4.8.1). coefficient τ_c is a function of ξ, ε/ξ and β where it is kept unchanged for all expressions as given in Eq. (4.3.5), while parameters a_i and b_i are defined as function of ξ and ε/ξ according to Eqs.(4.8.2) and (4.8.3), respectively,

$$\begin{Bmatrix} \bar{\lambda} \\ \bar{\mu} \\ \sigma_\lambda \\ \sigma_\mu \end{Bmatrix} = \begin{Bmatrix} a_1(\tau - \tau_c(1-e^{-\tau/\tau_c})^{b1} \\ a_2(\tau - \tau_c(1-e^{-\tau/\tau_c})^{b2} \\ a_3(\tau - \tau_c(1-e^{-\tau/\tau_c})^{b3} \\ a_4(\tau - \tau_c(1-e^{-\tau/\tau_c})^{b4} \end{Bmatrix} \tag{4.8.1}$$

$$a_i = c_i \xi^{d_i} \tag{4.8.2}$$

$$b_i = g_i + h_i(e^{j_i(\varepsilon/\xi)} - 1) \tag{4.8.3}$$

where i =1, 2, 3 and 4 corresponding to $\bar{\lambda}$, $\bar{\mu}$, σ_λ and σ_μ, respectively. The coefficients c_i, d_i, g_i, h_i and j_i are summarized and given in Table 4.8.1 for each quantity. The developed formulas for $\bar{\lambda}-\tau$,$\bar{\mu}-\tau$, $\sigma_\lambda-\tau$ and $\sigma_\mu-\tau$ response quantities, are proved to have the same general form with their corresponding coefficients a_i and b_i being expressed in terms of two independent variables ξ and/or ε/ξ while coefficient τ_c is expressed as a function of ξ, ε/ξ and β. Parameter ξ takes the frame influence and parameters ε/ξ and β consider the influence of brittle element. However, it is noticed that when ε/ξ getting smaller, the importance of β itself becomes less visible. The displayed curves for $\bar{\lambda}$, $\bar{\mu}$, σ_λ and σ_μ show also the relative importance of the mixed system yield strength ratio R_q over its corresponding initial stiffness ratio R_k, the tendency of which is indicated in ε formula as well. For specific brittle element, the importance of ξ is prevailing in determining the brittle element influence level on the frame inelastic response.

Table 4.8.1 Summary of formulas coefficients

Forms	$a_i(\tau - \tau_c(1-e^{-\tau/\tau_c}))^{b_i}$					
	$a_i = c_i\xi^{d_i}$			$b_i = g_i + h_i(e^{j_i(\varepsilon/\xi)} - 1)$		
	i	c_i	d_i	g_i	h_i	j_i
$\overline{\lambda}$	1	$2\pi^2$	1	1	0	0
$\overline{\mu}$	2	14.5	0.700	0.417	-0.000296	0.177
σ_λ	3	16.8	0.807	0.389	0.0226	0.102
σ_u	4	13.5	0.871	0.309	0.00556	0.115

4. 9 Fitting agreement

To know how well is the fitting agreement between simulation data and prediction estimates made by the analytical expressions already derived, fitting ratio termed f_r and defined as the prediction estimate divided by simulation value is investigated. It is found that f_r is mainly related to ξ and ε/ξ parameters, where f_r tends to increase when ε/ξ goes higher and if ε/ξ is kept constant, f_r will be higher for lower value of ξ. For most cases, it is found that f_r falls within the range (0.90-1.10) for the averages $\overline{\lambda}$ and $\overline{\mu}$, and within the range (0.85-1.15) for the standard deviations σ_λ and σ_μ. The upper limits of f_r are accompanied by lower value of ξ and/or higher value of ε/ξ. Nevertheless, still caution may be taken for some exceptional cases in which f_r goes beyond the above ranges of f_r. These cases especially arise when ξ is in the lowest level (0.0125) and simultaneously ε/ξ in the upper range, also, under this situation, simulation results with double curvatures are noticed for σ_λ. Generally, f_r is less for the averages than for the standard deviations which is preferable tendency as the importance of averages is much higher than the corresponding standard deviations.

On the other hand, the denominator of f_r ratio, i.e., simulation result is not

perfectly exact itself due to sample size limit, thus for reference, the confidence interval for averages $\bar{\lambda}$ and $\bar{\mu}$, and variances σ_λ and σ_μ are computed assuming normal distribution with 90% confidence level. Setting λ as an example, the following equation is utilized for computing the confidence interval of $\bar{\lambda}$:

$$<\bar{\lambda}>_{1-\kappa} = \bar{\lambda}(1 - z_{\kappa/2}\frac{\delta_{\bar{\lambda}}}{\sqrt{n}}; 1 + z_{\kappa/2}\frac{\delta_{\bar{\lambda}}}{\sqrt{n}}) \qquad (4.9.1)$$

where $\delta_{\bar{\lambda}}$ is the coefficient of variation given by $\delta_{\bar{\lambda}} = \sigma_\lambda / \bar{\lambda}$ and $z_{\kappa/2}$ is the distance from the average, measured in standard deviation which corresponds to probability of exceedance equals $\kappa/2$. The coefficient of variation for λ is found around the range (0.2-0.5) and if the upper range is used with sample size of 100, the confidence interval will be: $<\bar{\lambda}>_{0.9} = \bar{\lambda}$ (0.91; 1.09). Similarly, for ductility factor where μ is replacing λ in Eq. (4.9.1), the coefficient of variation is found around the range (0.4-0.6) and using the upper value gives confidence interval of $<\mu>_{0.9} = \bar{\mu}$ (0.90; 1.10).

The variance's confidence interval formula is given in Eq. (4.9.2) which is irrelevant of variance type,

$$<\sigma^2>_{1-\kappa} = (\frac{s^2}{1 + z_{\kappa/2}\sqrt{2/(n-1)}}; \frac{s^2}{1 - z_{\kappa/2}\sqrt{2/(n-1)}}) \qquad (4.9.2)$$

in which, s^2 is equivalent to σ_λ^2 or σ_μ^2, and n is sample size. Utilizing the same confidence level used for the average (90%), the variance's confidence interval is found as: $<\sigma^2>_{0.9} = (0.811;\ 1.31)s^2$. For comparison, instead of normal distribution, Chi-square distribution is used for evaluating the variance's confidence interval and for the same previous level of confidence, then the following equation is used:

$$<\sigma^2>_{1-\kappa} = (\frac{(n-1)s^2}{\chi^2_{\kappa/2}}; \frac{(n-1)s^2}{\chi^2_{1-\kappa/2}}) \qquad (4.9.3)$$

where χ^2 is a chi-square random variable with (n -1) degree of freedom and s^2 is the variance like before. From chi-square table and for (n -1)=99 degrees of

freedom, $\chi^2_{0.05} = 123.2$ and $\chi^2_{0.95} = 70.05$. Having these data, the confidence interval for variance will be $<\sigma^2>_{0.9} = (0.803; 1.28)s^2$. It is noticed that the two distributions give almost similar results proving that sample size is relatively large from statistical viewpoint.

For the averages, it can be noted that fitting ratios and confidence intervals are almost of the same order. Also, for standard deviation where confidence interval equals square root of the variance's confidence interval, fitting ratio and confidence interval can also be viewed as having the same order. As we seek rough estimation of $\bar{\lambda}$, $\bar{\mu}$, σ_λ and σ_μ for preliminary design purpose, it is believed that these response quantities are still estimated within acceptable resolutions.

4. 10 Relationships between response quantities

The relation between average ductility factor of frame element $\bar{\mu}$ and average normalized plastic energy dissipated by frame element $\bar{\lambda}$ is examined based on simulation data and the derived analytical expressions. Also similar investigation is performed between their corresponding standard deviations, i.e., σ_μ - σ_λ. Based on Eq.(4.8.1) and Table 4.8.1, $\bar{\mu}$ - $\bar{\lambda}$ relation can be written in the following general form,

$$\bar{\mu} = a_5(\bar{\lambda})^{b_5} \tag{4.10.1}$$

where $a_5 = a_2/(a_1)^{b_2}$ and $b_5 = b_2/b_1 = b_2$. In case of bare frames where the coefficients are function of ξ only, then a_5 and b_2 can be given as $a_5 = 0.735\xi^{0.283}$ and $b_5 = 0.283$. In a similar manner and using Eq. (4.8.1) and Table 4.8.1, σ_μ- σ_λ relationship can be written as,

$$\sigma_\mu = a_6(\sigma_\lambda)^{b_6} \tag{4.10.2}$$

in which $a_6 = a_4/(a_3)^{b_4/b_3}$ and $b_6 = b_4/b_3$. In case of bare frame where response is related to ξ only, then a_6 and b_6 are given by $a_6 = 1.44\xi^{0.230}$ and $b_6 = 0.794$ using Table 4.8.1 (bare frame; $\varepsilon/\xi = 0.0$).

It can be observed from $\bar{\mu}$ - $\bar{\lambda}$ and σ_μ - σ_λ relationships and their related coefficients that the overall characteristic of the main original relations $\bar{\lambda}$, $\bar{\mu}$, σ_λ and σ_μ being functions of ξ, ε/ξ, and β is maintained. Fig. 4.10.1 displays sampling simulation and prediction curves of $\bar{\mu}$-$\bar{\lambda}$ and σ_μ-σ_λ relationships for ε/ξ=10.0, ξ = 0.0125 - 0.05 and β = -0.2,-0.1 and -0.05. For example, Tables 4.10.1 and 4.10.2 show the values of the relevant coefficients for bare frame and mixed system (ε/ξ=10.0 and β = -0.1), respectively. Simulation data for mixed system are based on appropriate selection of R_q, R_k, β, and ξ values that correspond to $\varepsilon/\xi \approx 10$.

Table 4.10.1 (ε/ξ = 0.0)

formula / ξ	$\bar{\mu} = a_5(\bar{\lambda})^{b_5}$		$\sigma_\mu = a_6(\sigma_\lambda)^{b_6}$	
	a_5	b_5	a_6	b_6
0.0125	1.2101	0.4170	0.5241	0.7943
0.025	1.4724	0.4170	0.6146	0.7943
0.0375	1.6514	0.4170	0.6747	0.7943
0.050	1.7915	0.4170	0.7208	0.7943

Table 4.10.2 (ε/ξ = 10.0, β = -0.1)

formula / ξ	$\bar{\mu} = a_5(\bar{\lambda})^{b_5}$		$\sigma_\mu = a_6(\sigma_\lambda)^{b_6}$	
	a_5	b_5	a_6	b_6
0.0125	1.2077	0.4156	0.5070	0.7481
0.025	1.4709	0.4156	0.6102	0.7481
0.0375	1.6507	0.4156	0.6800	0.7481
0.050	1.7914	0.4156	0.7344	0.7481

Fig. 4.10.2 shows another example of the above relationships where R_q = 1.7, R_k = 14, and for β = -0.05, -0.1 and -0.2 which results in different values of ε/ξ. The idea behind these varieties is to present the concerned relationships for different conditions. The prediction curves are plotted based on Eqs. (4.10.1) and (4.10.2). Agreements between expected and predicted estimates seems to be satisfactory in most cases and for both $\bar{\mu}$-$\bar{\lambda}$ and σ_μ-σ_λ relationships. In case of bare frame with bilinear hysteretic model, Matsushima (1991) gave direct analytical expressions for the above relationships as:

$$\bar{\mu} = \rho\sqrt{\bar{\lambda}} + 1 \qquad (4.10.3)$$

where ρ is function of ξ and given by,

$$\rho = 1.15\xi + 0.649 \qquad (4.10.4)$$

and

$$\sigma_{\mu} = \psi\sigma_{\lambda} \qquad (4.10.5)$$

where ψ is also function of ξ and given by,

$$\psi = 2.14\xi + 0.406 \qquad (4.10.6)$$

The two relations as given in Eqs (4.10.3) and (4.10.5) are plotted by dotted lines in Figs. 4.10.1(a) and 4.10.1(b), where they correspond to the case of $\varepsilon/\xi = 0$ (bare frame). Also, they are plotted, for reference, in Fig. 4.10.2 corresponding to $R_q = 1.0$ and $R_K = 1$. It could be noticed that the general derived formulations in this study for bare frame/mixed system are in consistent manner with previous research.

The inelastic dynamic response of bare frame or ductile frame mixed with brittle element system could be efficiently predicted by making use of the derived closed form expressions for $\bar{\lambda}$, σ_{λ}, $\bar{\mu}$ and σ_{μ}. If β is kept constant, influence of brittle element on the response of the original frame is taken up through a single factor ε and entry for any expression is set through two separate variables; ξ which is a factor covering frame characteristic and input motion level and ε/ξ ratio which is an indicator of brittle element structural performance relative to ξ. In general, the above figures show that mixed systems experience less damage relative to bare frames, in particular when dealing with low to moderate input motion intensity.

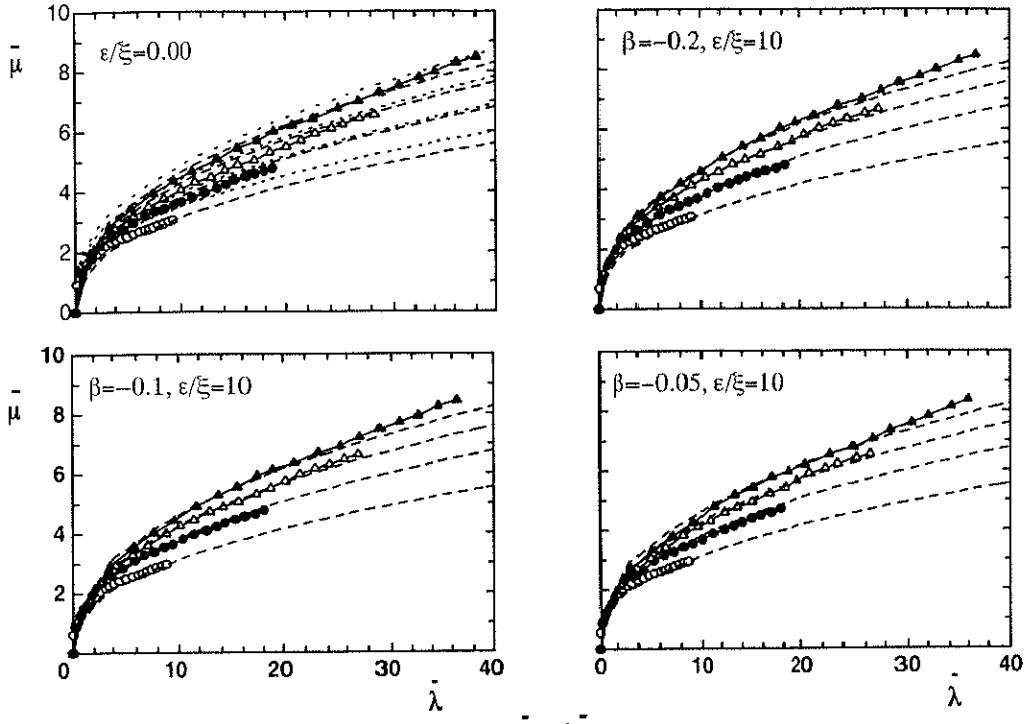

(a) $\bar{\mu} - \bar{\lambda}$

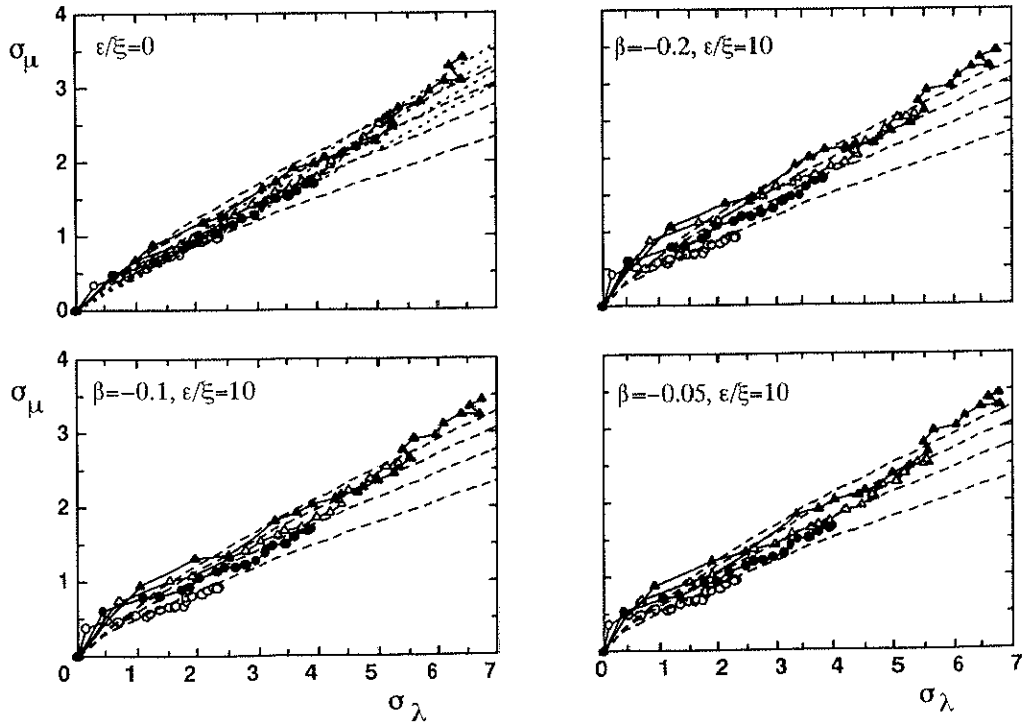

(b) $\sigma_\mu - \sigma_\lambda$

—○— ξ=0.0125, —●— ξ=0.05, —△— ξ=0.0375, —▲— ξ=0.05 : *(Simulated Curves)*

------ *(Predicted curves for bare frame; previous study)* , - - - - *(Predicted curves: this study)*

Fig.4.10.1 Relationships of (a) $\bar{\mu} - \bar{\lambda}$ and (b) $\sigma_\mu - \sigma_\lambda$ (ε / ξ = 0,10)

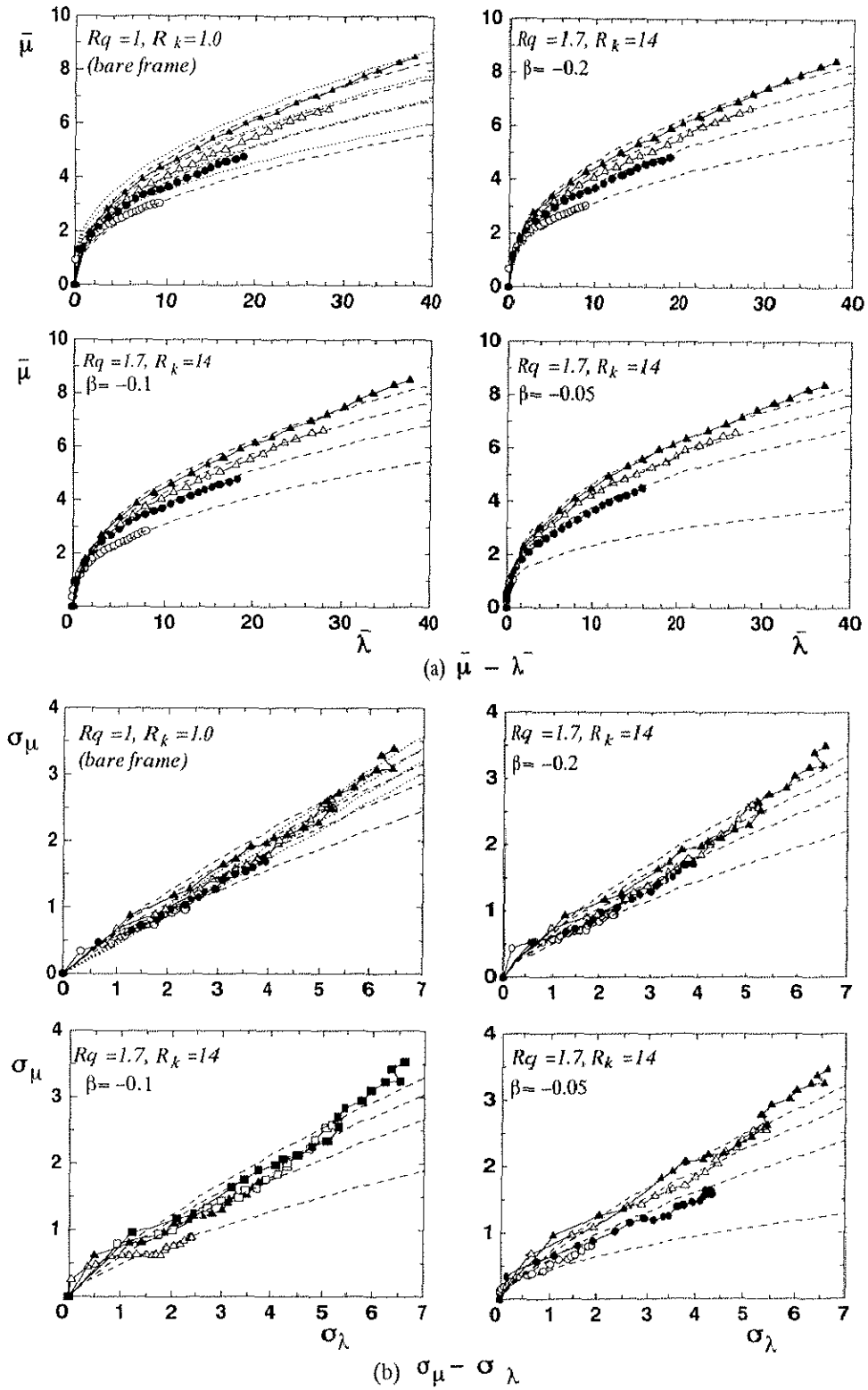

Fig. 4.10.2 Relationships of (a) $\bar{\mu}$-$\bar{\lambda}$ and (b) σ_{μ}-σ_{λ} ($R_q = 1.7, R_k = 14$)

4.11 General curves capturing the effect of brittle element on seismic response of the ductile frame

The general tendency of the overall seismic behavior of the frame element in a mixed system and the effect of relevant parameters could be easily traced through using the previously derived expressions for accumulated plastic energy and ductility factor and drawing the corresponding figures. In Fig. 4.11.1, plastic energy demand on frame elements in a mixed system ($\bar{\lambda}_{fw}$) is shown as a function of ε/ξ parameter (which falls in the range: 0.0-32.0). The curves are drawn for the full range of ξ = (0.0125,0.025,0.0375 and 0.05), β = (-0.2,-0.1, and -0.05), and for normalized time τ = (10, 20 and 40). The corresponding ductility factor experienced by frame element ($\bar{\mu}_{fw}$) is shown as well.

The effect of all relevant parameters in terms of $\bar{\lambda}_{fw}$ and $\bar{\mu}_{fw}$ are clearly viewed in Fig. 4.11.1. Effect of ε/ξ is deemed to be very important where higher value of ε/ξ leads to lower values of $\bar{\lambda}_{fw}$ and $\bar{\mu}_{fw}$, in such a way that the brittle element effectiveness is getting higher and frame element will be exposed to less plastic energy and ductility factor. The effect of ξ seems to contrast ε/ξ effect where higher the value of ξ higher the values of $\bar{\lambda}_{fw}$ and $\bar{\mu}_{fw}$ leading to more nonlinear deformation demands on frame element.

As far as the post-yielding stiffness ratio of the brittle element hysteretic model (β) is concerned, it is noticed that if β is getting higher and other parameters are held constant, less demand of $\bar{\lambda}_{fw}$ and $\bar{\mu}_{fw}$ are found, the effect of which coincides with ε/ξ one. Regarding the effect of normalized time τ, if other parameters are kept unchanged, the value of $\bar{\lambda}_{fw}$ is dramatically increased when the value of τ is getting higher, especially in case of bare frame. Also, the value of $\bar{\mu}_{fw}$ is increased by less degree comparing with $\bar{\lambda}_{fw}$ when τ is getting higher.

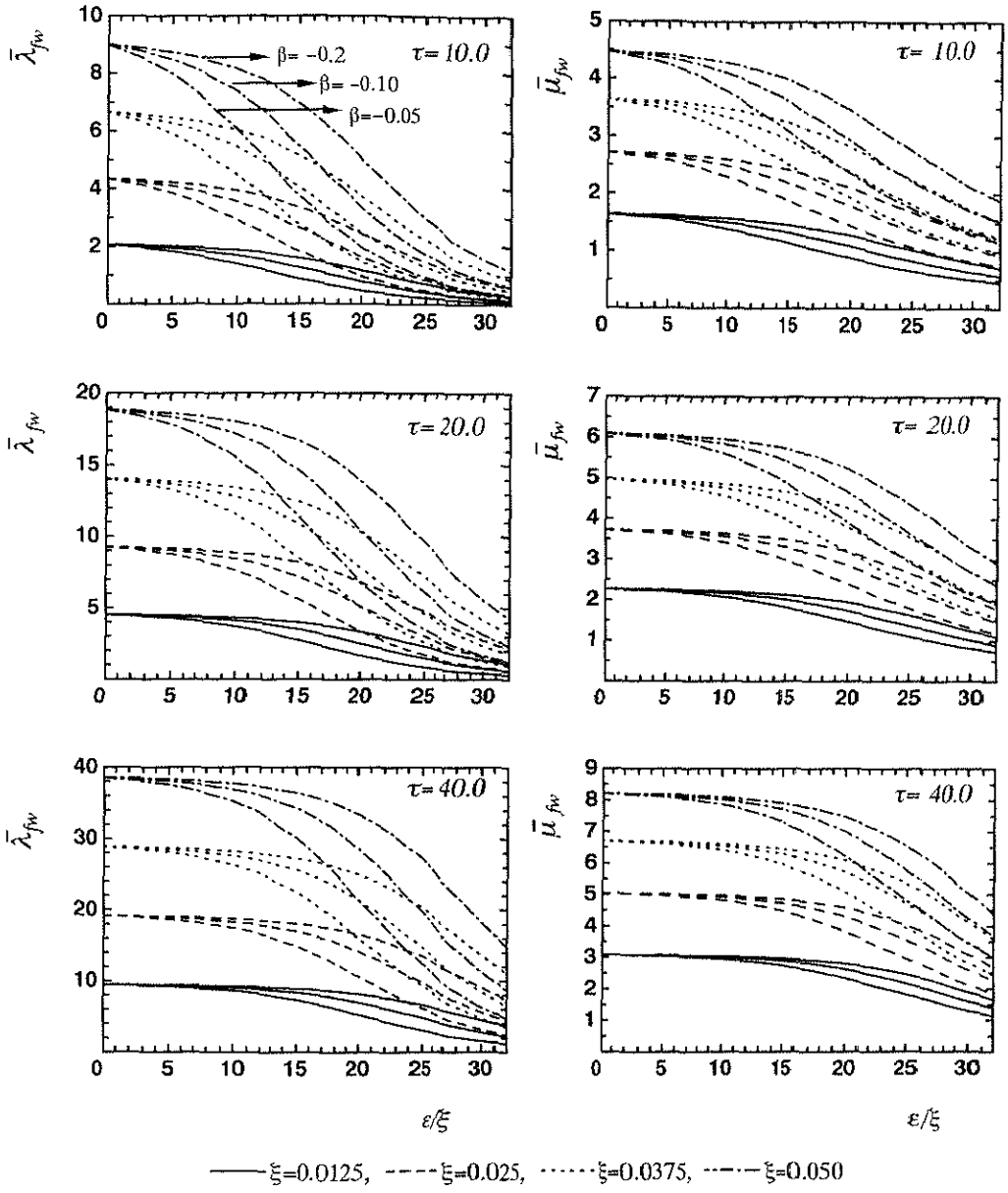

Fig. 4.11.1 Absolute response quantities based on prediction

The privilege of a mixed system over bare frame system is quantitatively investigated here by drawing the curves of the ratios ($\bar{\lambda}_{fw}/\bar{\lambda}_f$) and ($\bar{\mu}_{fw}/\bar{\mu}_f$) with respect to ε/ξ, and for full ranges of ξ and β. The curves are presented in Fig. 4.11.2 for sampling values of τ = 10, 20 and 40. The curves can show the degree of influence of all relevant parameters, where it can be seen that effect of ξ alone is almost diminished. The effects of ε/ξ and β, which are brittle element related parameters, are prevailing in giving the degree of the brittle element effectiveness in terms of $\bar{\lambda}_{fw}$ and $\bar{\mu}_{fw}$. If ε/ξ and β ratios are kept constant, the

influence on $\bar{\lambda}_{fw}$ is much higher compared to that on $\bar{\mu}_{fw}$. For example, if ε/ξ=15, β=-0.1 and τ=20 which are almost center points, $\bar{\lambda}_{fw}/\bar{\lambda}_f \approx 80$ % and $\bar{\mu}_{fw}/\bar{\mu}_f \approx$ 90 %; meaning that the brittle element have absorbed about 20% of the total plastic energy imposed on the system and reduced ductility factor demand on the frame element by 10%. In fact, the degree of influence is rapidly getting higher with increasing ε/ξ and β. As far as τ effect on the brittle element efficiency is concerned, it can be noticed from Fig. 4.11.2 that when τ is getting higher, the beneficial effect of the mixed system over pure frame system is getting lower.

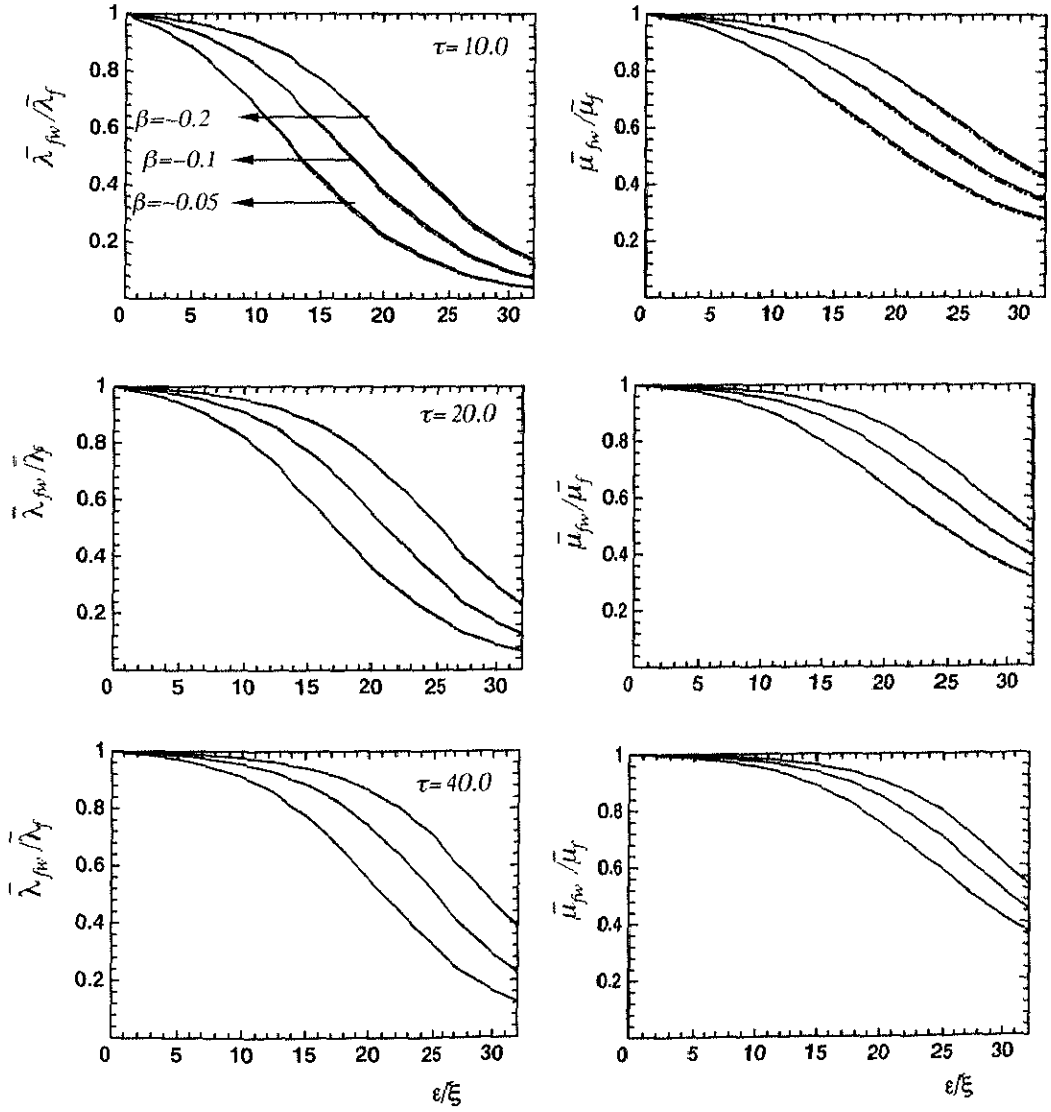

——ξ=0.0125, - - - -ξ=0.025, · · · ·ξ=0.0375, ——ξ=0.050

Fig. 4.11.2 Relative response quantities based on prediction

4. 12 Response under real earthquakes

For reference, the mixed system response under real earthquake ground motions are performed utilizing the horizontal north-south components of El Centro (1940), Taft (1952), Hachinohe (1968), Miyagiken-oki (1978) and Kobe (1995). The earthquake ground motions are processed before in the second chapter, where a part of each earthquake acceleration time history which is likely corresponding to stationary white noise is selected and used as a representative of the real earthquake for inelastic response analysis. Values of the parameters R_k, R_q and β are taken as R_k=6, R_q=1.4, 1.6 and 1.8, and β=-0.1. Examples for other values of β are also considered where the cases of R_k=8 and R_q=1.8 for β=-0.05 and -0.20 are analyzed as well, whereas ξ is taken as ξ=0.05 for all cases. Frame initial natural period T_0 is selected such that an integer value of τ_{max} is obtained having the relation $\tau_{max} = t_d / T_0$, where t_d is the time duration of the selected input motion as explained in chapter 2. Also, T_0 should not be out the range where the power spectral density of the input motion has reasonable value. Table 4.12.1 summarizes the values of T_0 for different earthquakes.

Table 4.12.1

Parameters / Earthquake	t_d (sec)	τ_{max}	T_0 (sec)
El Centro-Ns	11.0	10.0	1.10
Taft-Ns	11.8	15.0	0.787
Hachinohe-Ns	21.0	20.0	1.05
Miyagiken-oki(Ns)	10.0	15.0	0.667
Kobe-Ns	8.38	10.0	0.838

The response is also expressed in terms of accumulated plastic energy and ductility factor required by the original frame with respect to non-dimensional time τ, i.e., $\lambda-\tau$ and $\mu-\tau$, respectively. Results of simulation data under the earthquakes of El Centro, Taft, Hachinohe, Miyagiken-oki and Kobe are shown in Figs 4.12.1 through 4.12.5, respectively. Besides, Fig. 4.12.6 shows the corresponding response of bare frame system. The prediction estimates in terms of $\bar{\lambda}-\tau$ and $\bar{\mu}-\tau$ are also shown on the same figures together with the

fluctuation about the averages by adding and subtracting one standard deviation to the average estimates, i.e., $(\bar{\lambda} \pm \sigma_\lambda)$ and $(\bar{\mu} \pm \sigma_\mu)$. The response under real earthquakes will be changed once T_0 is changed; meaning that the response is not only function of τ, but also T_0 dependent. This is related to the fact that real input motions will never be stationary white noises. However, comparison between simulation data and the prediction estimates can be made possible if the response is calculated for many values of T_0 and average is taken, then it may approach the predicted estimates. Nevertheless, the present results could also be comparable if they are made on $(\bar{\lambda} \pm \sigma_\lambda)$ and $(\bar{\mu} \pm \sigma_\mu)$ curves.

Relationship between the accumulated plastic energy and ductility factor of frame element, λ-μ, is examined again here for real earthquakes where sampling cases are taken and plotted in Fig. 4.12.7 for each of the five earthquakes mentioned above. Also, the corresponding prediction estimates of $\bar{\lambda}$-$\bar{\mu}$ are shown on the same figures. It is of interest to see that relationships between response quantities themselves have generally better agreement with formulations compared with that of the response with time.

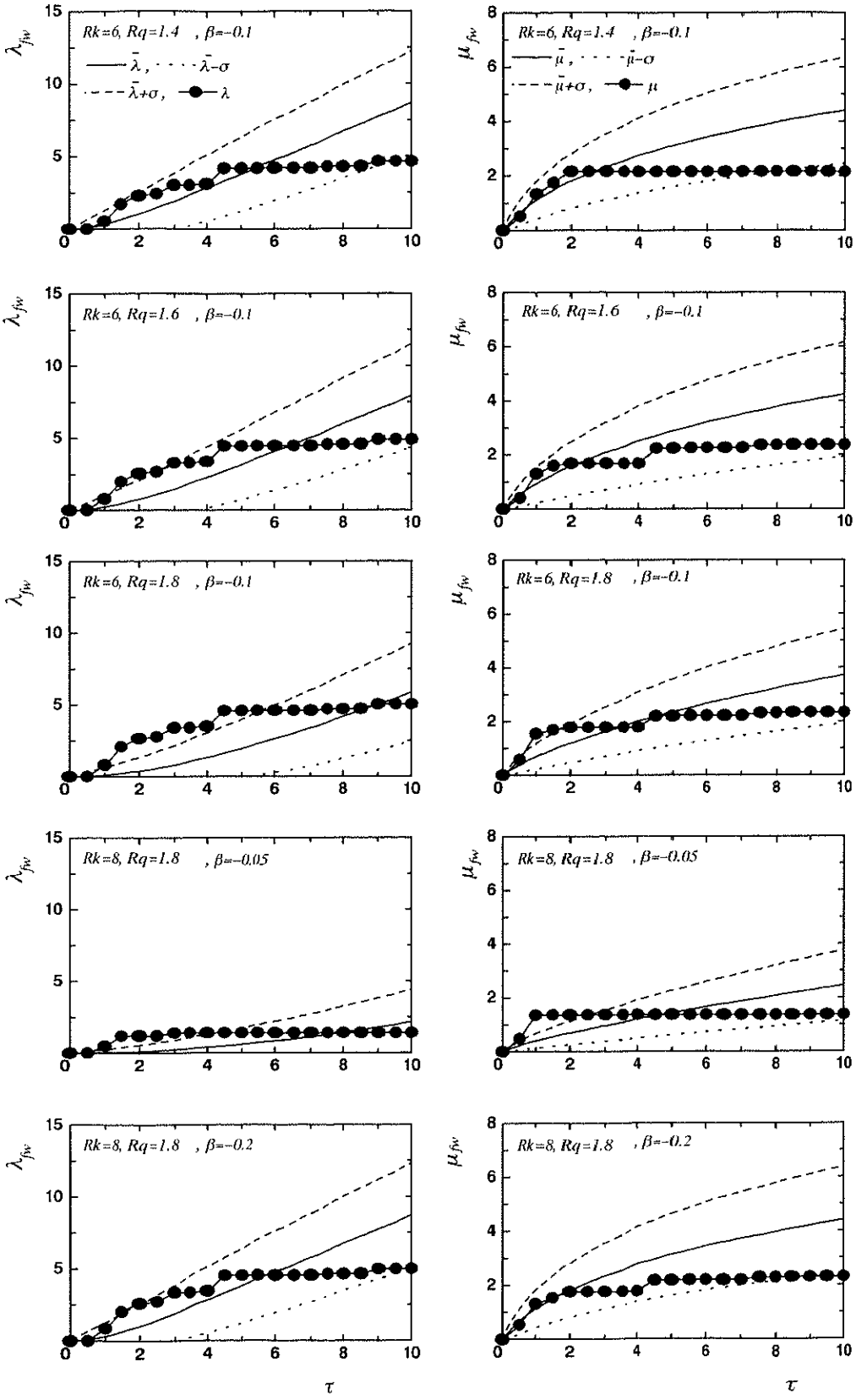

Fig. 4.12.1 Response under El Centro earthquake (ξ =0.05)

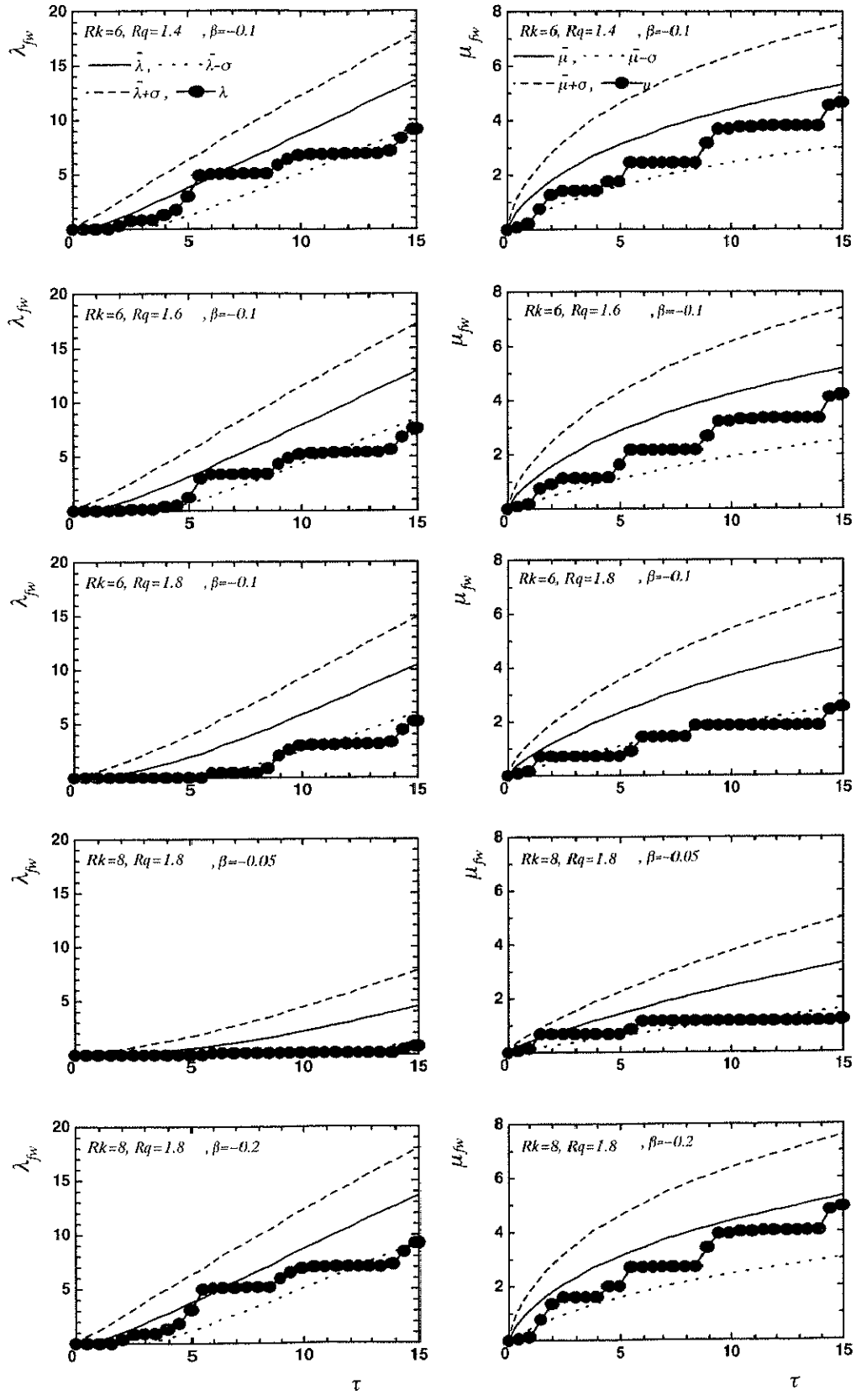

Fig. 4.12.2 Response under Taft earthquake (ξ=0.05)

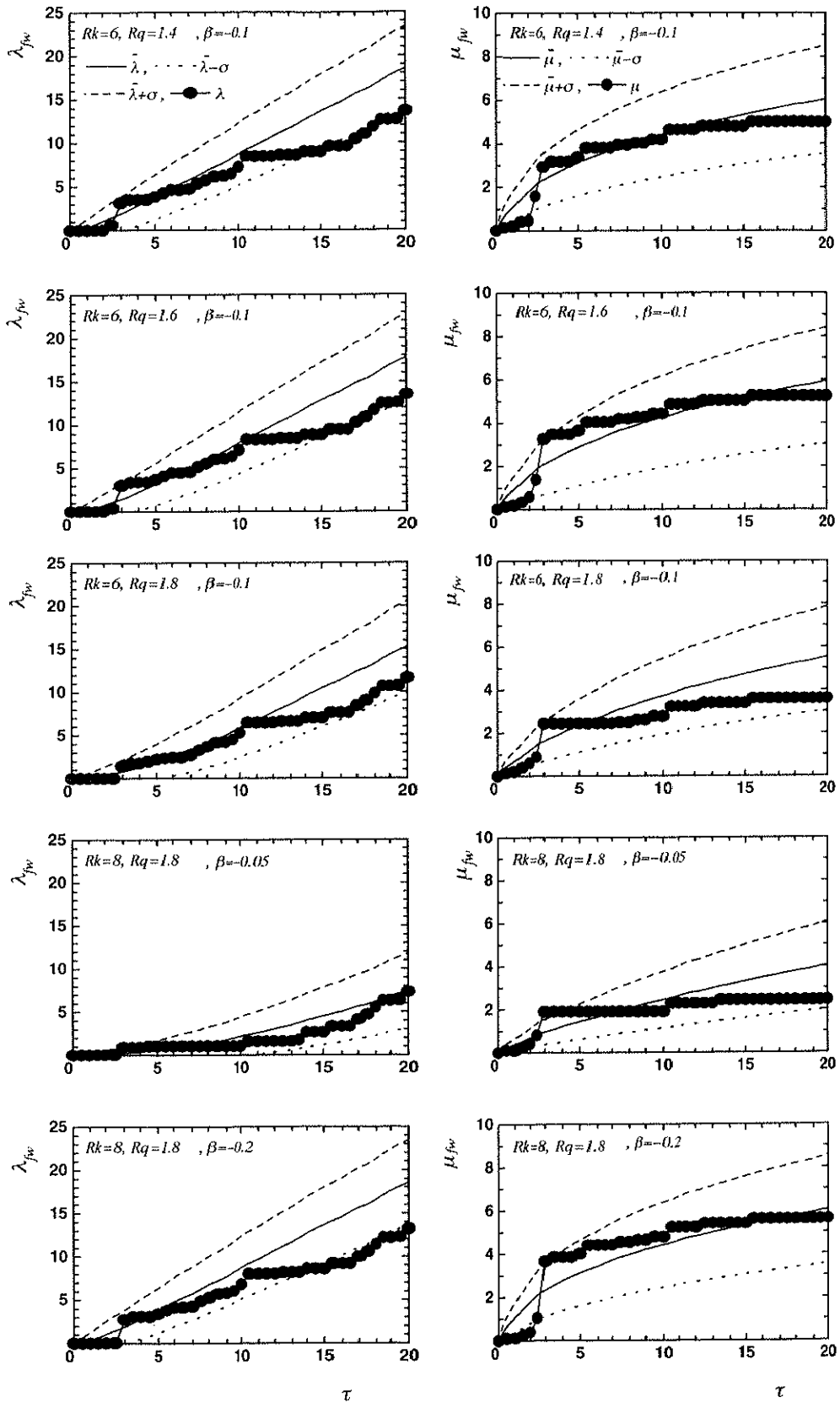

Fig. 4.12.3 Response under Hachinohe earthquake (ξ =0.05)

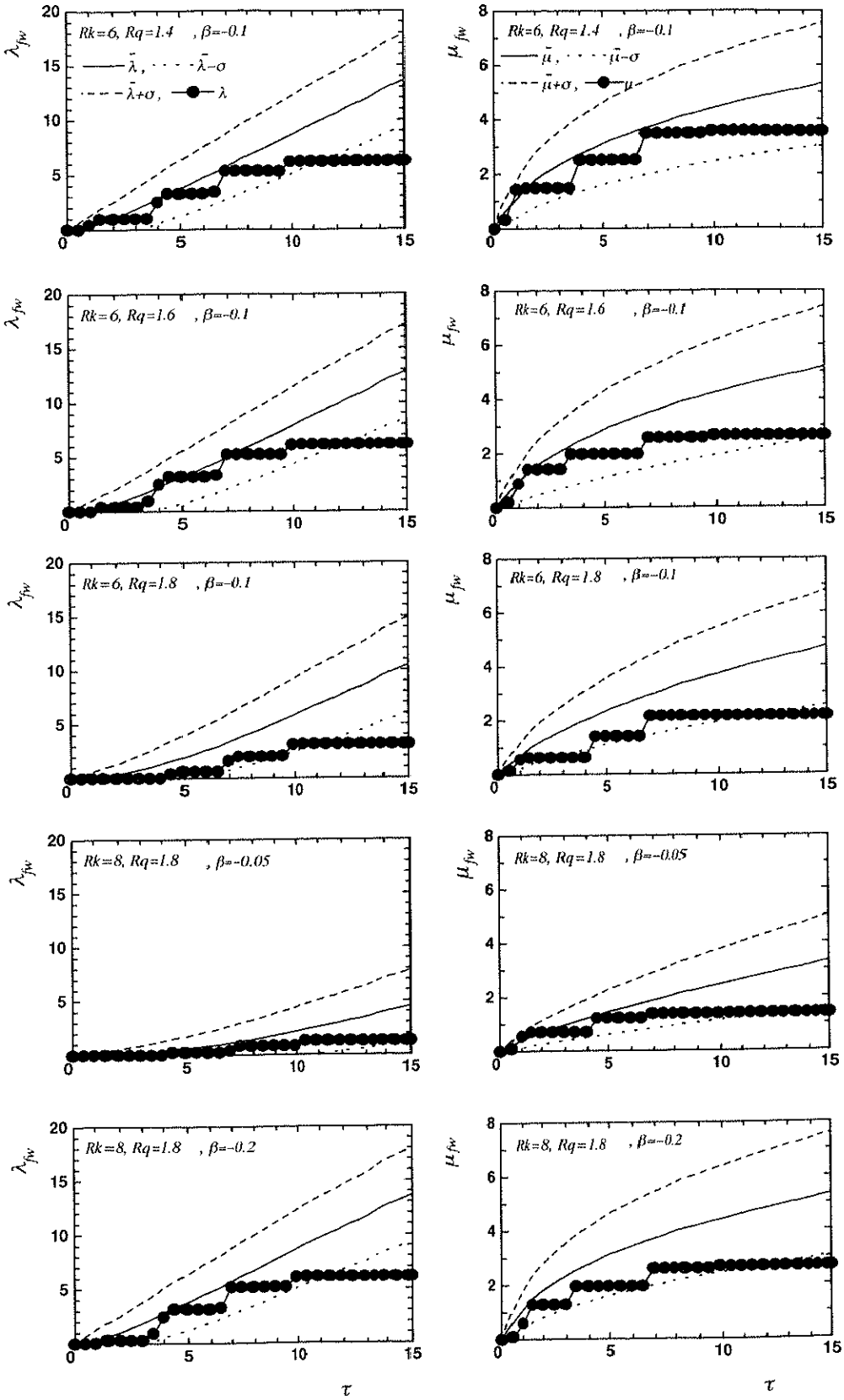

Fig. 4.12.4 Response under Miyagiken-oki earthquake (ξ=0.05)

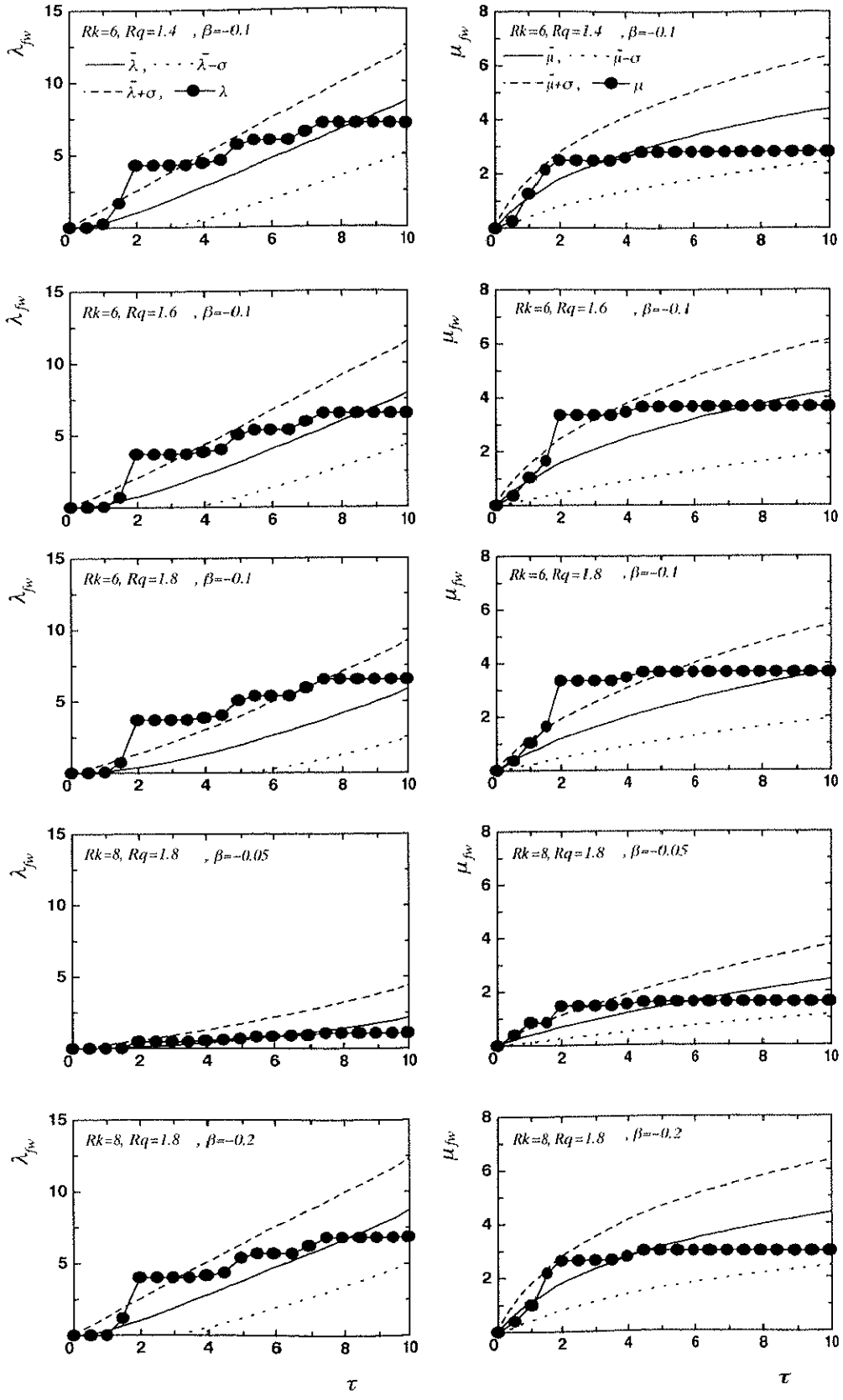

Fig. 4.12.5 Response under Kobe earthquake (ξ=0.05)

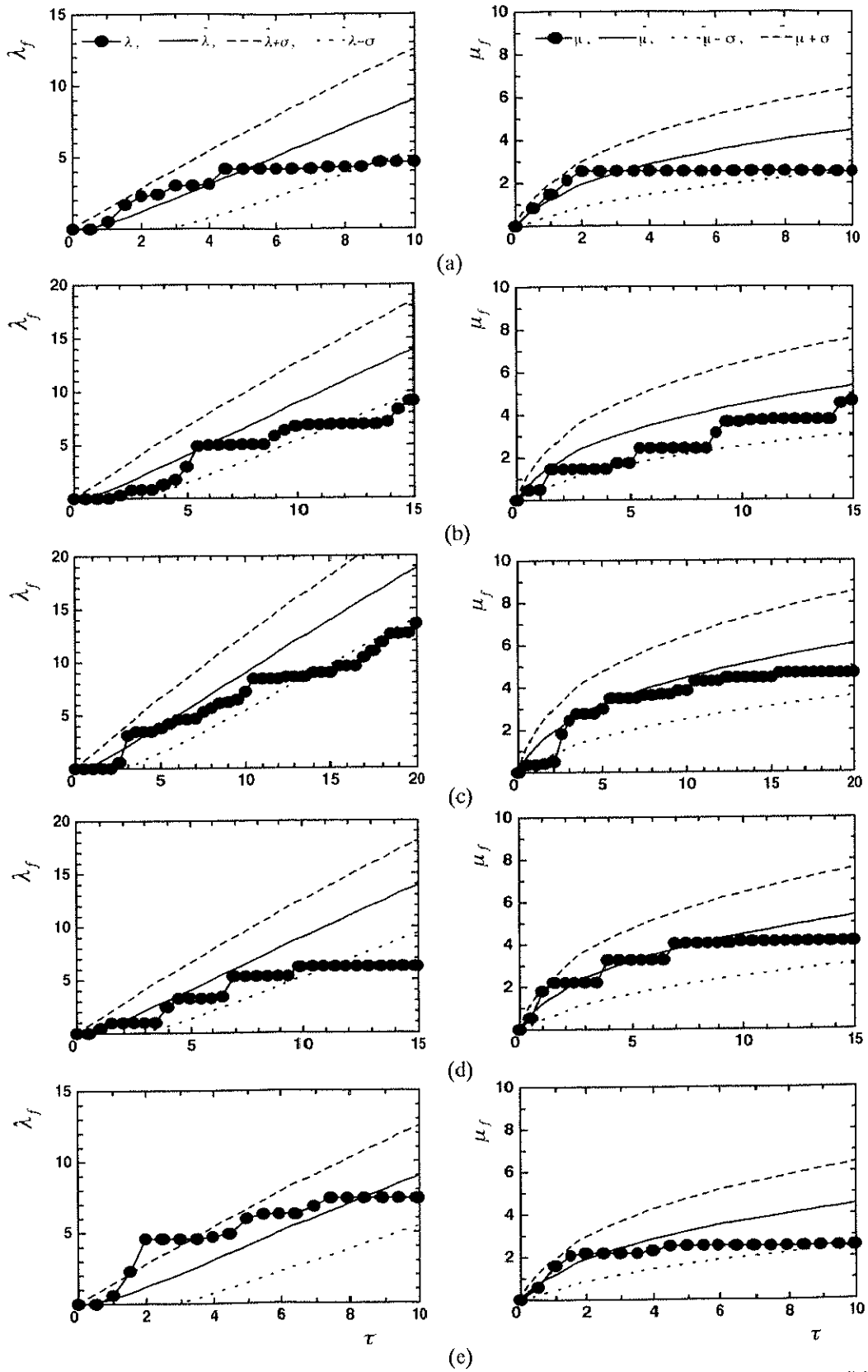

Fig. 4.12.6 Bare frame response under real earthquakes of (a) El-Centro; (b) Taft; (c) Hachinohe; (d) Miyagiken-oki and (e) Kobe (ξ=0.05)

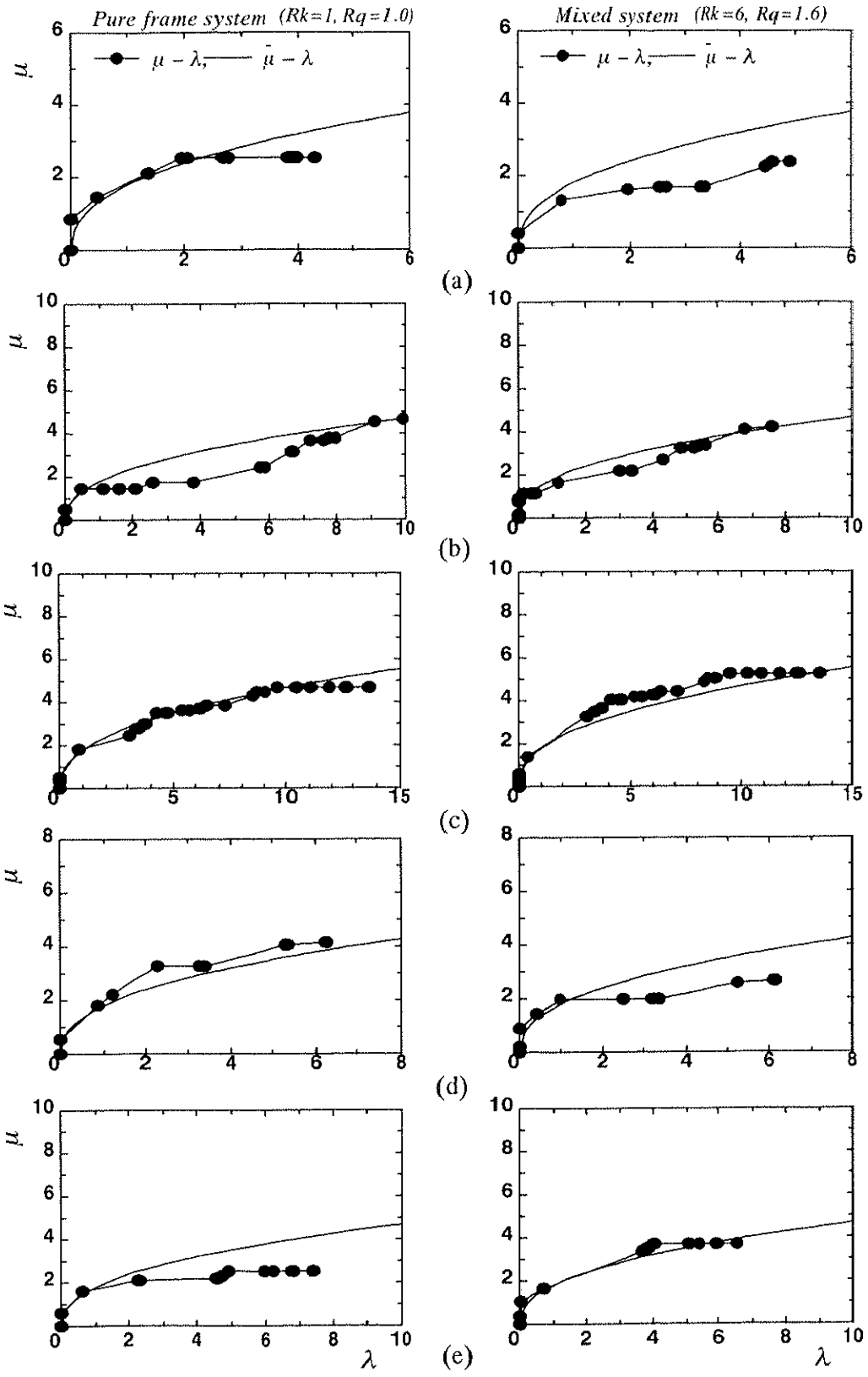

Fig. 4.12.7 μ - λ relationships under real earthquakes of (a) El-Centro; (b) Taft; (c) Hachinohe; (d) Miyagiken-oki and (e) Kobe (ξ =0.05)

Chapter Five

RELIABILITY ANALYSIS

5.1 Introduction

5.2 Reliability analysis

Chapter 5

RELIABILITY ANALYSIS

5 .1 Introduction

The structural reliability dealt with in this chapter quantitatively treats the unpredictability in the nonlinear response of the structure giving the uncertainty of the action that it is supposed to withstand. The application of structural reliability methods for bare frame systems had intensive research in the past few years. However, reliability application to mixed structural system has not been found in available literature; at least to the writer information. The importance of structural safety and reliability is well recognized and found its straight way in developing seismic design codes. Reliability function of the mixed system is defined here as the probability that the frame demands of accumulated dissipated plastic energy and/or ductility factor do not exceed some critical presumed levels beyond which the system is assumed to fail. Reliability assessments are performed by making use of the previously derived formulations for the averages and standard deviations of plastic energy $(\bar{\lambda},\sigma_{\lambda})$ and ductility factor $(\bar{\mu},\sigma_{\mu})$ in combination with appropriately selected probability density function (p.d.f). Other than these prediction estimates of reliability which are based on earlier formulations, reliability curves based on simulation data are traced as well.

5.2 Reliability analysis

Reliability functions for accumulated plastic energy λ and ductility factor μ, denoted by $R_{\lambda}(\lambda_F)$ and $R_{\mu}(\mu_F)$ respectively, are defined in the following

two integrals:

$$R_\lambda(\lambda_F) = \int_0^{\lambda_F} f_\lambda(\lambda)d\lambda \tag{5.2.1}$$

$$R_\mu(\mu_F) = \int_0^{\mu_F} f_\mu(\mu)d\mu \tag{5.2.2}$$

In Eq. (5.2.1), λ_F is a prescribed extreme value of λ after which failure occurs, which corresponds to μ_F in Eq. (5.2.2) when ductility-based reliability is dealt with. $f_\lambda(\lambda)$ and $f_\mu(\mu)$ are probability density function under which λ and μ are assumed to be distributed as shown in Fig. 5.2.1 as an illustrative example.

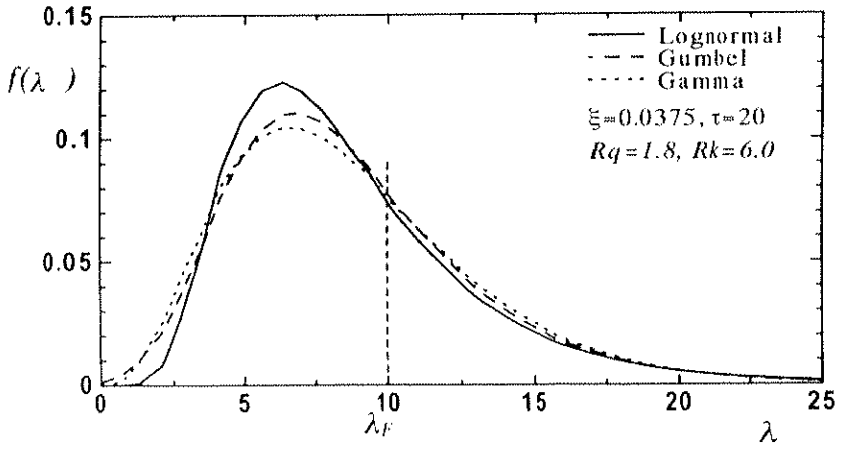

Fig. 5.2.1 Probability density functions of 3 distributions

To know what effect that different probability density functions may have on reliability functions, a typical system of $R_k = 6$, $R_q = 1.8$, and for $\xi = 0.025$-0.05 is analyzed for reliability utilizing three types of p.d.fs, namely, lognormal, Gumbel and gamma distributions. Gumbel probability density function $f_\lambda^{Gu}(\lambda_F)$ and cumulative distribution function $F_\lambda(\lambda_F)$ for accumulated plastic energy λ, are written in Eqs. (5.2.3) and (5.2.4), respectively,

$$f_\lambda^{Gu}(\lambda_F) = \frac{1}{\Phi_\lambda}\exp\left\{-\frac{\lambda_F - \Delta_\lambda}{\Phi_\lambda} - \exp[-(\frac{\lambda_F - \Delta_\lambda}{\Phi_\lambda})]\right\} \tag{5.2.3}$$

$$F_{\lambda}(\lambda_F) = \exp[-\exp(-\frac{\lambda_F - \Delta_{\lambda}}{\Phi_{\lambda}})] \tag{5.2.4}$$

where Φ_{λ} and Δ_{λ} are expressed as functions of the average and standard deviation of λ and given in Eqs.(5.2.5) and (5.2.6), respectively,

$$\Phi_{\lambda} = \sigma_{\lambda}\sqrt{6}/\pi \tag{5.2.5}$$

$$\Delta_{\lambda} = \bar{\lambda} - \upsilon(\sigma_{\lambda}\sqrt{6}/\pi) \tag{5.2.6}$$

where υ in Eq. (5.2.6) stands for Euler's constant which is equal to 0.5572. The probability density function for lognormal distribution of λ, is denoted by f_{λ}^{L} and given by Eq. (5.2.7),

$$f_{\lambda}^{L}(\lambda_F) = \frac{1}{\sqrt{2\pi}\eta_{\lambda}\lambda_F}\exp[-\frac{1}{2}(\frac{\ln(\lambda_F) - \theta_{\lambda}}{\eta_{\lambda}})^2] \tag{5.2.7}$$

where η_{λ} and θ_{λ} are expressed as functions of the average and standard deviation of the distribution for the process under consideration λ, that is

$$\eta_{\lambda} = \sqrt{\ln[(\frac{\sigma_{\lambda}}{\bar{\lambda}})^2 + 1]} \tag{5.2.8}$$

and

$$\theta_{\lambda} = \ln(\bar{\lambda}) - \frac{1}{2}\ln[(\frac{\sigma_{\lambda}}{\bar{\lambda}})^2 + 1] \tag{5.2.9}$$

As there is no closed form expression for cumulative density function, thus, integration prescribed in Eq. (5.2.1) must be solved using numerical integration method. Gamma probability density function is given in Eq. (5.2.10) where there is also no closed form expression for the cumulative density function and numerical integration must be performed,

$$f_{\lambda}^{Ga}(\lambda_F) = [1/\Gamma(\gamma_{\lambda})\varphi_{\lambda}^{\gamma_{\lambda}}]\lambda_F^{\gamma_{\lambda}-1}\exp(-\lambda_F/\varphi_{\lambda}) \tag{5.2.10}$$

where the coefficients γ_{λ} and φ_{λ} are also given as functions of the average and standard deviation of λ as the following:

$$\gamma_\lambda = (\bar{\lambda}/\sigma_\lambda)^2 \tag{5.2.11}$$

$$\varphi_\lambda = \sigma_\lambda^2/\bar{\lambda} \tag{5.2.12}$$

The function $\Gamma(\gamma_\lambda)$ is given by:

$$\Gamma(\gamma_\lambda) = \int_0^\infty e^{-u} u^{\gamma_\lambda - 1} du \tag{5.2.13}$$

and in case that γ_λ is integer value, then it could be given by

$$\Gamma(\gamma_\lambda) = (\gamma_\lambda - 1)! \tag{5.2.14}$$

When ductility-based reliability is to be considered, λ as an index or main symbol in Eqs. (5.2.3) through (5.2.14) shall be replaced by μ. The reliability curves of $R_\lambda(\lambda_F) - \tau$ and $R_\mu(\lambda_F) - \tau$ are shown in Figs. 5.2.2(a) and 5.2.2(b), respectively assuming failure levels of λ_F =10 and μ_F =5.

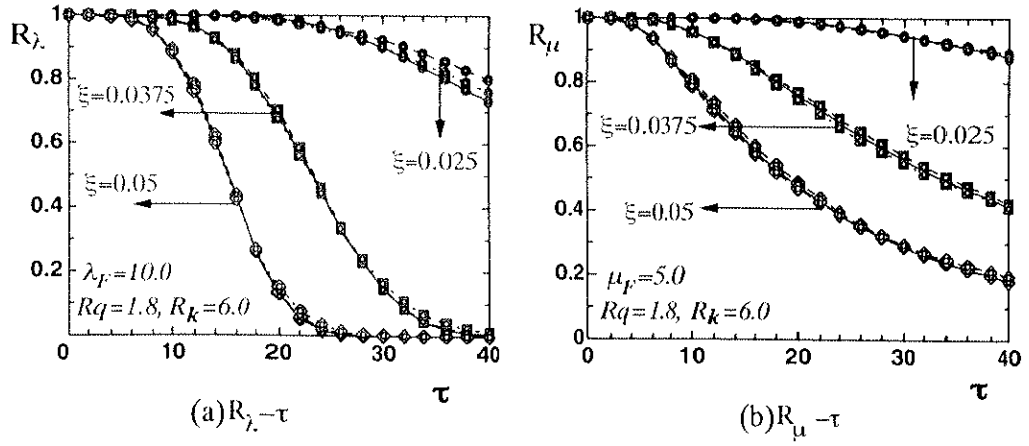

solid lines: Gumbel dist., dashed lines: lognormal dist., and dotted lines: gamma dist.

Fig. 5.2.2 Reliability curves based on three-probability distributions

It can be concluded from the above figures that $R_\lambda(\lambda_F) - \tau$ and $R_\mu(\lambda_F) - \tau$ curves are generally irrelevant to distribution type. As different distribution types have given almost similar results, typical other curves of $R_\lambda(\lambda_F) - \tau$ and $R_\mu(\mu_F) - \tau$ are computed and depicted in Figs. 5.2.3 and 5.2.4, respectively, with dashed lines using Gumbel distribution for values of ξ =0.025, 0.0375 and

0.05, R_q = 1.0, 1.6, 1.8 and 2, and for R_k =1, 6 and 8. Reliability curves based on simulation data are displayed in Figs. 5.2.3 and 5.2.4 (lines with symbols) in which $R_\lambda(\lambda_F)$ or $R_\mu(\mu_F)$ at specific value of τ refers to the percentage of samples that have not reached λ_F or μ_F at τ. It is noticed that satisfactory agreement is obtained between the prediction and simulation based reliability.

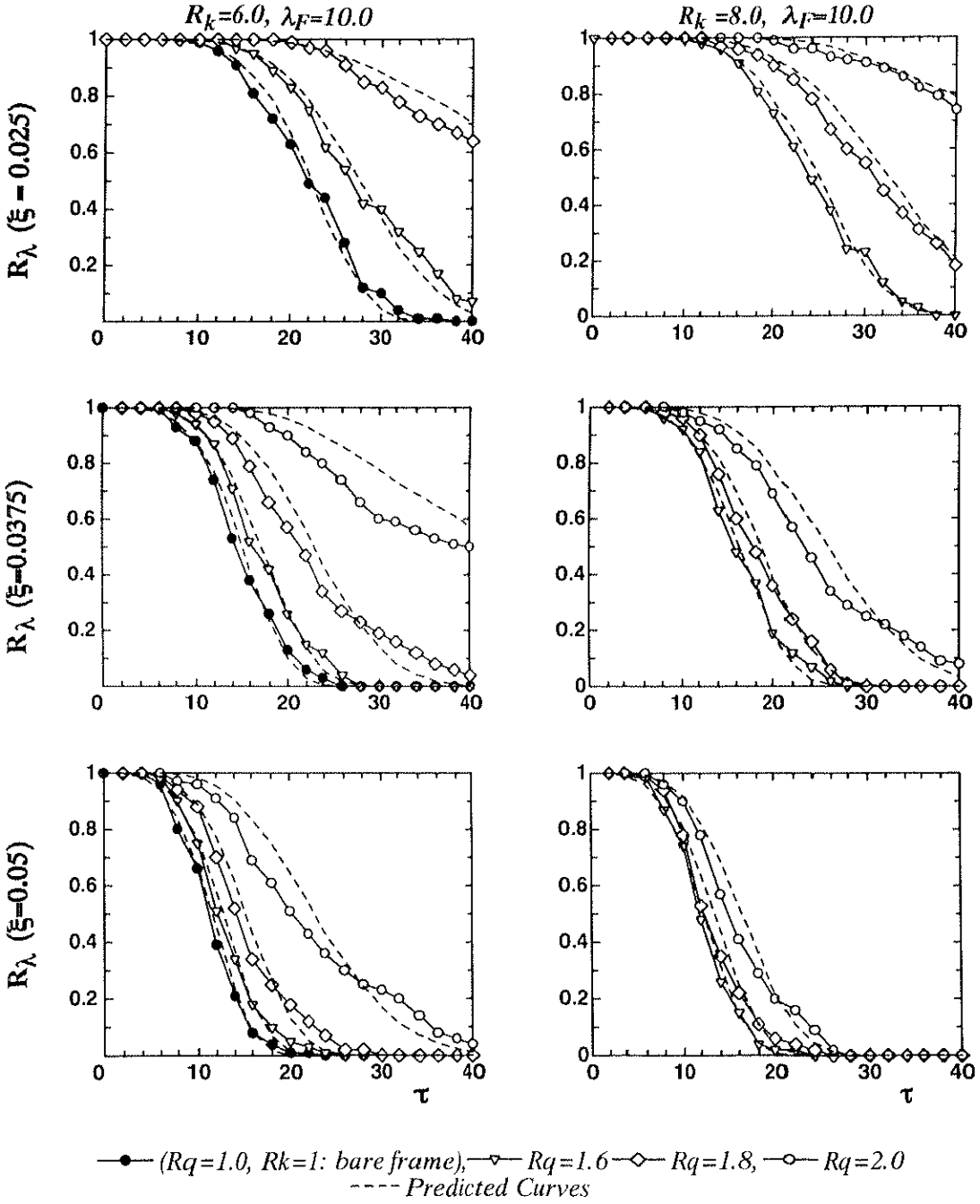

Fig. 5.2.3 Reliability curves based on plastic energy dissipation

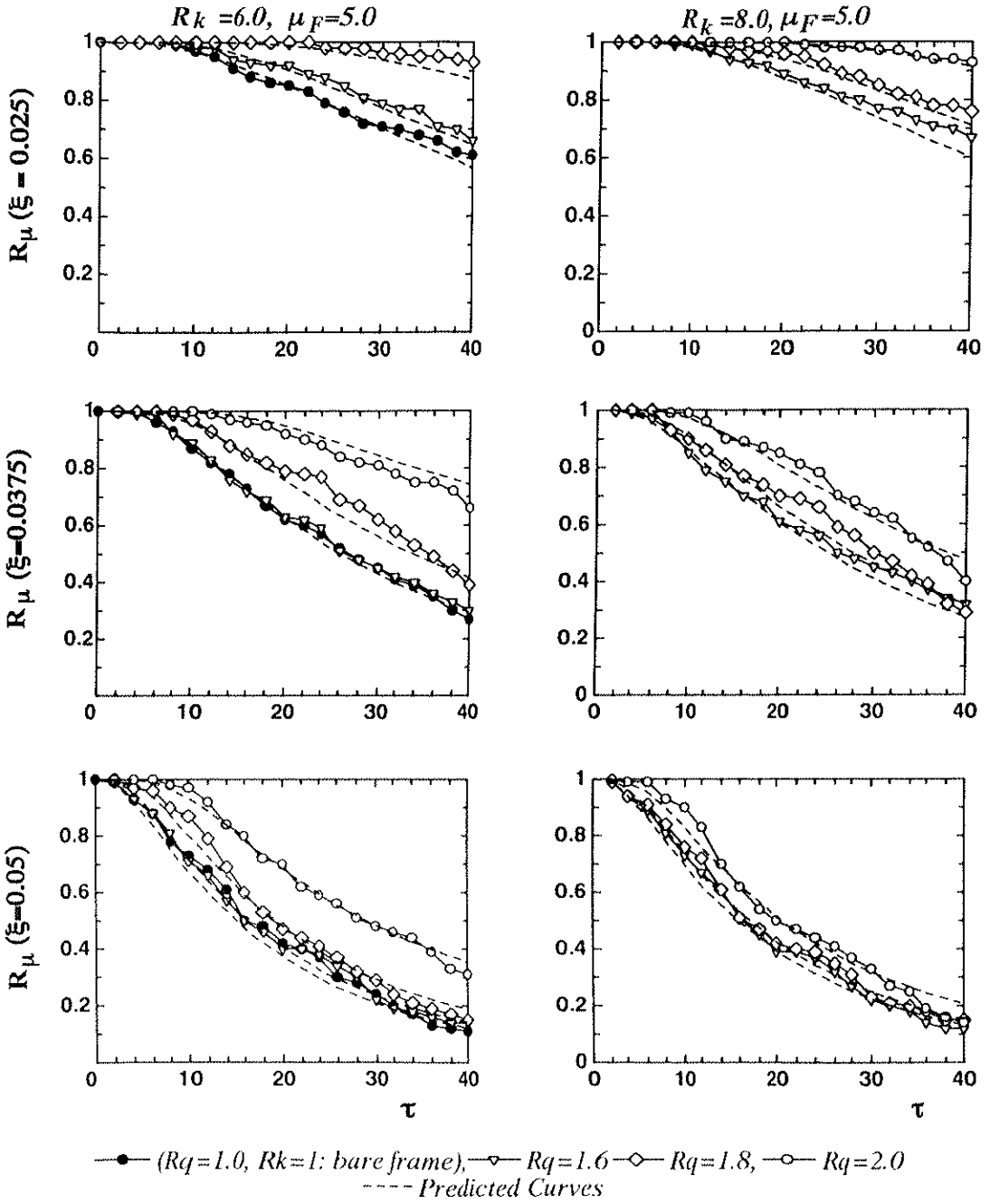

Fig. 5.2.4 Reliability curves based on ductility factor

Reliability simulation and prediction curves covering wider range of β, other than the central value of -0.1, are also computed and plotted in Figs. 5.2.5(a) and 5.2.5(b) where the parameters R_k and R_q are taken as (R_k=12 and R_q=1.6) and (R_k=8 and R_q=1.4), respectively. The fitting agreement is also seen reasonable in most cases.

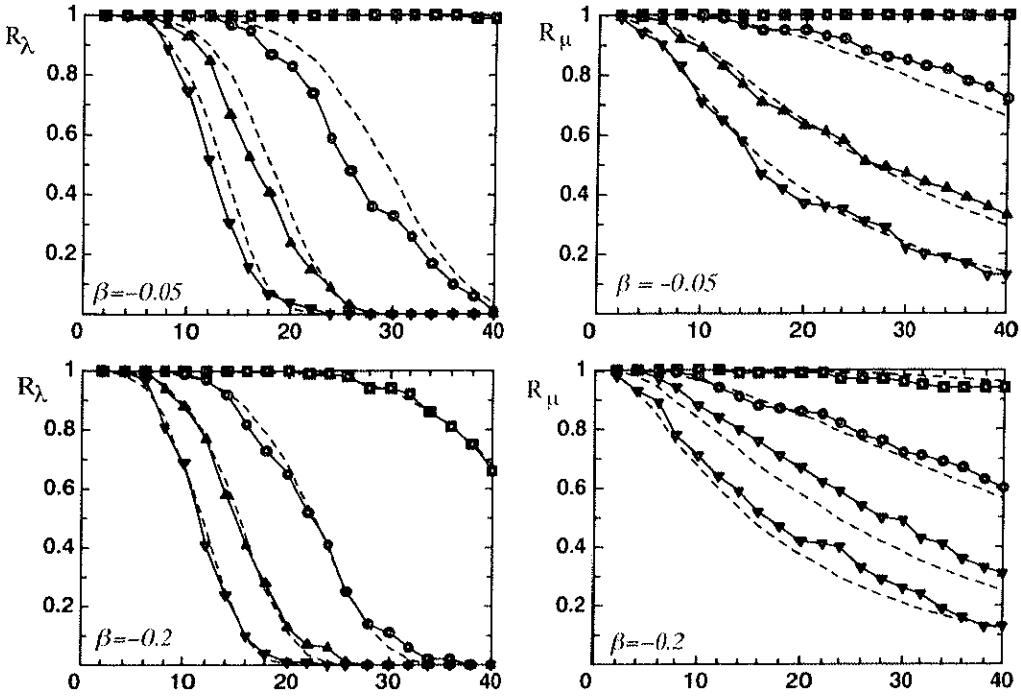

(a) : Rk=12, Rq=1.6

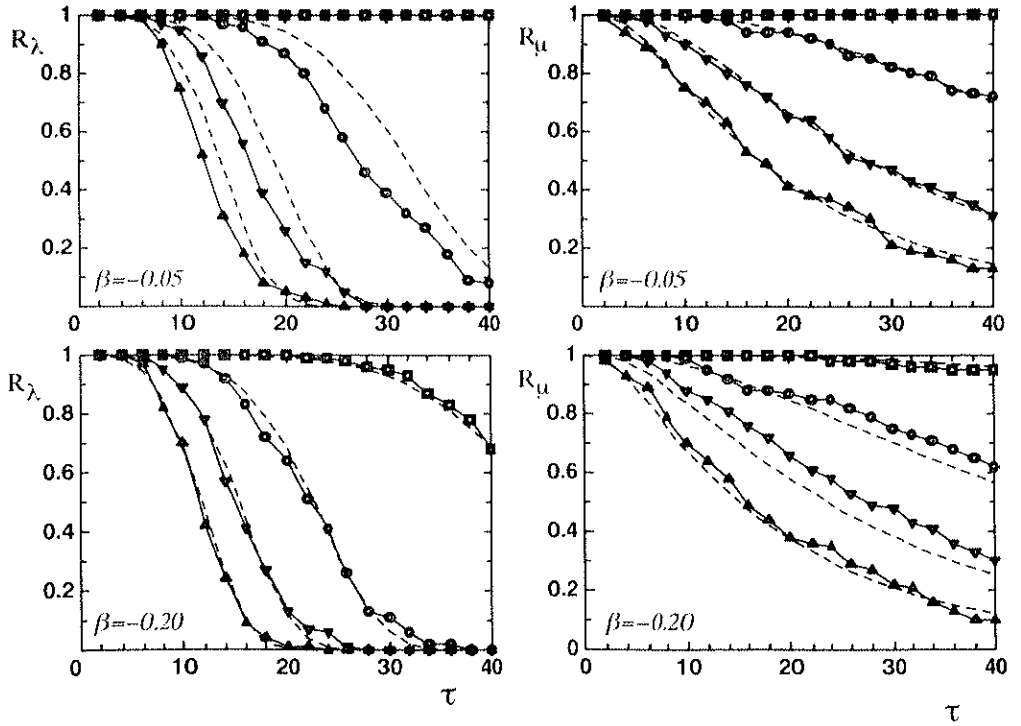

(b): Rk=8, Rq=1.4

ξ=0.0125, ξ=0.025, ξ=0.0375, ξ=0.05 *(Simulated Curves)*

Predicted Curves

Fig. 5.2.5 Reliability curves for β = –0.05 and -0.2

It is of important to mention that reliability curves are mainly aimed at showing how much brittle elements of different characteristics affect reliability of the frame in mixed system, and what parameters are controlling the degree of effectiveness. Also, these curves can be used for design purpose, for example, at the preliminary design stage, the system data (R_q, R_k, β, T_0, α, λ_F and/or μ_F) and excitation data (S_0 and t_d; where t_d is the time duration of excitation) are available, then the probability of safety which is expressed in term(s) of reliability function(s) R_λ and/or R_μ can be known from reliability curves (Figs. 5.2.3 through 5.2.5) having $\tau = t_d / T_0$. If the target safety level is found not appropriate, then system data have to be manipulated in order to get the prescribed target level of safety by means of trial and error methods. Reliability curves other than shown here can be easily predicted and drawn using the formulations and the methods mentioned above within the application limits for ξ, β and ε / ξ.

As concluding points, it is found that reliability of mixed system also depends on three parameters represented by ξ, ε / ξ and β. Parameter ξ is related to frame yield strength whereas ε / ξ and β are related to brittle element potential energy capacity. Higher the value of ξ lower the reliability and more plastic energy and ductility factor are required and vice versa. But higher ε / ξ higher reliability is available and less plastic energy and ductility factor are required from the frame element. This proved to indicate the important effect that brittle element may have, in some cases, on the overall seismic response and reliability of frame in mixed systems to the degree that must not be ignored. Mixed system as well as pure frame system reliability is treated here through covering uncertainty in seismic loads by using simulated input motions and allowing geometric and mechanical characteristics of the system to be variable parameters in a way that enables the design engineer to practically estimate and judge the effect of the used brittle elements on the behavior of the designed frames by means of response quantities and/or reliability function.

Chapter Six

CONCLUSIONS AND RECOMMENDATIONS

6.1 Conclusions

6.2 *Recommendations for future research*

Chapter 6

CONCLUSIONS AND RECOMMENDATIONS

6.1 Conclusions

Inelastic random earthquake response and reliability assessment of ductile frames when mixed with brittle elements is presented. The mixed frame system is modeled by undamped single-degree-of-freedom system and excited by simulated ground acceleration. The ductile frame element has elasto-plastic restoring force while the brittle element (like infill wall) has degraded stiffness and strength model. Referring to the contents and results of this study, the following main points could be outlined:

1. Approximate solutions for average and standard deviation of accumulated plastic energy and ductility factor demanded on the frame element, are derived as closed form expressions. The solutions are compared with the simulation estimates where acceptable agreement is found in most cases.
2. The influence of brittle element on the inelastic response and reliability of the frame is mainly related to the brittle element potential energy capacity relative to normalized input motion intensity.
3. The efficiency of the brittle element in reducing plastic energy and ductility demands on the frame and enhancing its reliability is recognized to a degree that depends on level and duration of input motion, brittle element potential energy capacity and the frame structural characteristics.
4. The overall relative seismic response of ductile frame mixed with brittle elements to that without brittle elements has nothing to do with input motion intensity as a separate variable. The main effective parameters are: Post-yielding slope ratio of brittle element restoring force model and the

ratio which determines the brittle element potential energy capacity to the input motion intensity.

5. Though more enhanced analytical research is needed, the provided pioneer formulations in this study may pave the way for endorsing an improvement in seismic design codes concerning the problem of mixed systems.

6.2 Recommendations for future research

The concluded formulations which summarize the effect and contribution of brittle-failure type elements on the whole seismic performance of the structural frame may be improved by:

1. Further improvement of the hysteretic model for the frame element may be considered like using Takeda's model or other RC nonlinear models if more precise results for RC structures are needed, but it is expected that more complicated formulations has to be dealt with due to increasing number of parameters.
2. Also, hysteretic model for the brittle element may be improved to allow for stiffness and strength deterioration at the same deformation levels under repeated cycles.
3. Viscous damping characteristics of the brittle element and frame element may have to be considered in future studies allowing another parameter to be represented in the formulations. However, it is unclear how much important that effect may be in terms of relative response of mixed frame system /pure frame system.
4. Simulated input motions rather than white noises can be used. Kanai-Tajimi power spectral density model and a deterministic envelope function can be considered for taking into account local site effect and transient phases of real input motions, respectively.
5. Because determining the brittle element characteristics seems to be difficult task and the range is wide, it may be visible to consider them as random variables in future study.
6. Mixed system like infilled frame continues to be built throughout the world and giving this large scale and problem complexities, research efforts based

on worldwide accumulated analytical and experimental researches as well as post-earthquake observations, should be directed towards much better and closer understanding of the mixed frame system seismic behavior among different institutions and researchers. That may hopefully and eventually leads to introduction of simple guideline usable by practitioners or design engineers to account for brittle element existence in the seismic design of frame structures in such a way that local conditions are taken into considerations as well.

REFERENCES

1. Abrams, D.P. 1992; "Strength and behavior of unreinforced masonry elements"; X WCEE, Vol.6, pp. 3475-3480, Madrid, Spain.
2. Al-Sadeq, H. and Matsushima, Y. 1998; "Reliability analysis of masonry infilled frame structures subjected to earthquake ground motions"; Proc. of the Tenth Japan Earthquake Engineering Symposium, Vol. 2, pp. 2535-2540, Yokohama, Japan.
3. Bycroft, G.N. 1960; "White noise representation of earthquake"; Proc. Paper 2434, Journal of Engineering Mechanics Division, ASCE, Vol. 86, EM2.
4. Broken, S.T. and Bertero, V.V. 1981; "Studies on effects of infills in seismic resistant RC construction"; Report No. UCB/EERC 81/12; Earthquake Engineering Research Center; Univ. of California at Berkeley.
5. Clough, R. W. and Penzien, J. 1975; "Dynamic of Structures "; McGraw-Hill, New York.
6. Gavrilovic, P. and Sendova, V. 1992; "Experimental and analytical studies of infill walls in reinforced concrete structures"; X WCEE, pp. 3309-3315, Madrid, Spain.
7. Goto, K. and Matsushima, Y. 1999; "Estimation of structural safety"; Master thesis, University of Tsukuba, Japan.
8. Housner, G.W. 1956; "Limit design of structures to resist earthquake"; Proc. of I WCEE, Berkeley, CA.
9. Kanai, K 1957; " Semi-empirical formula for the seismic characteristics of the ground"; University of Tokyo, Bulletin of the Earthquake Research Institute, Vol. 35, pp. 309-325.
10. Matsushima, Y 1991; "Random response of a single-degree-of-freedom system with bilinear hysteresis"; Journal of Structural and Construction Engineering, Transactions of AIJ, No. 420, pp. 101-110, (in Japanese).

11. Mehrabi, A.B., Shing, P.B., Schuller, M.P. and Noland, J.L. 1996; "Experimental evaluation of masonry-infilled frames"; Journal of Structural Engineering, ASCE, 122(3), pp. 228-237.
12. Myslimaj, B. and Matsushima, Y. 1998; " Earthquake motions in various soil conditions and its influence on the inelastic response of structures"; Doctoral thesis, University of Tsukuba.
13. Negro, P. and Verzeletti, G. 1996; " Effect of infills on the global behavior of R/C frames: Energy considerations from pseudo-dynamic tests"; Journal of Earthquake Engineering and Structural Dynamic, Vol. 25, pp. 753-773.
14. Richard, A.J. and Gouri, K. B. 1996; "Statistics: principles and methods"; 3rd ed., John Wiley & Sons, New York.
15. Smith, B. S. and Carter, C. 1969; "A Method of analysis for infilled frames"; Proc. ICE, Vol. 44, pp. 31-48.
16. Tajimi, H. 1960; "A statistical method of determining the maximum response a building structure during an earthquake"; II WCEE, Vol. II, pp. 781-797. Tokyo and Kyoto.
17. Teran-Gilmore, A., Bertero, V.V., Youssef, N. 1995; "Seismic rehabilitation of framed buildings infilled with unreinforced masonry walls using post-tensioned steel braces"; Report No. UCB/EERC-95/06, Univ. of California at Berkeley.
18. Tsai, K.C., and Li, J.W. 1994; "DRAIN2D+, A general purpose computer program for static and dynamic analysis of inelastic 2D structures "; Report No. CEER/R 83-03 , National Taiwan University.
19. Wakabayashi, M. and Martinez, R.E. 1988; "Design of earthquake-resistant buildings"; McGraw-Hill; New Jersey.

PUBLICATIONS

I - Referred Papers

1. Al-Sadeq, H. and Matsushima, Y. 1999; "Inelastic random seismic response analysis and reliability of ductile Frames filled with brittle elements"; Journal of Structural and Construction Engineering, Transaction of Architectural Inst. of Japan (AIJ), No. 516.
2. Al-Sadeq, H. and Matsushima, Y. 1998; "Reliability analysis of masonry infilled frame structures subjected to earthquake ground motions"; Proc. of the Tenth Japan Earthquake Engineering Symposium, Vol. 2, pp. 2535-2540, Yokohama, Japan.
3. Al-Sadeq, H. and Matsushima, Y. 1998; "Inelastic random seismic response analysis of unreinforced RC infilled frame Structures"; Proc. of the Sixth East Asia-Pacific Conference on Structural Eng. and Construction, Vol. 3, pp. 1507-1512, Taipei, Taiwan.
4. Al-Sadeq, H. 1992; " Analysis of linear and nonlinear behavior of space frames with infilled panels under static and seismic forces"; Proc. of the First International Symposium on Earthquake Engineering, Aleppo, Syria.(in Arabic).

II - Presentation Papers

1. Al-Sadeq, H. and Matsushima, Y. 1998; "Inelastic random seismic response of frames filled with brittle elements"; Summaries of Technical Papers of Annual

Meeting of Architectural Institute of Japan, Vol. B-2, pp. 395-396.

2. Al-Sadeq, H. and Matsushima, Y. 1997; "Effect of masonry infill on seismic response of RC frame structures"; Summaries of Technical Papers of Annual Meeting of Architectural Institute of Japan, Vol. B-2, pp. 987-988.

III - Master Thesis

Al-Sadeq, H. 1991; "Analysis of Linear and Nonlinear Behavior of Space Frames with Infilled Panel under Static and Seismic Forces," Publications of Institute of Earthquake Engineering and Engineering Seismology, University of "Kiril and Metodij", Skopje, Macedonia.

本学関係